PEOPLE'S DEMOCRATIC REPUBLIC OF ALGERIA

MINISTERY OF HIGHER EDUCATION AND SCIENTIFIC RESEARCH

UNIVERSITY M'HAMED BOUGARA-BOUMERDES

Institute of **E**lectrical and **E**lectroni**c** **E**ngineering

Doctorate Thesis

Presented by:

MALLATI Meftah

For a **PhD Degree** in**:**

Filière : **Génie électrique et électrotechnique**

Option : **Microelectronics**

Study of the effect of the temperature and the magnetic field on NBTI in the MOSFET devices

To be defended before the jury composed of :

Mr	RAHMOUNE Fayçel	Prof	(UMBB)	President
Mr	BENTARZI Hamid	Prof	(UMBB)	Supervisor
Mr	LAGHROUCHE Mourad	Prof	(UMMTO)	Examinateur
Mr	BENNAMANE Kamal	MCA	(UMMTO)	Examinateur

Année Universitaire 2019/2020

ABSTRACT

Negative Bias Temperature Instability (NBTI) is a serious degradation mechanism in nanoscale devices and circuits. It impacts mainly P-channel devices by generating traps at the Si/SiO_2 interface as well as in the oxide bulk. These generated traps cause the degradation of the most important transistor parameters such as threshold voltage, saturation current and channel mobility. Since the improvement of devices and circuit performance is the main target in nanotechnology, investigating the physics of the NBTI and its modelling is essential and highly useful. In this thesis, the study of NBTI degradation for pure-SiO_2 is undertaken and it shows that despite of many models that have been developed, none of them gets the consensus especially on the microscopic origin of fast and permanent components. The proposed models in the literature can be split into two big categories: Hydrogen based models or Reaction-Diffusion (RD) models and hole trapping detrapping models also called Energy Well (EW) models. Some authors attempts to propose models that combine both hydrogen and hole contribution, but they diverge on which of them is behind the permanent part or the fast recovery one. Although NBTI is extensively studied and several models have been proposed in the past, its physical mechanism has remained a field of great debate.

In this thesis, a new physical based model, which extends the two-stage model to account the hydrogen diffusion in the oxide, is proposed. In our model holes in correlation with hydrogens in the oxide are responsible of NBTI and in contrast to any other proposed model both hole and hydrogen related defects contribute to fast and long term recovery and the two components are correlated at stress uncorrelated in recovery period. The validity of the model equations is checked using COMSOL Multiphysics simulator.

Key word: MOSFET reliability, Negative Bias Temperature Instability (NBTI), oxide defects, Reaction-diffusion model.

الملخص

عدم الثبات الناتج عن تغير درجة الحرارة وعن فرق الكمون السلبي الذي يتعرض له الترانزستور اثناء أداء عمله يسمى Negative Bias Temperature Instability ويرمز له اختصارا NBTI-

(NBTI) هو آلية تدهور خطيرة في الأجهزة الالكترونية الميكرو والنانو سكوبيه. إنه يؤثر بشكل رئيسي على أجهزة P-channel عن طريق توليد الفخاخ في واجهة Si / SiO_2 وكذلك في الجزء الأكبر من أكسيد. وعلى الرغم من العديد من النماذج التي تم تطويرها، فإن أياً منها لا يحصل على إجماع على وجه الخصوص على الأصل المجهري لما يسمى بالمكونات السريعة والدائمة. يمكن تقسيم النماذج المقترحة في الابحاث إلى فئتين رئيسيتين: النماذج القائمة على الهيدروجين أو نماذج الانتشار-التفاعل (RD) ونماذج المعتمدة على حبس وتحرير الفجوات في الثقوب والذي المسمى أيضًا حائط الطاقة Energy Well (EW). لقد قدم بعض الباحثين نماذج تجمع بين كل من الهيدروجين ومساهمة الثقوب، لكنهم يختلفون حول أي منهم وراء الجزء الدائم أو السريع. على الرغم من دراسة NBTI على نطاق واسع، وعلى الرغم من كثرة النماذج في الماضي، إلا أن آليتها الفزيائية تظل موضوع نقاش حيوي.

في هذه الأطروحة، تم اقتراح نموذج فيزيائي جديد، يمتد نموذج Two-Stage لتفسير انتشار الهيدروجين في الأكسيد. في نموذجنا، تكون الثقوب المرتبطة بالهيدروجين في الاكسيد مسؤولة عن NBTI وعلى عكس أي نموذج آخر مقترح، فإن العيوب المرتبطة بالثقب والهيدروجين تساهم في الاسترداد السريع والطويل الأجل. يتم التحقق من صحة معادلات النموذج باستخدام محاكي COMSOL Multiphysics.

كلمات مفتاحية :تدهور الترانزستور. التذبذب الحراري السالب الكمون. نموذج التفاعل الانتشار.

Résumé

La dégradation du transistor à effet de champ (MOSFET), soumis aux contraintes de température et de polarisation négative, communément appelée Negative Bias Temperautre Instability (NBTI) est un problème sérieux de fiabilité dans les circuits et les composants microélectroniques. Le NBTI dégrade surtout le transistor à canal P par la génération des pièges de trous à l'interface entre Si et SiO_2 ainsi qu'à l'intérieur de l'oxyde. Ces pièges provoquent la dégradation des paramètres du transistor les plus importants tel que la tension de seuil, le courant de saturation et la mobilité des porteurs dans le canal. Parce que le but ultime de la nanotechnologie est d'améliorer la performance des composants et des circuits intégrés, la compréhension de la physique du NBTI et sa modélisation et très importante. Dans cette thèse, la dégradation NBTI est étudiée en détail pour les transistors à SiO_2 pure. Il est montré que malgré de nombreux modèles développés, aucun d'entre eux n'obtient le consensus notamment sur l'origine microscopique des composants dits rapides et permanents. Les modèles proposés dans la littérature peuvent être divisés en deux catégories principales : les modèles à base d'hydrogène ou les modèles de réaction-diffusion (RD) et les modèles de piégeage et de piégeage de trous également appelés modèles Energy Well (EW). Certains auteurs ont tenté de proposer des modèles qui combinent à la fois l'hydrogène et le peignage des trous dans l'oxide, mais ils divergent sur lequel d'entre eux se trouve derrière la partie permanente ou celui à récupération rapide. Bien que le NBTI soit largement étudié et que plusieurs modèles aient été proposés dans le passé, son mécanisme physique reste un sujet de débat vif.

Dans cette thèse, un nouveau modèle à base physique est proposé. Le modèle proposé étend le modèle Two-Statge en tenant compte de la diffusion de l'hydrogène dans l'oxyde. Dans notre modèle, les trous en corrélation avec les hydrogènes dans l'oxyde sont responsables du NBTI et contrairement à tous autres modèles proposés, les défauts liés au trou et à l'hydrogène contribuent à une récupération rapide et à long terme. Il est montré que les deux composantes sont à la fois corrélées au début de la période de stress est non corrélée en période de récupération. La validité des équations du modèle est vérifiée à l'aide du simulateur COMSOL Multiphysics.

Mots clés: Fiabilité des transistors MOSFET, Contraintes de température et de polarisation négative (NBTI), Défaut d'oxyde, Reaction-diffusion model.

ACKOWLEDGEMENTS

First of all, I would like to give thanks to God for making it possible for me to experience this great opportunity. I am indebted to my supervisor Professor H. Bentarzi at IGEE for his technical support, helpful suggestions, patience, scientific advices, and availability and this thesis would not have been possible without his invaluable guidance, generous support and constant inspiration. He has been excellent mentor during this thesis project.

I wish to acknowledge IGEE staff for providing support and suitable environment.

This acknowledgement would not be complete if I do not express the most sincere thanks to my family members for their support and encouragement, the patience they have shown throughout this work.

Table of contents

ABSTRACT I
الملخص II
RESUME III
ACKOWLEDGEMENTS IV
TABLE OF CONTENTS V
LIST OF FIGURES VII

CHAPTER I

INTRODUCTION 1

CHAPTER II

SILICON DIOXIDE AND ITS DEFECTS

II.1 Amorphous SiO_2 structure 6

II.2 -Defects in Si/SiO_2 system 7

II.3- Oxygen vacancy 8

II.4 E′ centers: 9
- II.4.1 E'_δ center: 9
- II.4.2 E'_γ Center 11
- II.5 P_b center: 12

II.6 Classification of charges in the oxide: 13

II.7 Hydrogen is SiO_2 15

II.8 Positive charges in the oxide classification 16

II.9 Conclusion 17

CHAPTER III

NBTI EXPERIMENTAL FEATURES

III.1. NBTI definition 18

III.2. History of NBTI degradation: 21

III.3. NBTI experiment set-up 22

III.4. Experimental features of NBTI: 25
- III.4.1 Charge Transport Independence 25
- III.4.2 Channel Hole Concentration 26
- III.4.3 Oxide Field Dependence 26
- III.4.4 Temperature Dependence 27

III.4.5. Time Dependence 28
III.4.6 Recovery of NBTI 29
III.4.7 Hydrogen dependence 29
III.4.8 Magnetic field dependence 31

III.5 Conclusion 32

CHAPTER IV
NBTI MODELLING

IV.1 Hydrogen-diffusion based models 34
IV.1.1 Reaction Phase 34
IV.2.4 Dispersive Transport 44

IV.2 Hole-trapping detrapping based model 47
IV.3.1 Two Stage Model 47
IV.3.2 Threshold Voltage Shift Expression 51

IV.3 Conclusion 52

CHAPTER V
NBTI PROPOSED MODEL

V.1 Positive charge classification 55

V.2. Model derivation: 56
V.2.1 Stress Period 57
V.2.2 Relaxation (Recovery) Period 59

V.3 Model simulation 63
V.3.1 Fast Recovery and Long Term Recovery 64
V.3.2 Power Law and Time Exponent 65
V.3.3 Stress Voltage and Temperature Dependence 66

V.4. Conclusion 69

CHAPTER VI

CONCLUSION AND PERSPECTIVES 70
APPENDIX 1 73
REFERENCES 103

List of Figures

Figure	Page
Figure I.1. Important milestones in the development of semiconductor electronics	3
Figure II.1 (a) SiO_4 structural unit of most forms of SiO_2, showing tetrahedral coordination. (b) Si_2O bonding configuration with Si-O-Si bond angle θ varying from 120° to 180° depending on the form of SiO_2.	8
Figure II.2: Si/SiO2 system atomic structure. Left: Ordered substrate Si. Right: Amorphic SiO2 structure	9
Figure II.3 (A) SiO2 structure. (B) Oxygen vacancy defect	10
Figure II.4 The defect levels arising from oxygen vacancies (neutral) or its positive counterpart Eδ′ centers.	11
Figure II.5. Structure of an E'γ center. The silicon atom on the left-hand side carries an electron in the dangling bond (DB). The positively charged silicon atom on the right-hand side is bonded to the back oxygen (BO). This atomic arrangement is also referred to as the puckered configuration	12
Figure II.7 Schematic of the defect levels originating from an E'γ centers. The energy levels for the capture of electrons (+/0) as well as the energy levels for the emission of electrons (0/+) are found to lie close to the silicon conduction band or the silicon valence band, respectively.	13
Figure II.8 The Pb configuration. a) for (111) surface. b) for (100) surface	14
Figure II.9 P_b center density of states and charge for p-MOSFET.	14
Figure II.10: Schematic diagram of MOS structure showing the distribution of defects	15
Figure II.11 Schematic representation of Hydrogen related configurations in amorphous SiO_2.	16
Figure II.12 The framework of positive charge. a) The contribution of each type in typical NBTI stress/recovery sequence. b) The charges during recovery c) charge during stress.	17
Figure III.1 ID - VG and gm -VG curves for fresh device (solid line) and after 10,000s of NBTI stress (dashed line) for a p-MOSFET	21
Figure III.2. Threshold voltage shift for p-MOSTFET and n-MOSFET under BTI stress	22
Figure III.3 Conventional charge pumping set-up	25
Figure III.4 Ultrafast charge pumping pulse waveform.	26
Figure III.5 Interface traps creation for p-MOSFETs for three different oxide thicknesses under similar gate voltage	27
Figure III.6 Interface traps density shift for constant gate voltage stress and for temperature ranging from 50°C to 200°C.	28
Figure III.7 Temperature dependence of measured NBTI time exponent obtained by conventional measurements with different time delays.	29
Figure III.8 Stress – recovery behavior of NBTI	31
Figure III.9 Threshold voltage shifts for hydrogen annealed and deuterium annealed devices	31
Figure III.10 ΔV_{th} at Vs=-60V for different applied magnetic fields at T=80°C	32
Figure III.11 Impact of magnetic field on ΔV_{th} recovery at Vs=-60V and T=80°C	33

Figure IV.1 The mechanism of Si-H bond breaking according to R-D model and reaction	37
Figure IV.2 Schematic representation of the R-D model principle in the context of Arrhenius behavior	38
Figure IV.3 The classical R-D model underlying mechanism representation. a) Hydrogen profile. b) Interface traps generation regimes.	40
Figure IV.4 The assumed triangular distribution of the released hydrogen atoms in the oxide.	41
Figure IV.5 The distribution profile of the released H^+ in the oxide.	43
Figure IV.6 Temperature dependence of measured NBTI time exponent.	46
Figure IV.7 Schematic representation of the dispersive transport of hydrogen species.	46
Figure IV.8. Schematic of the Reaction-Diffusion (RD) model during (a) stress and (b) recovery. The stochastic H2 hopping during recovery is illustrated	47
Figure IV.9 Two stage model principle. Stage one is based on the hole-trapping detrapping model for switching traps. Stage two illustrates a hydrogen transitions that results in the creation of an interface state.	49
Figure IV.10 Carrier capture and emission coefficients of an oxide trap at energy level ET	49
Figure V.2 NBTI model dynamics. Circles are stages of stress and rectangles are rate of transformation	57
Figure.V.3 Defects involved in NBTI degradation and their energy distribution with respect to silicon band gap	58
Figure V.4 – Time evolution of threshold shift for 1000 s of stress at – 1.5 V followed by 1000 s of recovery at 0 V	66
Figure V.5 – Threshold shift in a log-log scale. The extract power law time exponent is 0.26	67
Figure V.6 – NBTI degradation for different voltage stress at T = 200 °C	67
Figure V.7 – NBTI degradation for different temperatures at Vs = – 1.5 V	68

Chapter I

Introduction

Semiconductor devices used in microelectronics, photonics, and optoelectronics currently constitute the basic technologies of smartphones, tablets, PCs, GPS navigation systems, high definition flat screens, digital cameras, processing technologies that affect the luxury of our lives. Overall, microelectronic technology based on semiconductor devices and integrated circuits has changed our daily lives.

All of these technological advances have only been financially and physically possible thanks to the miniaturization of the basic components of integrated circuit (IC) chips. Integrated circuit (IC) chips are now much smaller and faster, and packaging is more efficient, reliable and cost-effective. In fact, it was the scaling of the device that led to the microelectronics revolution as described by Moore's law [1], which states that "Increasing the integration density by factor of two a year would minimize the cost per transistor".

Figure I.1 summarizes major milestones in the development of semiconductor electronics.

On guidance of Moore's law, the scaling of the MOSFET (specifically the gate length) continued without hindrance from 100 µm size to 100 nm. On reaching 100 nm (or the deep sub-micron channel length), maintaining the electrostatic integrity of the transistor became a major issue leading to serious challenges to scaling. Some of the major problems to MOSFET scaling in sub-100 nm channel length regime are:

1- Short channel effect (SE).
2- Drain induced barrier lowering (DIBL).
3- Increased off state current.

4- Increased gate leakage.
5- Poly gate depletion effects.
6- Source/Drain access resistance reduction.
7- High field mobility degradation.
8- Variability.

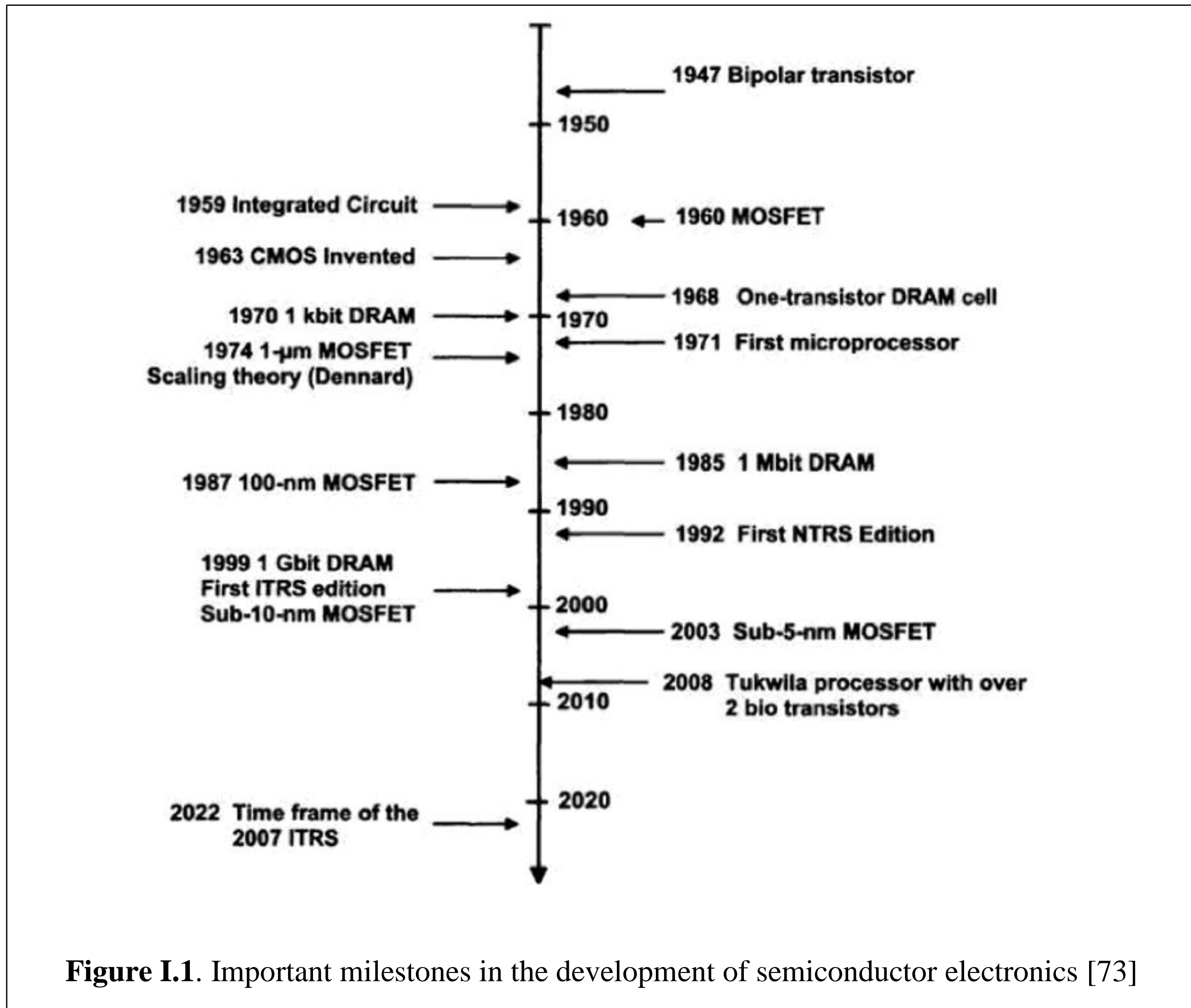

Figure I.1. Important milestones in the development of semiconductor electronics [73]

The history of the semiconductor industry has revealed that the miniaturization tendency has been constrained by the ability of the fabricated transistors to withstand the increasing operating stresses. The gate dielectric may indeed be the key structural element in the reliability of MOSFET transistor. It is the smallest dimensional element in a transistor and yet has to withstand the highest electric field. It must have low levels of fixed charge ($\sim 5 10^{10}\, cm^{-2}$) and interface states ($\sim 5 10^{10}\, cm^{-2}\, eV^{-1}$) and must remain reliable after years of high field stressing (~ 10 years) since it occupies a large fraction of the total chip area and thus can dominate yield.

The silicon dioxide (SiO_2) possesses those attributes to the extent that no other material does. The qualities of SiO_2 have made from it the mainstay of the industry for the past 40 years.

As the miniaturization has stepped into deep nanometer arena, major reliability issues arose. Some of them are Hot Electron degradation, Electromigration, Oxide Breakdown (TDDB), Bias Temperature Instability (BTI), Latchup and Soft errors. These problems have limited the miniaturization and pushed researchers to look up for new alternative material.

In the 1960s, one micrometer at that time was considered as the limit due to short-channel effects and optical problems in the manufacturing steps using lithography. During 1970s, the short channel effect was overpassed and 500 nm was considered to be the physical limit because of the increased resistance source/drain. The switch from buried channel to surface channel further boosted the miniaturization. At the end of 1970, the limit was 250 nm for reasons of leakage (tunneling current) through the gate oxide and dopant fluctuation in the channel. Once the problem of leakage current has been overcome, in the 1980s, 100 nm was considered the physical limit as many difficulties prevented the reduction of physical parameters of the Metal-Oxide-Semiconductor Field Effect Transistor (MOSFET). Finally, 10 nm has long been accepted as the physical limit for many reasons including that of the tunneling current between the source and the drain.

One of the most longstanding reliability problems that now is limiting the downscaling of the oxide is Negative Bias Temperature Instability (NBTI). It is a major reliability concern for modern complementary metal oxide silicon technology. It manifests itself as a shift in threshold voltage (V_{TH}) and a degradation in saturation drain–current ($I_{D,sat}$) in p-channel metal oxide silicon field effect transistors (pMOSFETs) subjected to negative gate bias at moderately elevated temperatures. It was observed as early as 1967 by Deal et al., but an apparently consistent explanation was only made much later in 1977 by Jeppson and Svensson, based the Reaction-Diffusion model.

In spite the fact that NBTI is heavily studied and many models have been proposed, no model can successfully explain all features of the BTI phenomenon and no consensus about the microscopic origin of the NBTI degradation.

The proposed models in the literature can be classified as follows [4-7]:

1. One component that is related to hydrogen instabilities in the oxide. The hydrogen behavior in the oxide is often modeled by Reaction-Diffusion (RD) model;
2. One component that is related to hole trapping/detrapping in the preexisting or stress-induced precursors;
3. Two independent components where the fast one is related to hole trapping/detrapping processes and the permanent one is due to hydrogen-related defects such as P_b-H and/or E'-H complexes;
4. Two independent components that result from generation and recovery of interface traps which are modeled by the RD model, together with hole trapping and detrapping in oxide defects;
5. Two independent components where the fast one is attributed to interface state passivation and the permanent one is ascribed to hole trapping in Deep-Level defects;
6. Two tightly coupled components where hole trapping in the oxide trigger E'-H complex formation by consuming P_b'-H and leaving a dangling Pb center be-hind.

With the advance in measuring techniques of NBTI, the assumption of one component is abundant and most relevant results ascribe NBTI to two components; one permanent and the other recoverable. The relation-ship between the two components and their microscopic origin are under heavy debate. In general, NBTI models proposed in the literature are trying to answer the following questions:

- **Q1:** What are the microscopic origins of the two components? And which of them is permanent (slow) or recoverable (fast)?
- **Q2:** What is the relation (correlation) between the two components: coupled (dependent) or decoupled (independent)?

In this work, I propose a new physical based model, which extends the two-stage model to ac-count the hydrogen diffusion in the oxide. In the context of the proposed model, the answer of the above-mentioned two questions is:

- The degradation is originated from P_b centers at the interface, E' centers in the oxide and E'-H complexes in the border of the Si-SiO_2 interface. The fast component is related

to E' center trapping/detrapping, whereas the slow component is shared between E'-H complex and P_b centers.

- The two components are coupled and decoupled at the same time. They are tightly coupled during stress where first E' centers are created which triggers the generation of P_b centers and the creation of E'-H complex. In contrast to the stress correlation, the degradation recovery is fairly decoupled and each of the three microscopic species created during stress recover independently to each other.

The ultimate goal of this thesis is to highlight the experimental foundation upon which the model is built and to make in evidence its mathematical derivation steps.

In this context, the thesis is structured as follows:

Chapter 1 (this chapter) is devoted to the general introduction.

Chapter 2 presents the theory of microscopic structure of the Silicon-Silicon Dioxide system. The different electrically active oxide defects at the Si/SiO_2 interface as well as in the oxide bulk are explained. A special attention is given to defects that are relevant for electronic device reliability. Based on these defects the macroscopic picture of proposed model will be given.

Chapter 3 outlines the theoretical background that serves as a foundation of our model. It focuses on the NBTI distinguishing it from other degradation mechanisms. Some techniques used in NBTI measurements are quoted highlighting their evolution from conventional Stress-Measurement-Stress (SMS) technique, known to underestimate the degradation because of its inevitable recovery, to ON-THE-FLY (OTF) method. This chapter ends out by studying NBTI features and signatures.

Chapter 4 gives an overview of common NBTI models. Two well-known models are explored; the first is a hydrogen-diffusion related model known as Reaction-Diffusion model. The second model is a hole-trapping and detrapping based model known as Two-Stage model.

My original contribution to the NBTI modeling is encapsulated in **chapter 5**. The proposed model is based the two-stage model and extends it by adding one of the most accepted feature of NBTI which is the hydrogen diffusion in the oxide. The proposed model is simulated using COMSOL Multiphysics.

Finlay conclusion and perspective will be highlighted in **chapter 6**.

Chapter II

Silicon dioxide and its defects

Silicon dioxide (SiO_2) has been playing a central role in most contemporary electronics and photonics technologies including fiber optics for communications and satellite data bus applications. It is a primordial ingredient of the oxides of 90% of all contemporary metal-oxide-semiconductor (MOS) based devices. For this reason, it is not a surprise that the SiO_2 has been one of the most studied materials in materials science. Actually, knowing the SiO_2 structure and defects a crucial step to layout the foundation upon which any reliable NBTI model will be built.

This chapter gives a brief introduction to the structure of the amorphous SiO_2 and also discusses the nature and properties of defects that have been encountered in these materials.

II.1 Amorphous SiO_2 structure

Most of the studies of SiO_2 comes from the study of the glass structure which the SiO_2 is a common fundamental constituent. Two models have been leading the scene to describe the structure of amorphous SiO_2, the continuous random network model first proposed by Zachariasen [2]) and the microcrystalline model of Randall [Reference , 3]. In the continuous random network model, the local structural unit (SiO_4 tetrahedron) remains unchanged, with each tetrahedron corner shared with another tetrahedron, as in the crystalline forms (figureII.1). However, the Si-O-Si bond angle will vary from one tetrahedron corner to another, yielding a "continuous random network". In the microcrystalline model, the SiO_2 is constructed from

microcrystallites of the various allotropic forms of crystalline SiO_2 or alternatively, sub-unit-cell-sized crystallites of one form of SiO_2. In the limit of small crystallites, the two models converge.

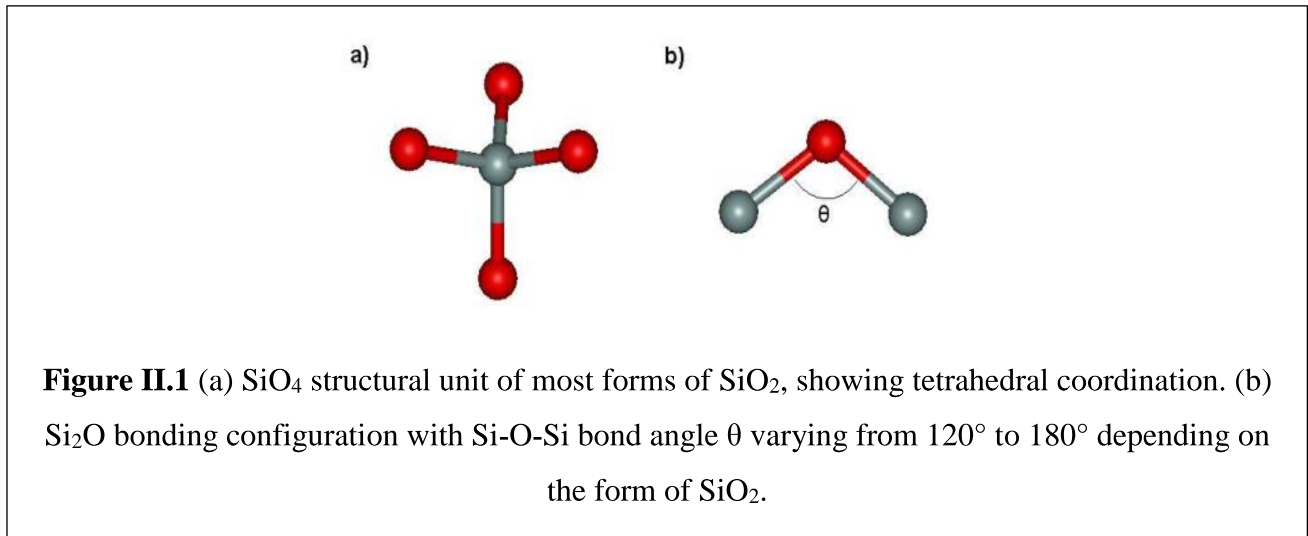

Figure II.1 (a) SiO_4 structural unit of most forms of SiO_2, showing tetrahedral coordination. (b) Si_2O bonding configuration with Si-O-Si bond angle θ varying from 120° to 180° depending on the form of SiO_2.

Experimental studies confirming these two models give Si-O to be 0.16 nm, O-O 0.262 nm, Si-Si 0.313 nm and bond angles vary from 120° to 180° [4] [5].

II.2 -Defects in Si/SiO_2 system

In crystal silicon dioxides (α-quartz), which are characterized by a long-range atomic order, a defect is any deviation from the long-range order. When it comes to amorphous materials (a-SiO_2), the concept of defect has no sharp definition as in crystals. However, amorphous SiO_2 is a network of Si-O chains and rings. This structural peculiarity is a result of the fact that the constituent atoms preserve their coordination and juxtaposition; that is., every Si atom is 4-fold coordinated and every O atom is 2-fold coordinated and Si atoms always connect to oxygens and vice versa. It is in these terms of disruptions and ordering one can define intrinsic defects in amorphous SiO_2 (figure II.2).

Defects that are relevant for electronic device reliability are those electrically active; i.e., those that can trap or exchange chares with the silicon substrate or the gate in MOS based devices.

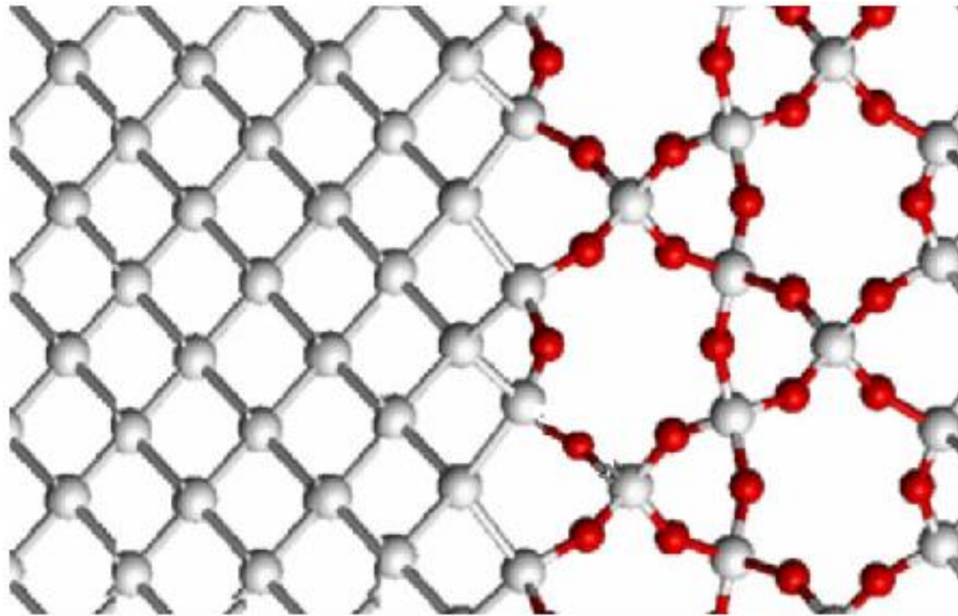

Figure II.2: Si/SiO_2 system atomic structure. Left: Ordered substrate Si. Right: Amorphic SiO_2 structure

In the following I will go through the most relevant electrically active defects.

II.3- Oxygen vacancy

In an ideal structure of SiO_2 Si has to be followed by an O and every O has to be followed by a Si. If an O atom is missing from a Si-O chain, the two neighboring Si atoms may undergo some relaxation and produce a (usually strained) Si-Si bond, or at least one of the silicon atoms may relax behind the plane of its three remaining oxygen neighbors and bind to one network oxygen or silicon atom (puckering) as shown in figure II.3.[6]

Calculations of the neutral oxygen vacancy using ab-initio and semi-empirical methods predict that the Si–Si bond length to be between 2.3 and 2.7 A. This bond length is close to the Si–Si distance in elemental silicon and strongly reduced with respect to the initial Si–Si distance of ≈3.2 A, reflecting the flexibility of the SiO_2 network and the strength of the Si–Si bond [7].

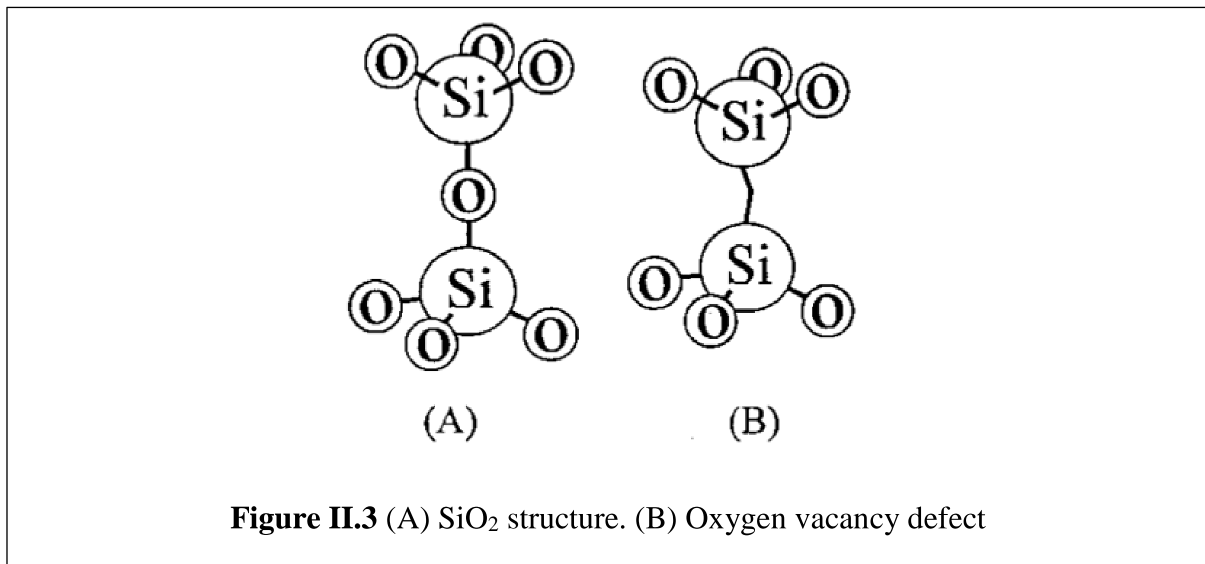

Figure II.3 (A) SiO_2 structure. (B) Oxygen vacancy defect

Oxygen vacancy is of great importance for defect studies as it represents the precursors of many electrically activated defects both positively and negatively charged [8]. The experimental observations suggest, however, that the electron capture cross section of the neutral electron traps is 2–3 orders of magnitude smaller than that of the hole. For this reason negative counter part of oxygen vacancy centers proved to be difficult to observe and identify experimentally [9].

II.4 E′ centers:

E'-center is the most studied defect in silica. It was discovered in 1956 by R.A. Weeks [10]. He used electron paramagnetic resonance (EPR) and identified a number of distinct resonances. He attributed these resonances to a single unpaired electron (therefore the name E', where E stands for electron and a prime suggesting a single electron).

The basic variant of E'-center defects correspond to a hole trapped in oxygen vacancy. . These defects are labeled by subscripts α, β, γ, δ to distinguish species characterized by different EPR parameters.

II.4.1 E'_δ center:

The oxygen vacancy can capture a hole. In this case a repulsion between the two electropositive silicon atoms occurs and results in a stretching but not in a breakage of the Si- Si bond. At this configuration the oxygen vacancy becomes E'_δ center. E'_δ center is the positively charged counterpart of the oxygen vacancy [11]. .

The missing negative charge within its bond causes a repulsion between the two electropositive silicon atoms and results in a stretching but not in a breakage of the Si- Si bond [12] .

An oxygen vacancy is neutral and after capturing a hole (or emitting an electron), it becomes positive; symbolized by $E_{0/+}$. In contrast, the E'$_\delta$ center is positive an after emitting a hole (capture of electron) it becomes neutral; symbolized by $E_{+/0}$.

The figure II.4 shows the defect levels of oxygen vacancies (neutral; E0/+) and its positive counterpart E'δ centers in amorphous SiO_2. Due to the amorphous nature of SiO_2, the defect levels E+/0 are spread widely over an energy range from - 1.5eV to + 0.4eV. By contrast in the case of the neutral oxygen vacancy the impact of the surrounding network can be neglected due to the strong Si- Si bond so that the distribution of E+/0 levels is narrow [13].

However, the E'$_\delta$ center is rarely found in device-grade gate oxides and is an unlikely candidate to provide substantial contribution to the NBT instabilities [7].

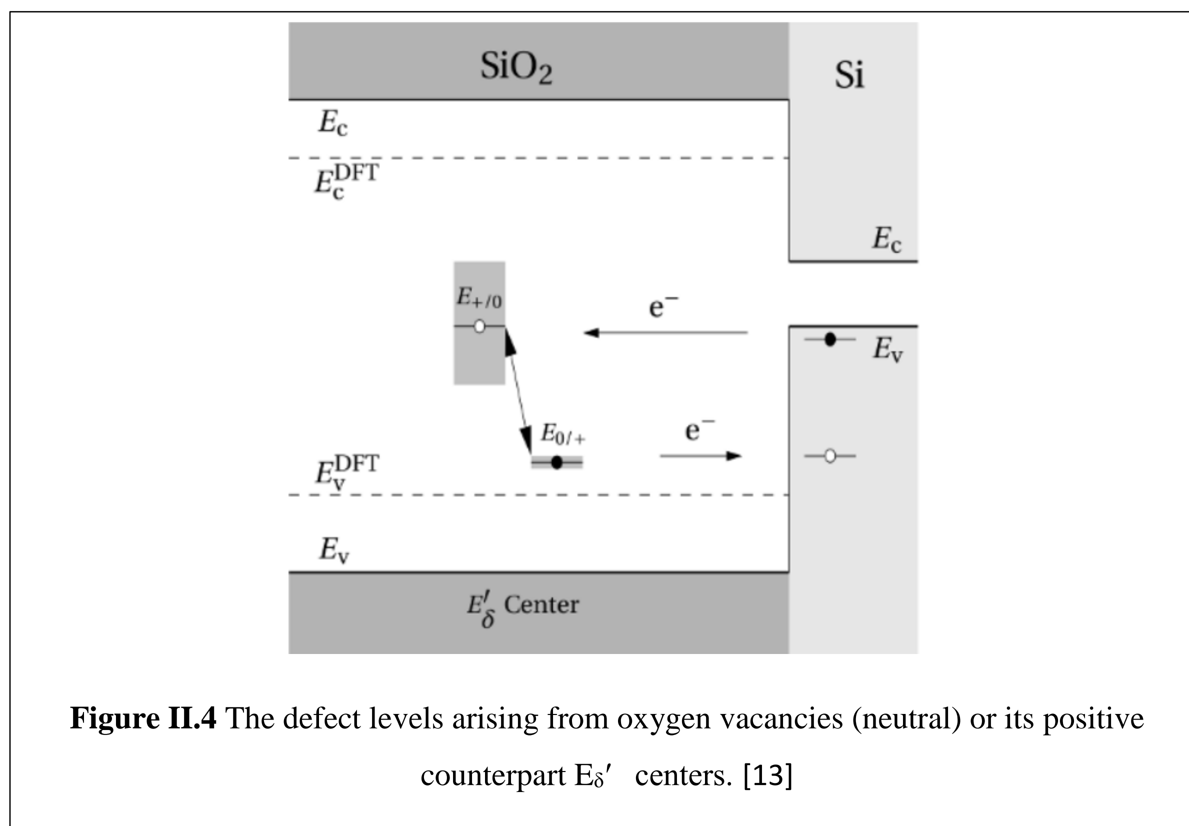

Figure II.4 The defect levels arising from oxygen vacancies (neutral) or its positive counterpart E_δ' centers. [13]

II.4.2 E'_γ Center

The existence of the E'_γ center as an additional metastable configuration of the oxygen vacancy has been confirmed and the name of E'_γ is given by Griscom et al because this center is relevant in oxide subjected to γ-ray radiation [11] [14].

Starting from the E'_δ center, one side of the defect undergoes a transformation called ‘puckered’. During this, the dimer bond is disrupted and the ‘puckered’ silicon atom moves through the plane defined by its three oxygen neighbors where this new configuration is stabilized via a back bond to a nearby oxygen atom.

This new configuration is stabilized via a weak bond of Si atom to a further nearby bridging O atom. On the other side of this defect, an unpaired electron in a dangling bond is left behind. The respective configuration is depicted in Figure II.5.

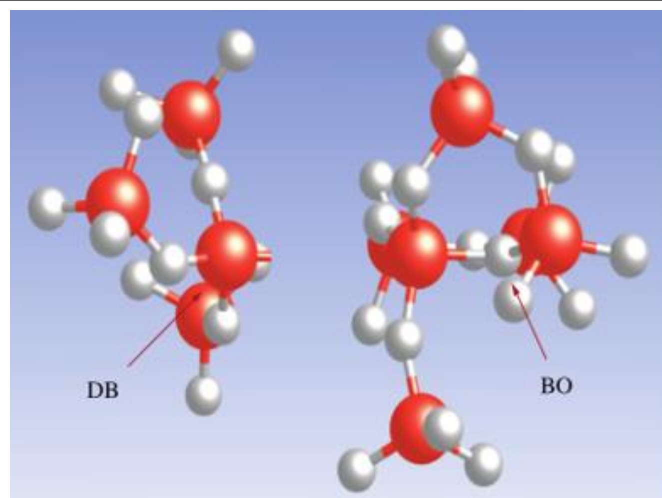

Figure II.5. Structure of an E’γ center. The silicon atom on the left-hand side carries an electron in the dangling bond (DB). The positively charged silicon atom on the right-hand side is bonded to the back oxygen (BO). This atomic arrangement is also referred to as the puckered configuration. [13]

In contrast to the Oxygen vacancy, the E’γ center exhibits only a small spread in its defect levels because the dangling bond on the left-hand side of Figure II.6 undergoes only.

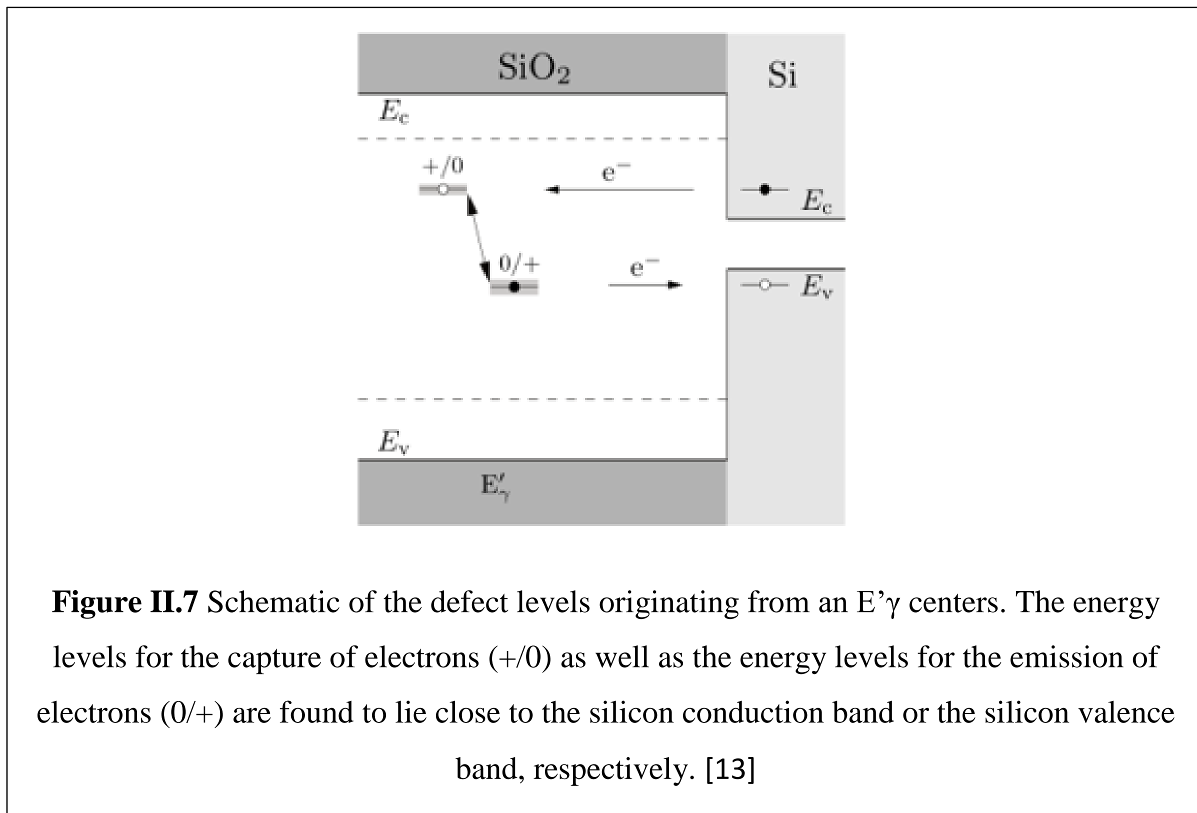

Figure II.7 Schematic of the defect levels originating from an E'γ centers. The energy levels for the capture of electrons (+/0) as well as the energy levels for the emission of electrons (0/+) are found to lie close to the silicon conduction band or the silicon valence band, respectively. [13]

II.5 P_b center:

Due to the difference in the chemical potential of silicon and oxygen atoms and the morphology of Si (crystalline) substrate and $Si0_2$ (amorphous) dielectric, the Si-$Si0_2$ interface often lacks the required smoothness. The unwanted roughness at the atomic scale is created by the lack of a homogeneous oxidation of the Si atoms at the substrate surface. The unoxidized Si atoms at the interface generally contain unsaturated valency, also called "dangling bonds"; this dangling bonds are P_b centers, or in other words, the P_b center is a trivalent Si defect at the $Si0_2$/Si interface (a silicon atom bonded to three other Si atoms) with an unpaired electron in an orbital pointing out to a vacancy. It is represented by the chemical formula •Si≡Si3 [6].

P_b centers are readily generated in thermal oxidation, but emerge in slightly different configurations depending on the crystallographic orientation of the Si substrate (Figure II.8). On Si (111), the P_b, center is a Si atom bonded to three other Si atoms at the interface with an unpaired electron in an orbital pointing out to a vacancy. For the technologically important Si (100), there are two types of Pb centers. One is the P_{b0} center which is essentially similar to the P_b variant on Si (111), but with two possible orientations. The other, called the P_{b1} center, is tentatively assigned to the •Si≡$Si_2$0 structure (i.e., a partially oxidized Pb, center). These interface defects introduce energy levels in the bandgap of SiO_2 and participate in the trapping and detrapping of carriers.

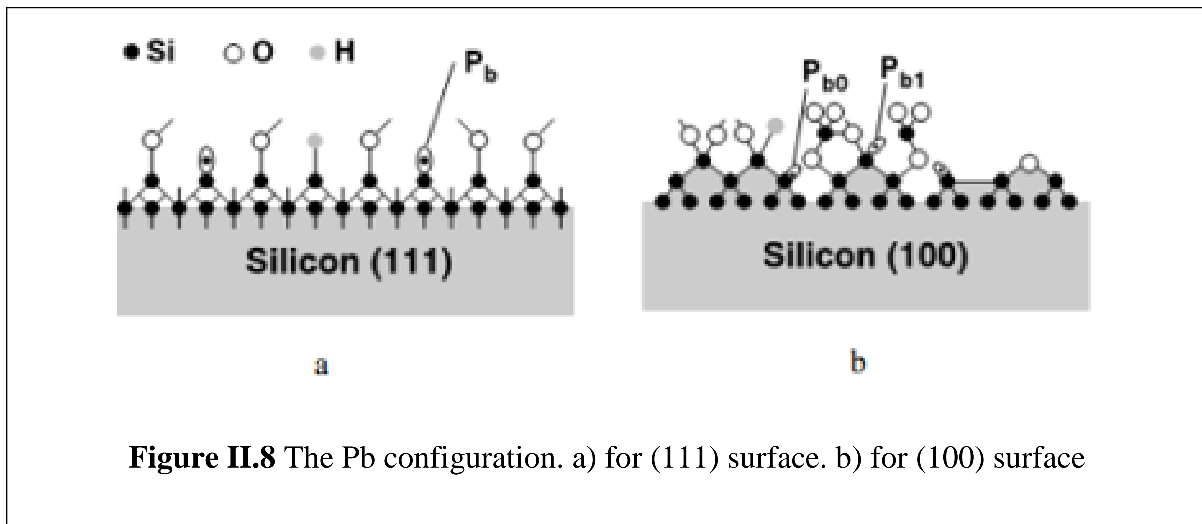

Figure II.8 The Pb configuration. a) for (111) surface. b) for (100) surface

The P_b defect is believed to be amphoteric, that is its charge condition can be positive, negative or neutral; figure II.9. The P_b centers whose energy level is in the lower part of the Si bandgap are donor interface defects. They are positively charged when empty and electrically neutral when occupied by an electron. The P_b centers whose energy level is in the upper part of the Si bandgap are acceptor like and is negatively charged when occupied by electron and electrically neutral when empty [15].

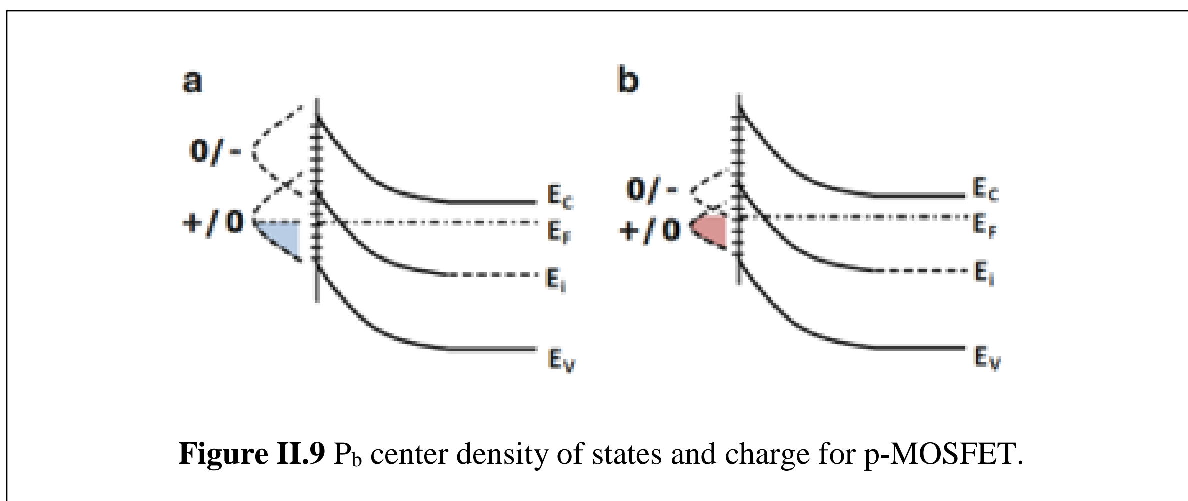

Figure II.9 P_b center density of states and charge for p-MOSFET.

II.6 Classification of charges in the oxide:

Ideal SiO_2 is neutral, and one of the direct consequences of defects is the creation of charges; positive or negative. Electrically active defects are classified depending on their location, electric and physical structure. [16] [17]. Figure II.10

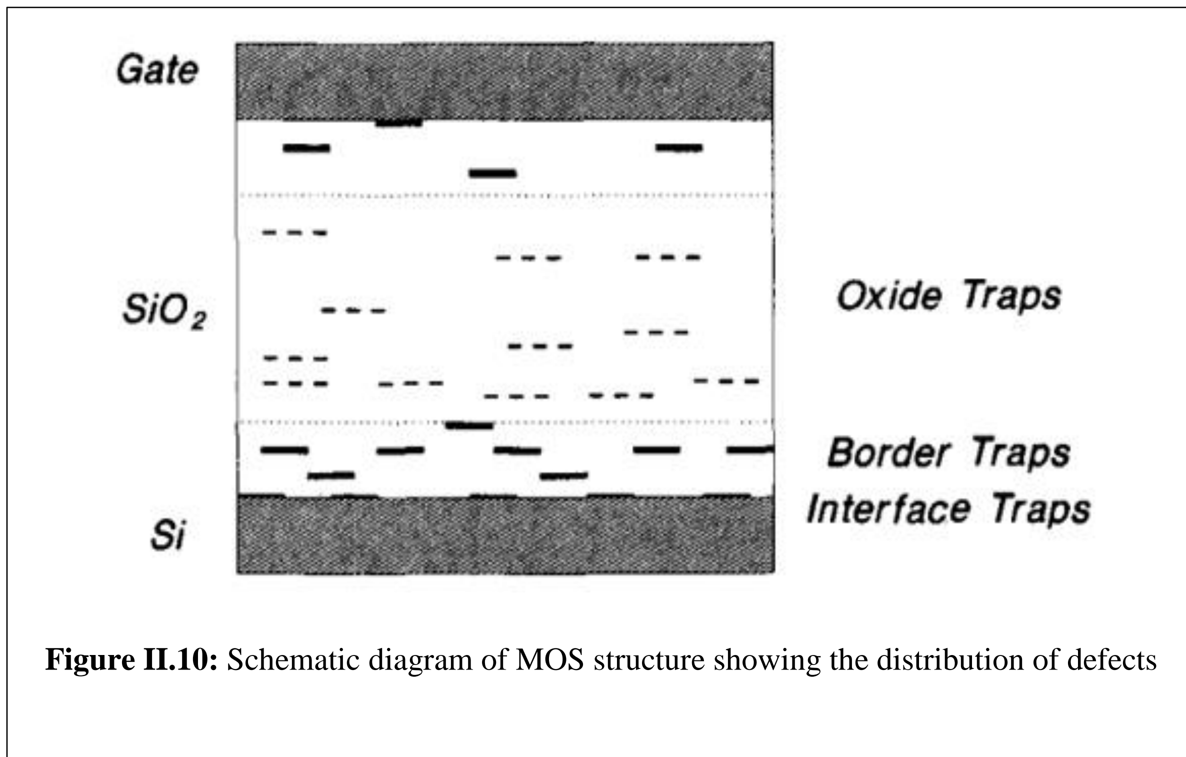

Figure II.10: Schematic diagram of MOS structure showing the distribution of defects

Often the terms trap and state are used interchangeably although they have specific meaning. The term trap empathies on lactation of the defect; one says interface trap and border trap to refer to the location with respect or the Si-SiO_2 interface. Whereas, the term state is used to refer the electrical behavior; one says fixed or switching state. Fixed charge can be positive, negative or even neutral. Switching state is charge that can exchange charge with silicon substrate. They can switch between positive and neutral state for donor-like traps and can switch between negative and neutral state for acceptor-like traps.

Depending on the location of the charge in the oxide they are classified into three groups:

1- Interface states: Interface traps are traps located at the interface between the oxide and the silicon substrate and the gate. Interface traps are by nature switching states because fixed interface states have not been observed, for this reason the term interface states and interface traps are used interchangeably without losing clarity.
2- Border traps: Border traps are those in the oxide and can exchange charge with the Si substrate or the gate on the window of the measurement time. The probability of an oxide trap to communicate with its surrounding layer (Si substrate or gate) decreases exponentially by the increasing the distance of the defect from the interface.
3- Oxide traps: Defects deep into the oxide further from the interface are called oxide traps.

Experimentally, it is very difficult, if it is not possible, to measure one group of charges without being contaminated by the others, because there is no clear border between them. This can lead to contradictory interpretations of the experimental results.

II.7 Hydrogen is SiO_2

Hydrogen plays an important role in MOSFETS as it is intentionally introduced to passivate defects (primarily Si dangling bonds) at the Si–SiO_2 interface. In fact, during oxidation SiO_2 growths over the Silicon substrate and passivates the Si interface states through binding of substrate Si to oxygen. But the passivation is incomplete such as an intolerable amount of native Si dangling bond-type interface states (1-5x10^{12} cm^{-1} in standard thermal Si/$Si0_2$) remain [18]. These were early recognized as a major obstacle in MOS device technology through their detrimental electrical activity as trapping and/or recombination centers [19]. It turns out that post thermal treatment in H_2 passivate the remaining dangling Si atom at the Si/SiO_2 interface. It is this hydrogen passivation that payed indispensable role in the MOS success story. Since then, hydrogen has long been known to be involved in many degradation processes, with much attention being devoted recently to bias-temperature instability (BTI) [20][7].

As we already noted, hydrogen is introduced intentionally during a post-metallization anneal in order to passivate dangling bonds at the Si–SiO_2 interface. Hydrogen introduced during gate oxidation and other post-oxidation annealing steps can also passivate defects in the oxide, e.g., non-bridging oxygens, oxygen vacancies, and so on. Figure II.11 shows three likely configurations of H in amorphous.

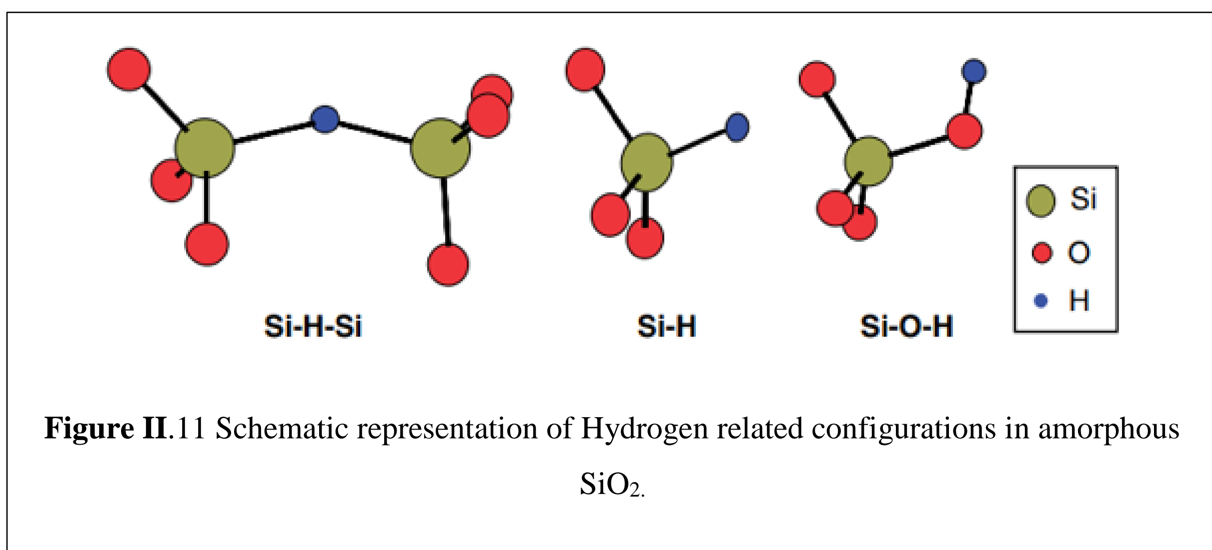

Figure II.11 Schematic representation of Hydrogen related configurations in amorphous SiO_2.

II.8 Positive charges in the oxide classification

Positive charges have been extensively studied as they behave in a complex way and different names have been used to capture its relevant behaviors. Zhang, J. F et all proposed a framework to name different types of positive chares that exists in oxides [21][22]. The distinction between positive charges in the oxide in the proposed framework is based on the different charging discharging properties of these positive charge.

In the context of this framework, positive charges in the oxide consist of three different types (Figure II.12):

1- as-grown hole traps (AHT),

2- cyclic positive charges (CPC), and

3- antineutralization positive charges (ANPC).

As-grown hole traps (AHT) are traps located far below the top edge of Si valence band (EV). They will not be charged under a relatively low oxide field. To fill AHT hot holes must be used. AHT can be created during fabrication process as well as during device life time. Possible mechanism of generation are cited in [21][22].

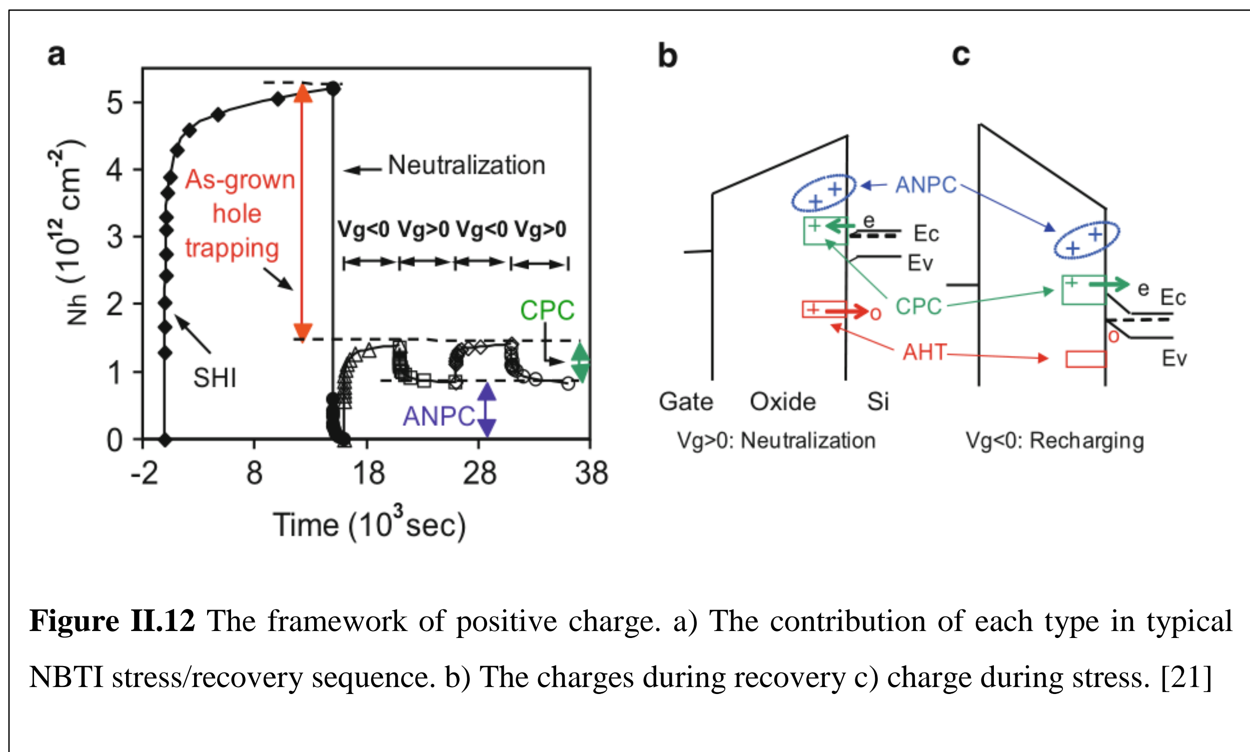

Figure II.12 The framework of positive charge. a) The contribution of each type in typical NBTI stress/recovery sequence. b) The charges during recovery c) charge during stress. [21]

After some period of stress, part of stress-generated positive charge can be repeatedly neutralized and recharged, so that they are called as cyclic positive charge (CPC). CPC has an energy level around Ec. Another of stress generated positive charge has energy level above Ec, so that their neutralization is more difficult than charging and they are referred to as antineutralization positive charge (ANPC).

II.9 Conclusion

The quality of the SiO_2 is a determing factor in the reliability of MOS based devices. Studying the structure of SiO_2 and the electrical and optical properties of its defects is a crucial step towards understanding the microscopic origin of any reliability problem in modern electronic devices. This chapter has reviewed the amorphous structure of SiO_2 and its defects, passing through hydrogen and its role in defect annealing and ending with the classification of defects and positive charge in SiO_2-based oxides. The positive charge classification is adopted to be used in our proposed model.

Chapter III

NBTI experimental features

Since their first commercialization, MOSFETs transistors have dominated the microelectronic industry. MOSFETs transistors have proved to be more reliable compared to their counterparts. To continue having leading place, their reliability should be improved in response to the industry ongoing strive for scaling and lower consumption. The scaling tendency along with the constant operation voltage adopted in the industry has increased the oxide field and the operating temperature therefore exacerbating the reliability of the device.

One of the most reliability critical issues is the Negative Bias Temperature Instability (NBTI). Its first symptoms were known since the beginning of the era of microelectronics by 1960. Since then, it became an important concern with the introduction of Silicon Oxynitride (SiON) gate dielectrics, and it continues to remain as an issue for High-K Metal Gate (HKMG) based planar MOSFETs and FinFETs [23].

In this chapter, a comprehensive literature review of the NBTI degradation will be presented together with methods of assessing and extracting of parameter related to NBTI. The main NBTI key features distinguishing it from other reliability issues are highlighted.

III.1. NBTI definition

Negative Bias Temperature Instability (NBTI) results in a gradual buildup of positive charges in the gate insulator of the transistor under the application of a negative stress gate bias and relatively elevated temperature, and causes a shift in parameters such as threshold voltage,

transconductance, subthreshold slope, linear and saturation drain current, gate-to-drain capacitance , etc. over time. The parametric shift partially recovers after the removal causing lower degradation for AC compared to DC stress [24].

From the basic characteristics of a simple pMOSFET, the threshold voltage is given by:

$$V_{th} = \Phi_{MS} - \frac{qN_{ot}}{C_{OX}} - \frac{qN_{it}}{C_{OX}} - 2\Phi_F - \frac{\left|\sqrt{4\varepsilon_s \Phi_F q N_D}\right|}{C_{OX}} \quad \text{(III.1)}$$

where :

- V_{th} : Threshold voltage;
- Φ_{MS} : Metal-Silicon potential;
- q: Elementary charge;
- N_{OT} : Oxide trap concentration;
- C_{OX} : Oxide capacitance;
- N_{it} : Interface trap concentration;
- Φ_F : Fermi potential;
- ε_s : Silicon permittivity;
- N_D : Substrate dopant concentration.

Assuming that the substrate doping (N_D) and the oxide capacitance are both constant the observed shift in threshold voltage (ΔV_{th}) must arise from a change in the numbers of oxide and/or the interface trapped charges (ΔN_{ot} and ΔN_{it}). Actually the majority of researchers have been agreed that oxide and interface traps are behind NBTI-induced degradation. However, the role of each type of defect is still actively debated [25].

Figure III.1 shows the impact of a NBTI stress on transistor. The solid line represents the fresh device (before NBTI stress), and the dashed line represents the device after stress. It is clearly shown a shift of threshold voltage and a reduction of mobility manifested by a decreasing of the transconductance. Generally, it is observed that after an NBTI stress:

- The transconductance gm decreases,
- The linear drain current Id,lin and saturation current Id,sat, decreases

- The channel mobility μeff, degrades,
- Subthreshold slope S, decreases
- The absolute value of the threshold voltage VT increases.

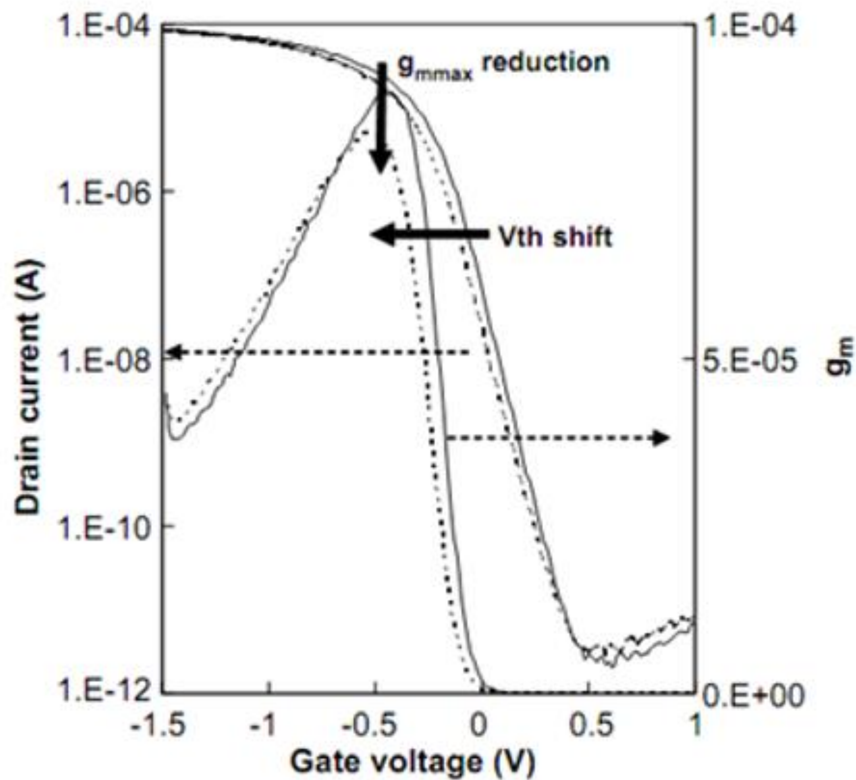

Figure III.1 ID - VG and gm -VG curves for fresh device (solid line) and after 10,000s of NBTI stress (dashed line) for a p-MOSFET.[30]

Actually the instability is observed in both configuration n-MOSFET and p-MOSFET and under positive or negative bias voltage as illustrated in Figure III. 2. But p-MOSFET under negative stress is experimentally shown to be the most vulnerable device to NBTI. This is way NBTI is a reliability phenomenon which is widely related to p-MOSFET transistors.

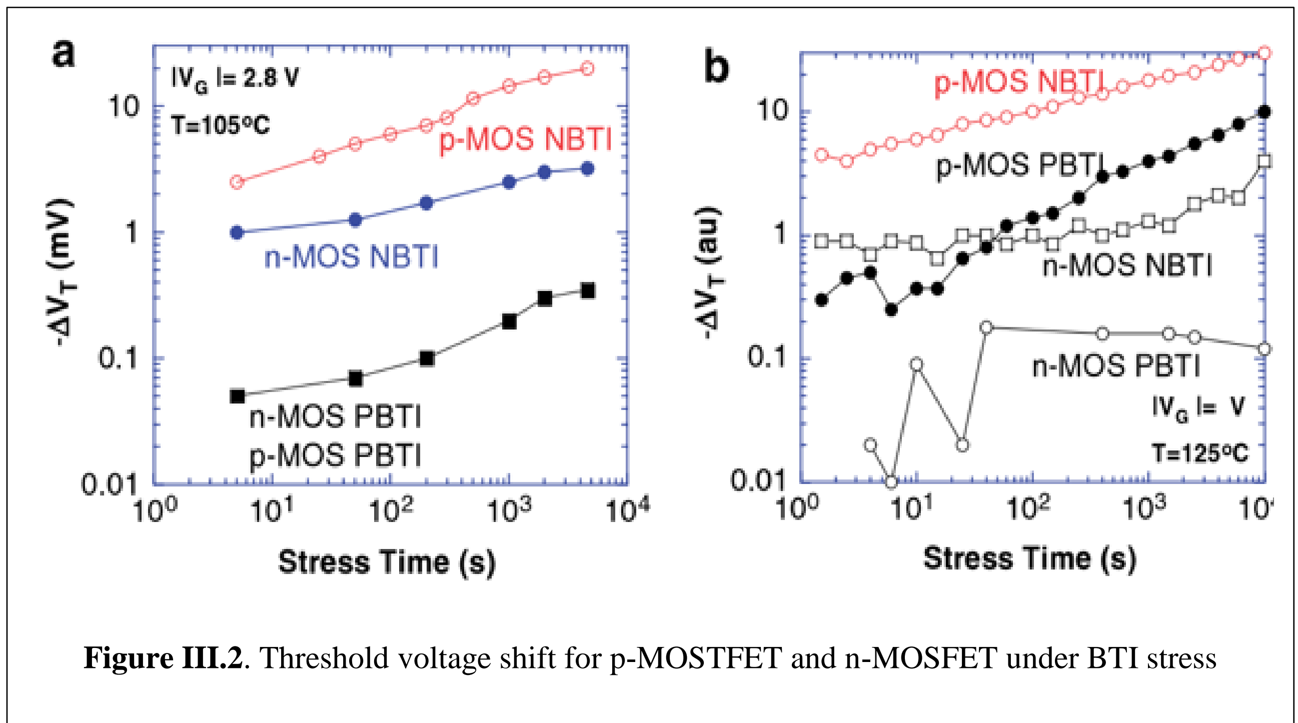

Figure III.2. Threshold voltage shift for p-MOSTFET and n-MOSFET under BTI stress

III.2. History of NBTI degradation:

The silicon based field effect transistor made its first steps in microelectronics field in the late 1960s. At that time, work focused mainly on the development of reliable thermally grown oxide layer to form the gate dielectric of the transistor. Extrinsic contamination (sodium ion Na^+, chloride ion Cl^-, potassium ion K^+) was very problematic and limiting the integration of MOS devices [26]. The diffusion through the oxide of these mobile ions is affected by the temperature and the electric field. One of the ways to reveal ionic contamination degree is to apply a negative bias under high temperature constrained. Under these conditions, the random behavior of mobile ions makes the electrical parameters unstable. These phenomena were called Negative Bias Temperature Instability or NBTI. Subsequently, this term continued to be used to describe any drift in electrical parameters during an NBT constraint. In 1967, the B.E. Deal team of the laboratory research and development at Fairchild Semiconductor in California in 1967 were the first to exhibit a creation of electrically active defects during NBT stress [27]. They realize that when a negative electric field is applied at high temperature, the appearance of a positive charge is not this time due to extrinsic contamination as in mobile ions, but is indeed due to an intrinsic origin in the device and strongly linked to the SiO2 / Si interface and the diffusion of silicon atom-based species.

The first widely accepted explanation of NBTI was made by K.O. Jeppson and M. Svensson published in 1977 [28]. They broke down the NBTI degradation mechanism into two parts: the first, dominant at a low electric field and limited by the diffusion phenomenon, and the second, appearing at a stronger electric field and controlled by the injection by tunnel effect of carriers in the hole trapping. They proposed the first version of what is called the "Reaction - Diffusion" (R&D) model. The R&D model has since been generalized and refined and even other models has been proposed to explain the experimental observation of the NBTI.

III.3. NBTI experiment set-up

Many methods, for the extraction of the threshold shift, have been used such as conventional stress measurement stress method (SMS) and On-The-Fly method (OTF).

In earlier time, threshold voltage shift was extracted using the stress measurement stress method. The stress is periodically interrupted and the ID-Vg characteristic is extracted by performing a gate voltage sweep while measuring the drain current at a slightly forward biased drain contact (linear regime). Vth shift is obtained by comparing the ID-Vg characteristic before stress with the ID-Vg characteristic obtained after stress. The fact that the stress is interrupted each time to measure Vth shift gives the method its name: stress measurement stress method (SMS).

The observation of post-stress recovery of NBTI [29](as will be discussed later in this chapter) has complicated the threshold voltage extraction. Since then, the attention of scientists shifted towards looking for new measurement set-up where the time of measurement can be reduced or even suppressed if possible.

A method called On-The-Fly measurement was developed. The transconductance gm, the drain current in the linear regime $I_{d,lin}$, and the threshold voltage shift ΔVT can be extracted while keeping the gate stress voltage nearly constant.

In the On-The-Fly measurement [30], the source and bulk contacts are grounded while the drain contact is slightly biased with typically −25mV. One first measures the pre-stress Vth (Vth0) by ID-VG sweep and drain current (ID0) at t0 (time-zero delay which is ≥ 1ms for the Slow-OTF and ~1µs for the Fast-OTF) [31]; then the stress at the gate contact is permanently applied and superimposed upon pulses which are small compared to the stress voltage. The transconductance gm of the transistor, which is defined as the change in drain current as a result of a change of gate voltage, can then be extracted as:

$$g_m = \frac{\partial I_{d,lin}}{\partial V_g} = -\frac{\partial I_{d,lin}}{\partial V_{th}} \tag{III.2}$$

From this relation ΔI_D is obtained. The threshold voltage shift can then be extracted using [13]:

$$\Delta V_{th} = \left| \frac{(V_G - V_{th0})\Delta I_D}{I_{D0}} \right| \tag{III.3}$$

It is important to know that the measured I_{D0} is assumed to be the "degradation-free" I_D, based upon which subsequent I_D shifts are calculated. Due to a finite delay before I_{D0} measurement can be made following the application of the gate stress voltage, degradation may already have occurred, resulting in an underestimated degradation-free I_{D0}. This underestimation affects the extracted V_{th} shift especially for early time of the stress. The smaller time-zero (t_0) is the more accurate data are.

To determine the interface state density and its distribution in the band gap, several techniques have been proposed such as the deep-level transient-spectroscopy technique (DLTS), the 1/f noise and the charge pumping method (CP) [32]. CP method is widely used to extract the interface state density in a transistor because of its capability for measurement on small area MOSFET devices. In the context of NBTI, modified CP methods were developed to minimize the time of measurement to prevent the recovery of NBTI [Reference , 33].

In a conventional CP method the stress is off during the measurement. The source and drain are tied together and weakly reverse-biased (Figure III3) [34]. The gate is driven by a pulse generator from strong inversion to accumulation. The substrate is grounded through a Pico-ammeter to measure the charge pumping current.

The CP current is given by [32]:

$$I_{CP} = \overline{D_{id}} 2qfA_G k_B TLn(v_{th} n_i \sqrt{\sigma_e \sigma_{th}} \sqrt{t_{em,e} t_{em,h}} \tag{III.4}$$

where:

$$t_{em,e} = \frac{|V_{FB} - V_T|}{\Delta V_A} t_f \tag{III.5}$$

$$t_{em,h} = \frac{|V_{FB} - V_T|}{\Delta V_A} t_r \tag{III.6}$$

where

- D_{it}: the mean density of interface states,
- f: the pulse frequency
- A_G: the gate cross-sectional area
- k_B: Boltzmann constant
- v_{th}: thermal velocity
- σ_e, σ_h : electron and hole capture cross section of a trap respectively

Since the stress in the conventional method is interrupted during measurement and NBTI generated interface traps are believed to recover, the accurate interface trap density is hardly obtained. Many researchers attempt to developed On-The-Fly CP. Ang et al. [33] have developed an ultrafast CP method. At a given interval, a series of positive 100 ns gate pulses of amplitude |Vgs| + 1 V are injected, at periods of 10 µs each. The pulses switched the device between inversion and accumulation repeatedly, inducing a dc surface recombination current measured, with sub-pA resolution, at the source/drain terminal. The pulse waveform is presented in Figure III.4.

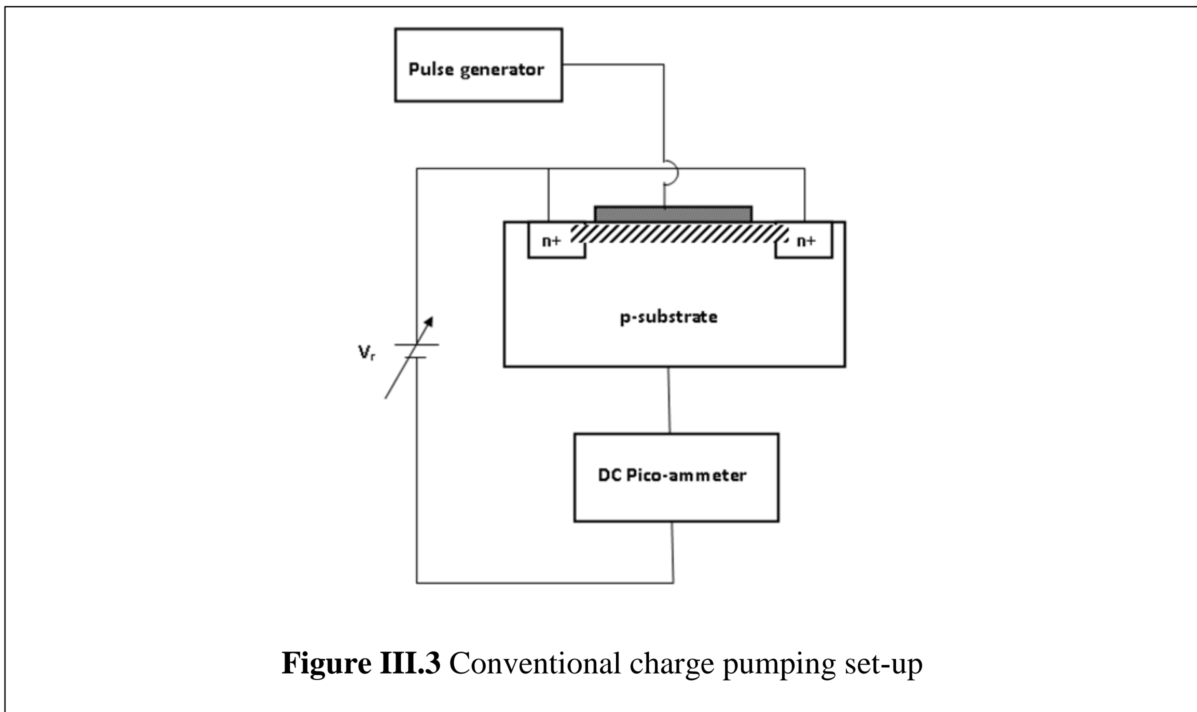

Figure III.3 Conventional charge pumping set-up

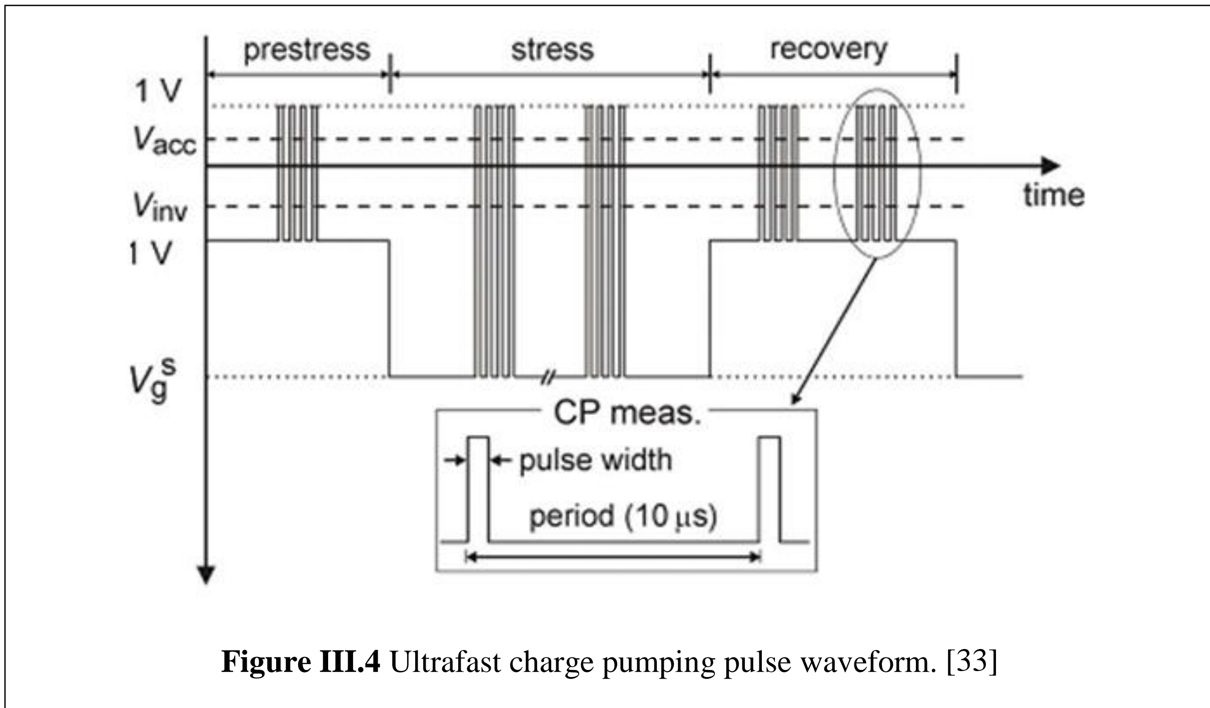

Figure III.4 Ultrafast charge pumping pulse waveform. [33]

The charge pumping current is believed to be solely due to interface traps contribution. However Ang et al. [35] give evidence that the CP current is contaminated by the contribution of interfacial oxide traps that participate to the CP recombination process. They attribute the recoverable part of the I_{cp} current to the tunneling of hole from Si substrate to the interfacial oxide traps and the permanent component of I_{cp} to the interface traps contribution. Ang et al. question the accuracy of the CP method for the determination of interface state density [35] [36][37][38]

III.4. Experimental features of NBTI:

NBTI features are the experimental observations related to the degradation behavior that distinguish it from the other reliability wearout mechanisms. Any model of NBTI could be qualified as reliable only if it succeeds in explaining these features. In the following I give some relevant features.

III.4.1 Charge Transport Independence

Unlike the other wearout mechanisms such as hot-carrier injection, oxide breakdown or electromigration where the charge transport activates directly or indirectly the degradation, NBTI is confirmed to be independent from carrier transport in the channel because NBTI degradation is observed even if both source and drain are grounded.

III.4.2 Channel Hole Concentration

It is recognized that the presence of holes is essential for NBTI degradation to occur, but whether their concentration has any impact on the NBTI degradation or not is controversial. Huard et al. and many other scientists believe that NBTI does not depend on the channel-hole concentration [39][30][29][40] However Alam and his group [41] [42][43] always treat NBTI degradation as a hole-concentration dependent phenomenon.

III.4.3 Oxide Field Dependence

It is widely accepted by the NBTI scientist community that NBTI is an oxide field dependent phenomenon rather than gate voltage dependent. Huard et al. [30] investigated the interface traps creation under NBTI degradation for different gate oxide thicknesses, ranging from 2.1 nm to 10 nm-thick while keeping the gate voltage constant.

When the oxide field is increased, the electrical parameters show a clear increase of their degradation (Figure III.5). These results demonstrate the importance of the oxide field.

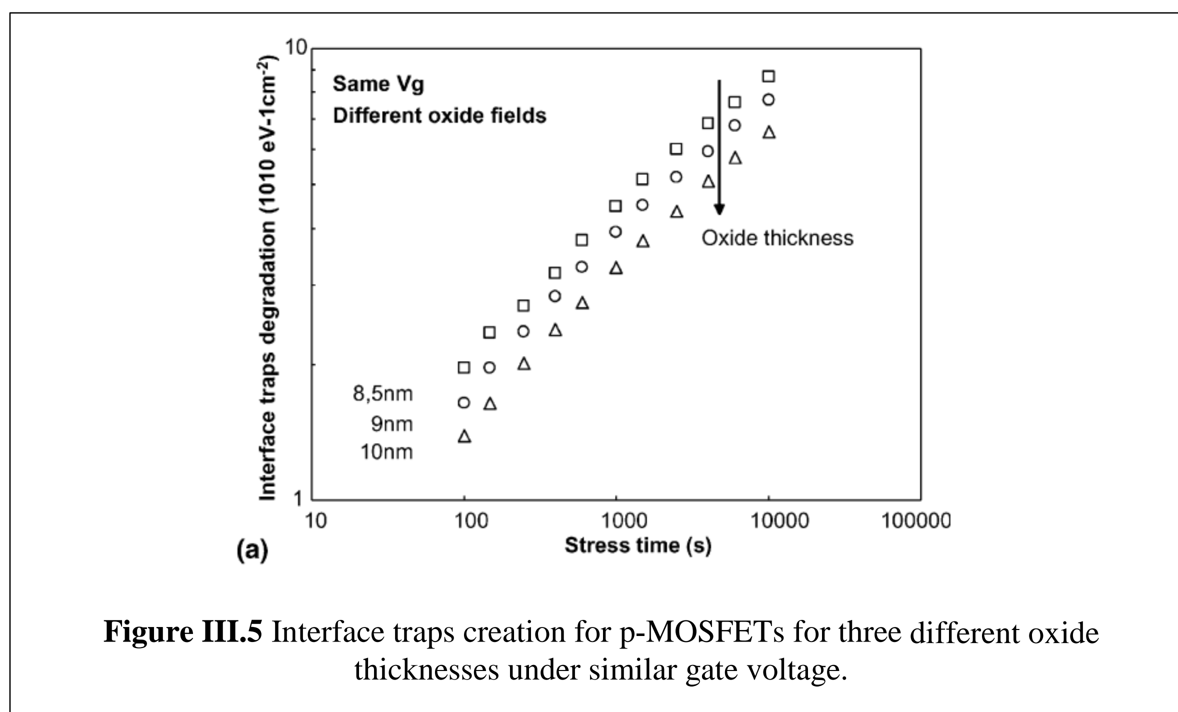

Figure III.5 Interface traps creation for p-MOSFETs for three different oxide thicknesses under similar gate voltage.

When the oxide field is increased, the electrical parameters show a clear increase of their degradation (Figure III.5). These results demonstrate the importance of the oxide field.

The results obtained by Huard et al. are consistent with the results of reference [40] which demonstrated that the oxide field is the driving force of the interface traps creation during

NBTI degradation.

The actual gate oxide field dependence of the NBTI damage is still a source of very active research. At this point two empirical models have being adopted [43]:

- Exponential model:
- power-law model

III.4.4 Temperature Dependence

Besides the importance of the oxide field, the NBTI degradation is also activated by temperature. Figure III.6 shows the effect of the temperature on the interface state density.

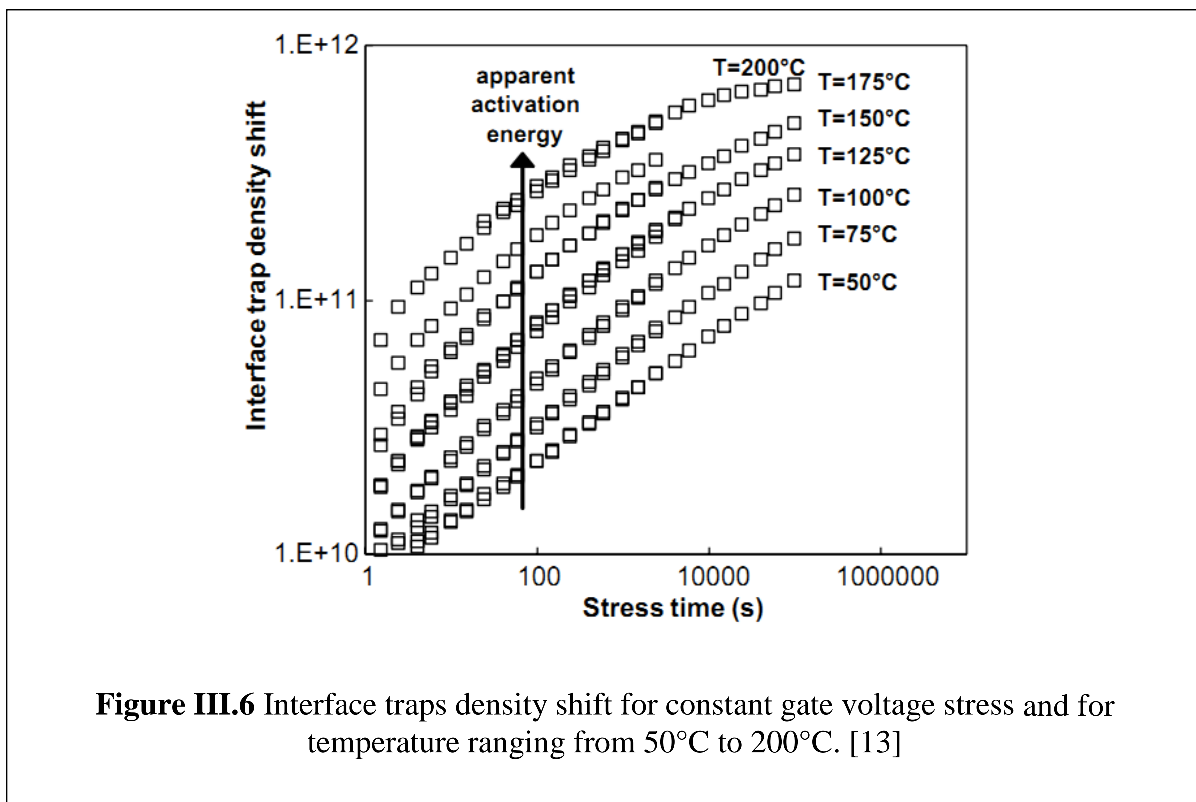

Figure III.6 Interface traps density shift for constant gate voltage stress and for temperature ranging from 50°C to 200°C. [13]

The NBTI temperature dependence is often modeled to follow Arrhenius' law $\exp(\frac{-E_a}{KT})$, with activation energy Ea. However, very different values are measured for the activation energy. An activating energy of 0,12 - 0,15 is often given [39].

Many reported data show that the power law exponent increases with temperature [30][44]. This has led some scientists to argue a non-Arrhenius's law.

However, there are other researchers who stand behind the Arrhenius-like behavior attributing the apparent dependence between the time exponent and the temperature to a measurement artifact [42].

Alam et al. [42] explains the temperature dependence of the time exponent by the inherent measurement delay in the classical measurements. Such delays lead to significant error in determining the true NBTI exponents (see Figure III.7) and therefore any temperature-dependent variation of these parameters cannot be used to reach specific conclusions regarding the mechanics of NBTI degradation. Once the ‘‘zero-delay’’, on-the-fly measurements are used, the temperature dependent degradation curves becomes parallel to each other confirming the Arrhenius like behavior.

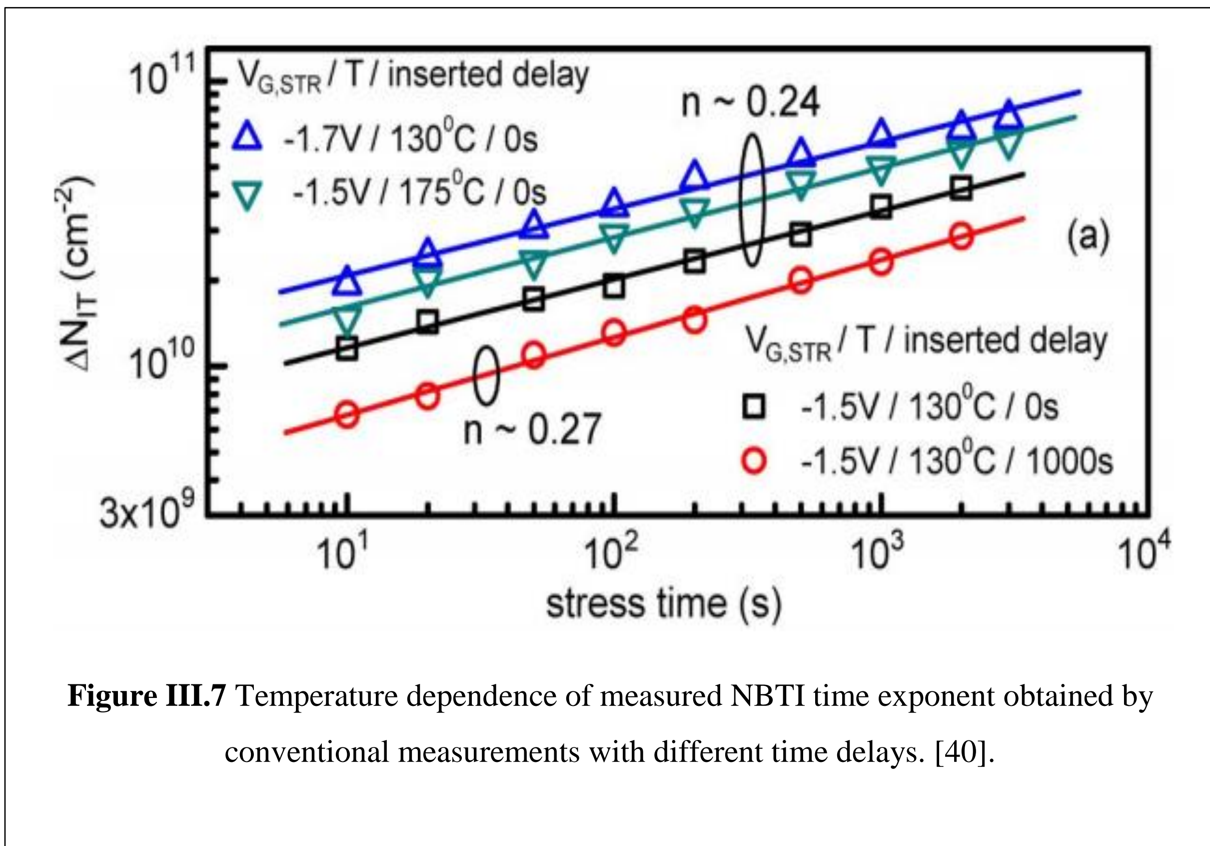

Figure III.7 Temperature dependence of measured NBTI time exponent obtained by conventional measurements with different time delays. [40].

III.4.5. Time Dependence

One of the most important features of NBTI is the slope of the time dependence of the threshold shift when plotted in a log-log scale. The value of this slope called the time exponent (n).

A time dependence of NBTI degradation is clearly observed since as long as the stress lasts more defects are created. It is widely accepted that NBTI follows a power law with different values of the time exponent as reported in the literature depending on the authors. A value of 0.25 was often given in early experiments, but values less than 0.25 have been also reported [43].

The time exponent n is very sensitive to the measurement time. Varghese et al. show that n = 0.14 for ‘‘no delay’’ measurements and n > 0.14 when there is a delay between stress and measurement. For nitrided oxide n can be as small as 0.10 [39].
Some researchers claim saturation of the degradation i.e. decreasing of the time exponent at latter stage. Again this is explained by the delay inserted during the measurement [42].

It is important to emphasize that caution must be exercised when comparing NBTI time evolution data with different experimental setups and different stressing and testing procedures. These observations may be inconsistent and lead to wrong insights on the physics of the NBTI damage and possible NBTI modeling.

III.4.6 Recovery of NBTI

Many experimental studies have reported generation and partial recovery of interface traps (ΔNIT) during and after NBTI stress, using Charge Pumping [29], [29], [45], Direct-Current IV (DCIV) [46], Low Voltage Stress Induced Leakage Current (LV-SILC) [47] and subthreshold slope (ΔS) [48] techniques.

Rangan et al. [49] were the first to explore the recovery effect using the uninterrupted stress technique. They showed that the recovery mechanism is temperature activated. A device subject to NBTI at room temperature or below will recover nearly to its original state; while a device stressed at a higher temperature displays less recovery.

Recent reports claim logarithmic time (log t) dependence of NBTI recovery based on the ultrafast measurement [50]. Also the recovery of NBTI is reported to be enhanced when it recovers under positive voltage.

III.4.7 Hydrogen dependence

While the exact nature of the complex NBTI mechanism is still unknown, it is widely accepted that interface traps are generated by breaking of hydrogen-passivated silicon bonds at the interface and subsequent diffusion of hydrogen [24].

Experiments demonstrate that NBTI is an activated process with activation energies of 0.12–0.15 eV [9–16]. Replacing hydrogen with deuterium during interface passivation reduces NBTI [10].

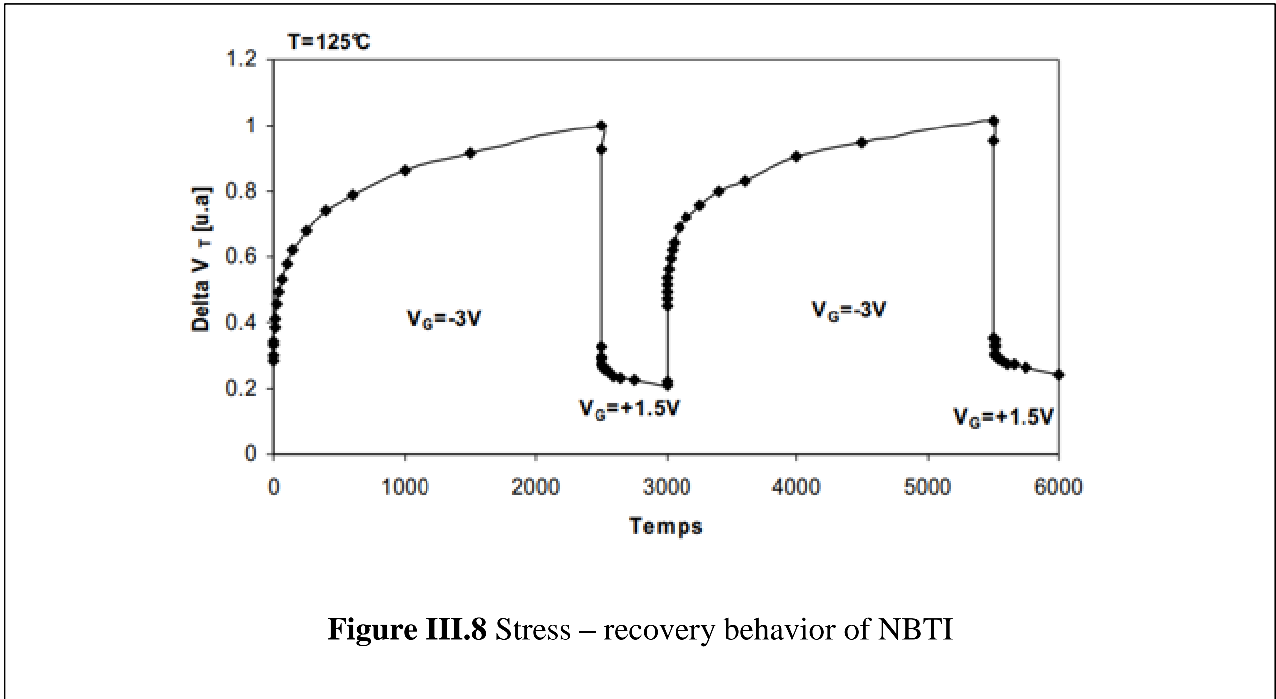

Figure III.8 Stress – recovery behavior of NBTI

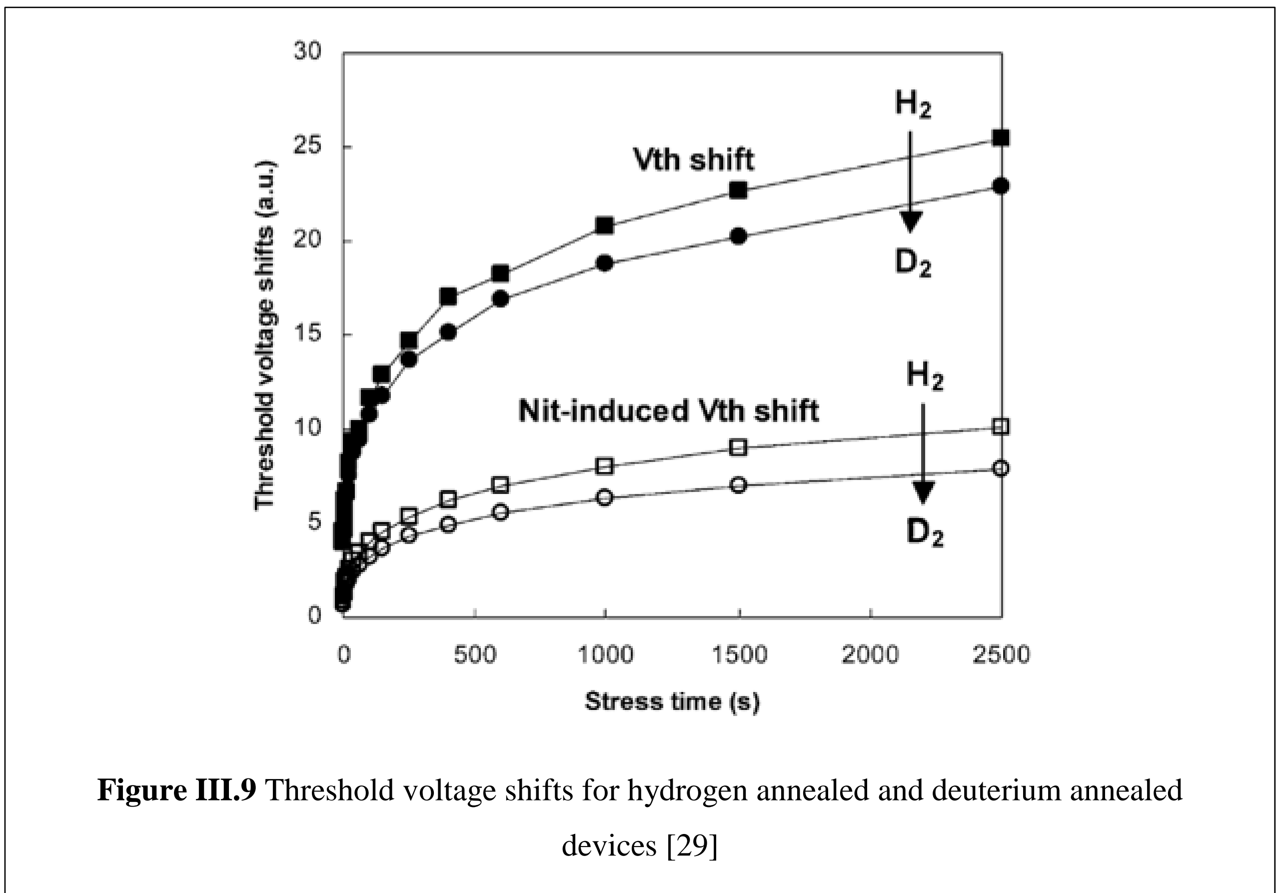

Figure III.9 Threshold voltage shifts for hydrogen annealed and deuterium annealed devices [29]

III.4.8 Magnetic field dependence

In a recent study conducted in the Centre de Développement des Technologies Avancées in Alegria (CDTA) [51], experimental evidences have been reported on the impact of applied a low magnetic field (B<100 Gauss) during negative bias temperature instability (NBTI) stress and recovery, on commercial power double diffused MOS transistor (VDMOS).

It is shown that that both interface (ΔN_{it}) and oxide trap (ΔN_{ot}) induced by NBTI stress decrease by applied magnetic field (figure III.10). This decrease is more pronounced as the magnetic field is high. In addition, the recovery of NBTI induced threshold voltage shift (ΔV_{th}) is relatively important with applied magnetic field figure III.11).

One explanation of decreased ΔV_{th} under magnetic field is diminishing of the contribution of paramagnetic defects (P_b center at the interface and E' center in the oxide) to the degradation under the effect of a magnetic field. The application of a magnetic field allows the orientation (polarization) of the unpaired electrons of paramagnetic defects and free electrons of the conduction band of the substrate (silicon). This reduces the trapping of electrons by the paramagnetic traps, according to the Pauli exclusion theorem which stipulates that the electrons cannot be in the same location (same energy state) in the same quantum state [52].

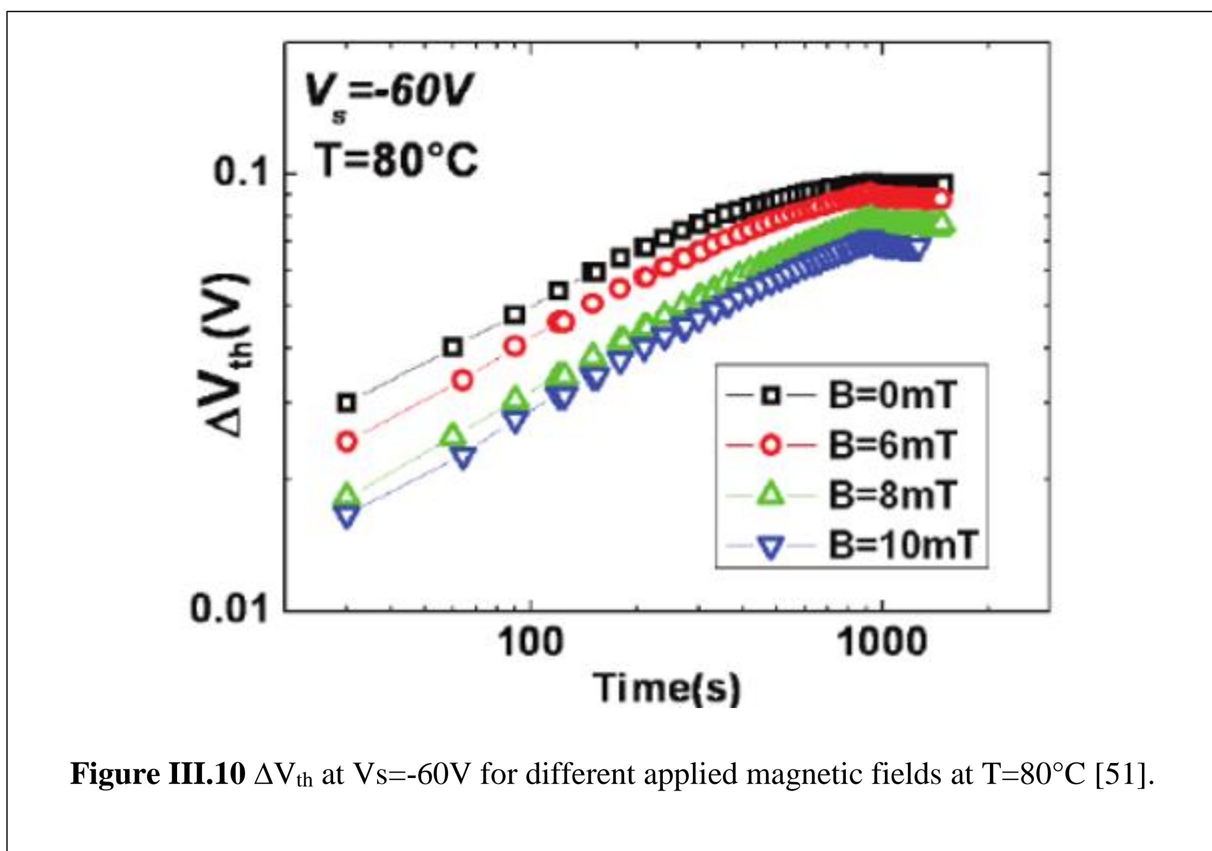

Figure III.10 ΔV_{th} at Vs=-60V for different applied magnetic fields at T=80°C [51].

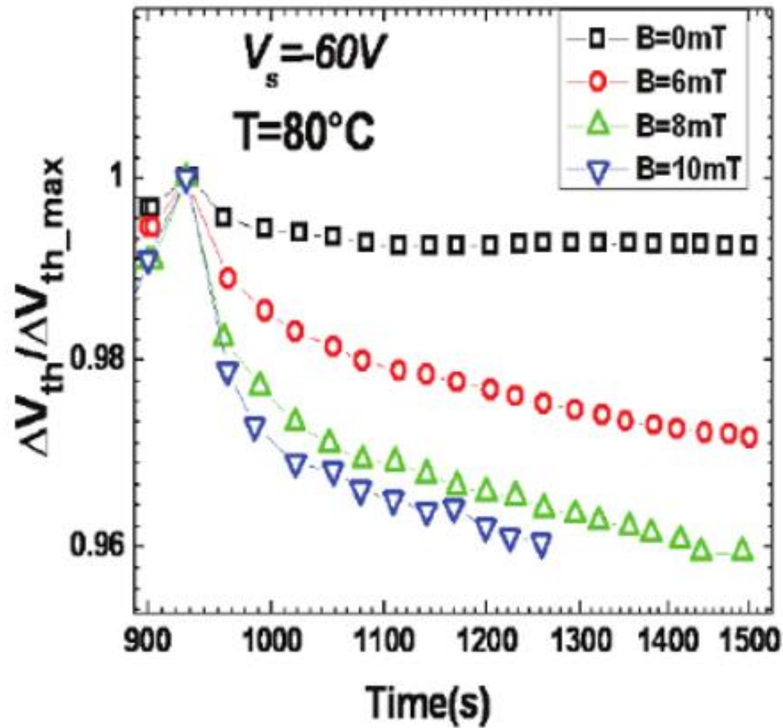

Figure III.11 Impact of magnetic field on ΔV_{th} recovery at Vs=-60V and T=80°C [51].

III.5 Conclusion

NBTI is one of the long-standing reliability issues in microelectronics. It is characterized by the shift of the most critical parameters of a pMOSFET transistor under negative bias and at a relatively high temperature. In this chapter, we have looked at the most common feature of NBTI that sets it apart from other reliability issues. No NBTI model can be described as comprehensive unless it consistently explains the above observations in a common framework. The goal of this paper is to develop such a comprehensive framework by generalizing the classical reaction–diffusion (R–D) model for NIT generation. This would allow us to identify the roles of hole density, hydrogen diffusion, oxide thickness, and interface quality that affect NBTI reliability.

Chapter IV

NBTI Modelling

The NBTI physical mechanism has remained a subject of great debate, and several explanations of the underlying mechanism behind NBTI and modeling attempts have been given over the years to explain the experimentally observed data. The earliest one is the Reaction Diffusion model first proposed by Jeppson and Svensson [42] thirty years ago and which has been continuously refined since then. Although the Reaction-Diffusion model is able to explain many experimentally observed characteristics of NBTI, the microscopic details are still not well understood. Recently, various alternative models have been put forward contradicting the standard reaction-diffusion model.

The proposed models in the literature can be classified into two broad categories:

- Hydrogen-diffusion based models
- Hole-trapping detrapping based models

In this chapter, I will explore an example of each category. The Reaction-Diffusion model is the well-known hydrogen-diffusion based. I will study the model from the earliest (classical) model proposed by Jeppson et al. and ending by highlighting some refinements introduced to the model to meet the experimentally observed behaviors that the model failed to predict.

For the hole-trapping detrapping based model, the two-stage model proposed by Grasser [50] is chosen and discussed.

IV.1 Hydrogen-diffusion based models

The observed increase of the interface trap density during NBTI stress and the role of hydrogen in the passivation of interface traps during the annealing process have led to the conclusion that NBTI is a hydrogen related phenomenon. The substitution of hydrogen by deuterium which is shown to attenuate NBTI degradation [53] is another proof of hydrogen importance for NBTI. For this reason the Reaction-Diffusion RD model has been proposed and it is accepted to be one of the best models describing the mechanism of generation of defects at the interface SiO_2/Si.

NBTI, in the context of this model, is regarded to be due to the depassivation and passivation of Si-H (reaction regime) and the behavior of the released hydrogen inside the SiO_2 (diffusion regime).

This "conventional" RD model suggests depassivation of H passivated defects at the Si/SiO2 interface, and subsequent diffusion of Hydrogen (as atomic H or molecular H2, after dimerization of H into H2) during stress, and the reverse processes during recovery after stress. It was also suggested, that the released H atoms (after depassivation) can diffuse and react with bulk H passivated defects to simultaneously generate interface traps and positive fixed gate insulator charges during stress. The degradation passes through the following phases:

IV.1.1 Reaction Phase

This phase starts just after the application of the stress. The interface traps are generated at the Si-SiO_2 interface. The microscopic mechanism behind the interface trap generation is not clear. The following table summarizes some suggestions:

Figure IV.1 illustrates the mechanism of reaction 5 in table IV.1. A channel hole can tunnel to a Si-H bond during inversion of the p-MOSFET and takes one electron from the covalent bonding thus weakening the Si-H bonds. The hydrogen now can easily be detached from the Si atom and diffuses away leaving a positively charged interface trap behind.

Reaction	Equation
1	$Si_3 - Si - H + H_2O \leftrightarrow Si_3 \equiv Si\bullet + H_3O^+$
2	$Si_3 - Si - H + h^+ \leftrightarrow Si_3 \equiv Si\bullet + H^+$
3	$Si_3 - Si - H + h^+ \leftrightarrow Si_3 \equiv Si^+\bullet + \frac{1}{2}H_2$
4	$Si_3 - Si - H + h^+ \leftrightarrow Si_3 \equiv Si^+\bullet + H^0$
5	$Si_3 - Si - H + H^+(\text{from substrate}) \leftrightarrow Si_3 \equiv Si^+\bullet + H_2$

Table IV.1 Proposed reactions of the interface trap generation [74]

The R–D model describes the rate of generation of interface traps by following equation:

$$\frac{dN_{it}(t)}{dt} = k_f(N_0 - N_{it}) - k_r N_{it} N_H \qquad x = 0 \qquad \text{(IV.1)}$$

Where

- x = 0 denotes the Si–SiO2 interface and x > 0 is (in the oxide) towards the gate,
- Nit is the number of interface traps at any given instant,
- N0 is the initial number of unbroken Si–H bonds;
- NH is the hydrogen concentration,
- kf is the oxide field dependent forward dissociation rate constant,
- kr is the annealing rate constant.

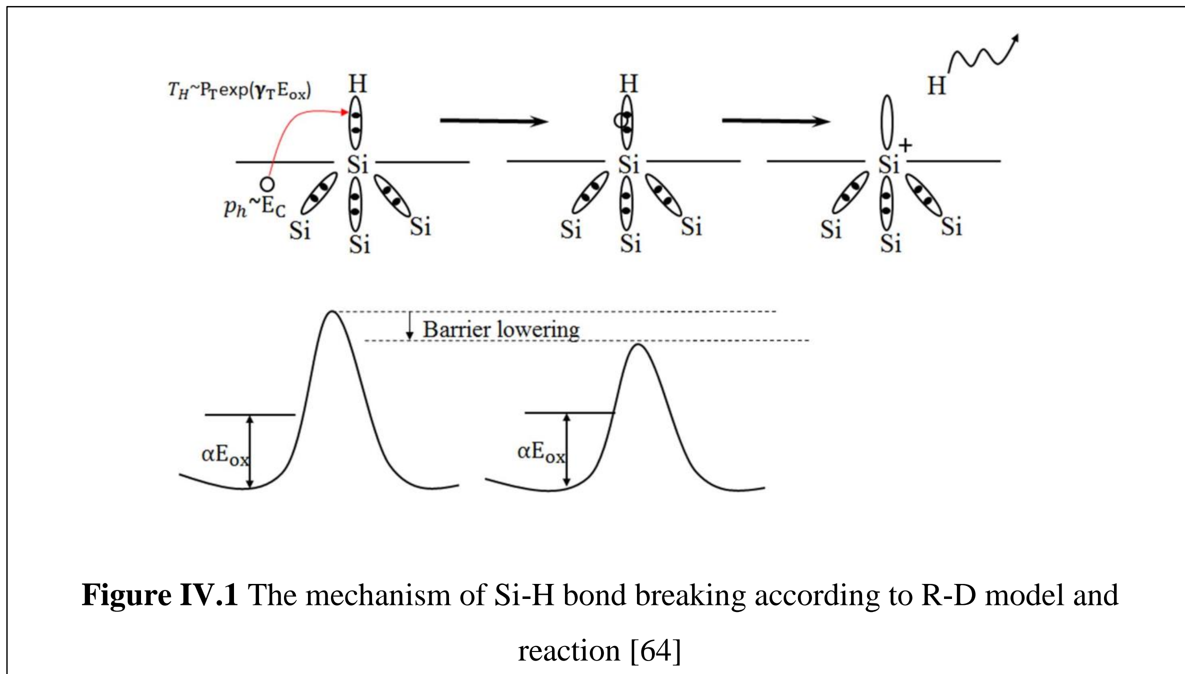

Figure IV.1 The mechanism of Si-H bond breaking according to R-D model and reaction [64]

The microscopic details of the trap generation and trap annealing processes that occur within a few Angstrom of the Si/SiO_2 interface are hidden in the constants k_f and k_r.

IV.2.2 Diffusion Phase

The diffusion medium is the amorphous SiO_2. The released hydrogen moves into the oxide by jumping between potential wells. Two approaches here are often used. The first one is to suppose that these potential wells are equal and uniformly distributed across the oxide as shown in Figure IV.2 (Arrhenius approach). In the second, potential wells are not equal and randomly distributed across the oxide as shown in Figure IV.7 (dispersive approach) [44].

IV.2.3 Arrhenius-like Diffusion

Figure IV.2 is a schematic representation of Arrhenius-like diffusion of the hydrogen where the entire potential walls have the same height.

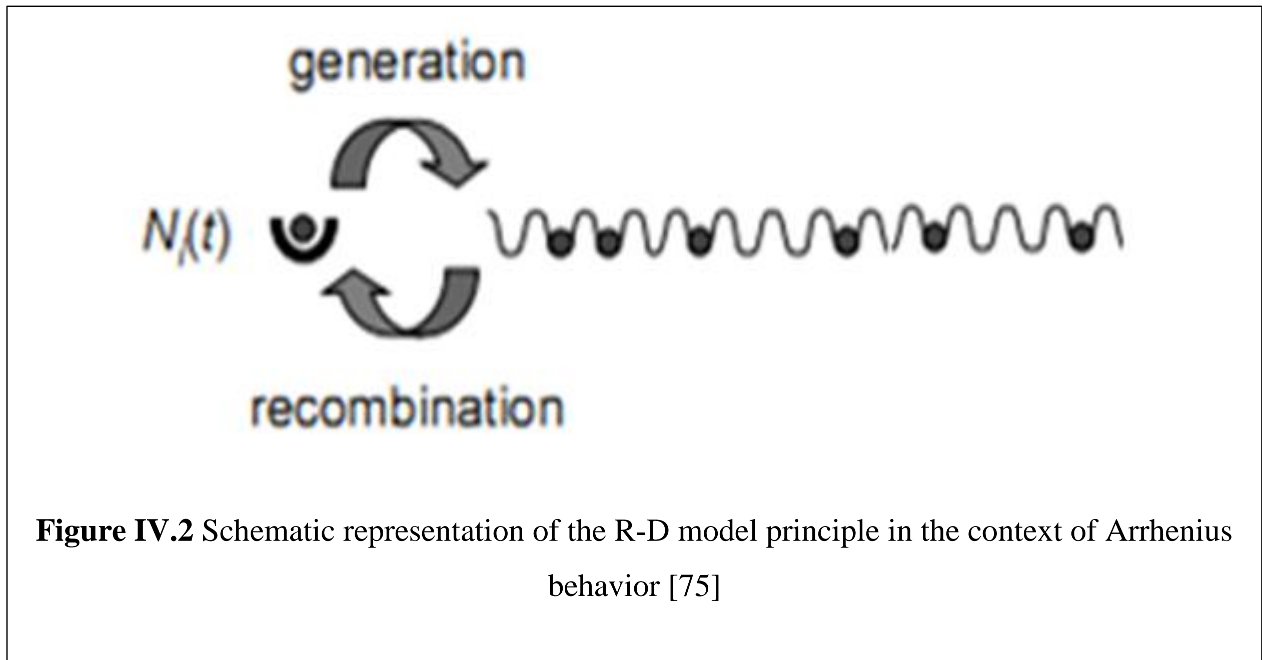

Figure IV.2 Schematic representation of the R-D model principle in the context of Arrhenius behavior [75]

The Arrhenius process is described by the following equations:

$$D_H = D_0 \exp\left(\frac{-E_D}{KT}\right) \quad \text{(IV.2)}$$

$$\frac{dN_H}{dt} = D_H \left(\frac{d^2 N_H}{dx^2}\right) \quad \text{(IV.3)}$$

Where:

- D_H is the hydrogen diffusion coefficient,
- k is Boltzmann constant,
- T is temperature in Kelvin,
- ED is the activation energy of hydrogen diffusion.

For the diffusion phase, the solution of the R-D model can be split up into six different regimes and each regime is characterized by its own time exponent. Figure IV.3 summarize these six regime.

Regime 1: Initially, the N_{it} and N_H values are very low and the reaction is limited only by forward reaction rate k_f and so giving a time dependence of n = 1.

$$N_{it} = k_f N_0 t \tag{IV.4}$$

Regime 2: After some time, when the amount of hydrogen at the interface is large, the forward reaction reaches quasi-equilibrium with the backward reaction therefore

$$K_f N_0 = k_f N_{H(x=0)} N_{it} \tag{IV.5}$$

With N_{it}=N_H we obtained:

$$N_{it} = \sqrt{\frac{k_f N_0}{k_r} t^0} \tag{IV.6}$$

with a resulting time dependence of n = 0.

As long as the diffusion of hydrogen away from the interface has not reached a large magnitude, there is no further degradation of the interface.

Regime 3: Regime three starts when the diffusion of hydrogen away from the interface starts and acts as a limiting factor for the degradation. In this phase the diffusion front has not reached the polysilicon gate, therefore:

$$\frac{dN_H}{di} = D_H \left(\frac{d^2 N_H}{dx^2} \right) \tag{IV.7}$$

Every dangling Si bond is associated with a free H atom in the oxide. The density of H in the oxide during diffusion can be approximated by a triangular profile [40], with the end front equal to $\sqrt{D_H t}$, thus the interface trap density is given by:

$$N_{it}(t) = \frac{N_H^0}{2} \sqrt{D_H t} \tag{IV.8}$$

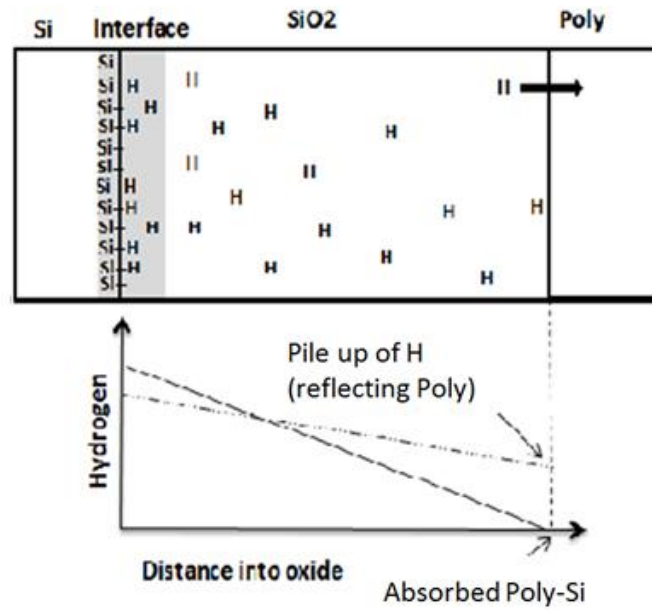

(a)

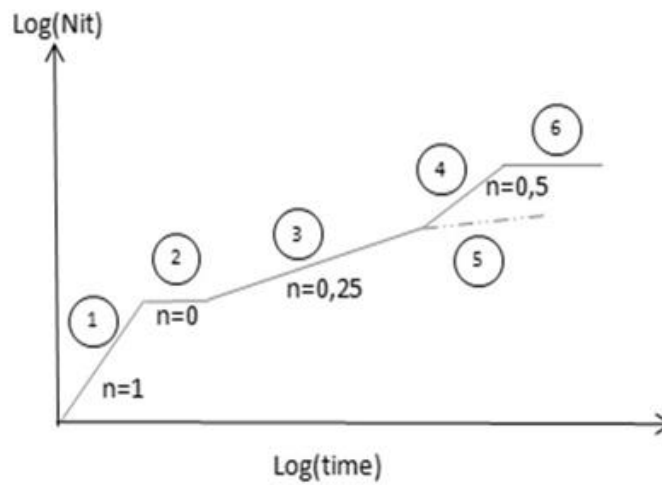

(b)

Figure IV.3 The classical R-D model underlying mechanism representation. a) Hydrogen profile. b) Interface traps generation regimes.

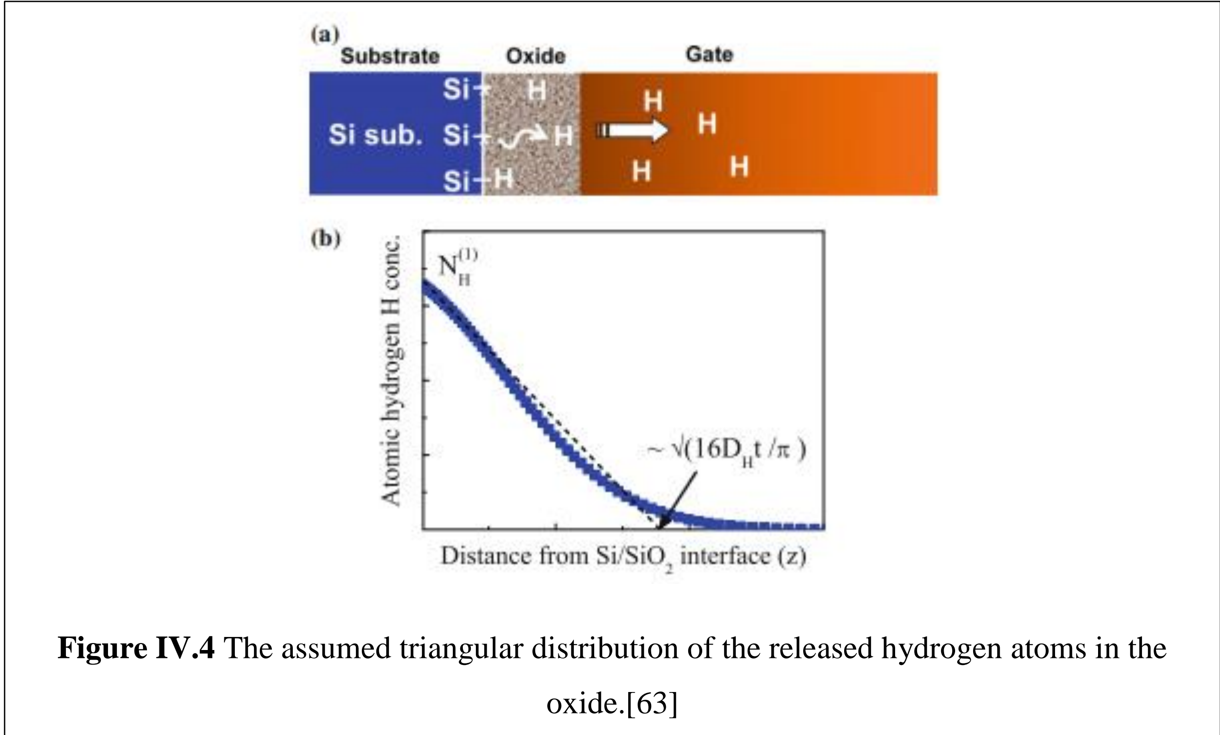

Figure IV.4 The assumed triangular distribution of the released hydrogen atoms in the oxide.[63]

The rate of interface generation is supposed to be constant during this period of the model then the term $\frac{dN_{it}}{dt}$ is neglected and so:

$$N_{it}N_H^0 = \frac{K_f N_0}{K_r} \tag{IV.9}$$

By combining eq. (IV.9) with eq. (IV.8) we obtained:

$$N_{it}(t) = \sqrt{\frac{K_f N_0}{2K_r}}\left(D_H t\right)^{\frac{1}{4}} \tag{IV.10}$$

which gives the time-exponent (n = 0.25) of NBTI when only H diffusion is taken into account.

Regime 4: When the diffusion end front reaches the polysilicon gate contact the time exponent changes again. In this model it is assumed that the hydrogen species diffuses into the poly-silicon gate with high diffusion constant. That is, the gate electrode acts as an absorber for the diffusing species. For this case a time exponent of n = 0.5 is derived.

Regime 5: If the poly-silicon gate reflects the hydrogen species, they pile up at the oxide gate interface causing the concentration gradient of the hydrogen in the oxide to decrease. As a consequence, the flux of hydrogen species decreases also. The NBTI degradation shows a sign of saturation as illustrated in Figure IV.3-a

Regime 6: When regime 6 is reached, theoretically, all interface bonds N_0 are broken and no further degradation can occur in this model. Therefore the change in N_{it} is zero thus the time exponent n is zero also.

The basic RD model (depassivation and atomic H diffusion) could explain the observed temporal kinetics of ΔNIT (power-law time slope, n ~ 0.25) during DC stress and frequency (f) independence of ΔNIT during AC stress. However, the experimental value of n ~ 0.25 found in earlier reports was attributed to recovery artifact.

In the previously described R-D model, only H diffusion is considered. However, it is known that atomic H is unstable and it would convert to molecular H_2 after it is released from the Si-SiO_2 interface. Activation energies observed from NBTI measurements support that the dominant diffusing hydrogen species are H_2 [43][29]. Therefore, it is worth repeating the derivation of the R-D model by replacing H by H_2.

In the H_2 diffusion-based model, after dissociation of Si−H bonds, the released H atoms transform to the hydrogen molecule according to the following reaction:

$$H + H \leftrightarrow H_2 \quad \text{(IV.11)}$$

The conversion between H and H_2 would be given by the law of mass action:

$$\frac{N_H(0)^2}{N_{H_2}} = const \quad \text{(IV.12)}$$

Following the same derivation as for the case of H, we obtain:

$$N_{it}(t) \propto \left(\frac{k_f N_0}{k_r}\right)^{\frac{2}{3}} \left(D_{H_2} t\right)^{\frac{1}{6}} \quad \text{(IV.13)}$$

When only the diffusion of H_2 is taken in consideration the time exponent is 1/6. This

reflects less degradation because the transformation H-H2 blocs the diffusion of H atoms allowing them to stay at the interface for more time, then more interface states are passivated.

In addition to the H and H_2 cases, another case is worth considering; when the diffusing species are protons H^+. The NBTI degradation is now drift limited rather than diffusion limited. The profile of the H^+ is approximated to a triangle as shown in Figure IV.5 [26]. The number of interface states is given by:

$$N_{it}(t) = N_H(0)\mu_H E_{ox} t \tag{IV.14}$$

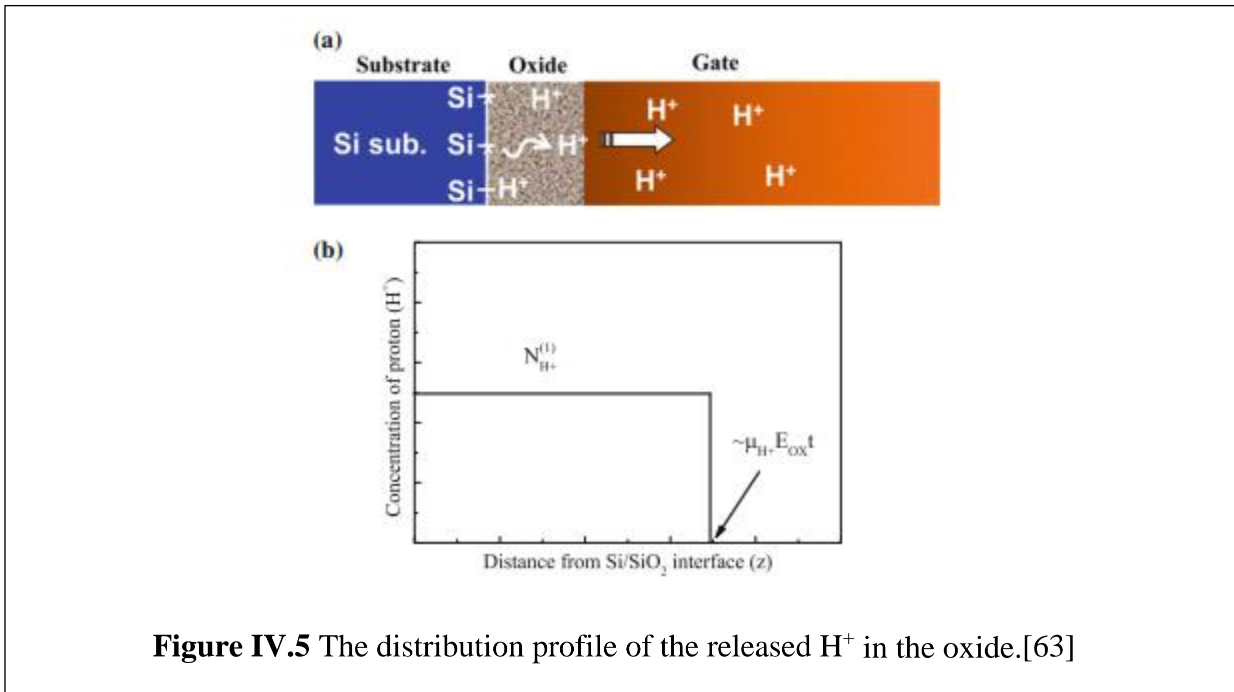

Figure IV.5 The distribution profile of the released H^+ in the oxide.[63]

From eq. (IV.13) and eq. (IV.9), N_{it} is given by:

$$N_{it}(t) = \sqrt{\frac{K_f N_0}{K_r}} (\mu_H E_{ox} t)^{\frac{1}{2}} \tag{IV.15}$$

The time exponent of 1/2 has never been seen in NBTI measurements, leading one to conclude that NBTI degradation through proton transport is unlikely [39][54] [42].

The following table summarizes the predicted value of the time exponent depending on the

diffusing species:

Species	**n**
H^0	0,25
H_2	0,162
H^0, H_2	0,25-0,165
H^+	0,5

Table IV.2 Value of the time exponent for different diffusing species [34]

The reaction-diffusion model predicts the temperature and the electric-field dependence of NBTI implicitly within the k_f and k_r coefficients. The oxide-field dependence (exponential dependence) is included in the k_f term and the temperature dependence of the degradation is incorporated through the activation energies of k_f, k_r and D_H in the form of Arrhenius activation.

In the recovery phase, when the stress is turned off, the forward reaction coefficient k_f is zero and only the backward reaction takes place. The quantity of hydrogen available at the interface rapidly repassivates the dangling bonds. Afterward the repassivation is diffusion controlled. It is governed by the following equation [55]:

$$N_{it} = N_{it}^{(0)} \left(\frac{1 - \left(\frac{\xi t}{t_0} \right)^{\frac{1}{2}}}{1 + \left(\frac{t}{t_0} \right)^{\frac{1}{2}}} \right) \quad (t > 0) \qquad \text{(IV.16)}$$

Where

t_0 time when the stress is stopped,

$Nit^{(0)}$ the number of traps generated at t_0,

ζ= ½ for one sided diffusion.

IV.2.4 Dispersive Transport

The Reaction-diffusion model described above assumes hydrogen species to diffuse into the oxide according to an Arrhenius-like activated transport. If we assume k_f, k_r and D_H to be given as follows [42]:

$$k_f = k_{f0} \exp\left(-E_F / KT\right) \quad \text{(IV.17)}$$

$$k_r = k_{r0} \exp\left(-E_R / KT\right) \quad \text{(IV.18)}$$

$$D_H = D_0 \exp\left(-E_D / KT\right) \quad \text{(IV.19)}$$

Where:

- E_F is the activation energy of the forward reaction rate,
- E_R is the activation energy of the backward reaction rate and
- E_D is the activation energy of the hydrogen diffusion.

Then the interface state density will be given by [42]:

$$N_{it}(t) \infty \left(\frac{k_{f0} N_0}{K_{r0}} \right)^m D_0^n e^{-\frac{m(E_F - E_R) + nE_D}{KT}} t^n \quad \text{(IV.20)}$$

Where n, m depends on the diffusion species.

Therefore for the Arrhenius transport (Diffusion nature) , the threshold shift curves plotted in a log-log scale at various temperatures as a function of time should be parallel to each other (n is independent of temperature). In contrast, the obtained curves show that the time exponent n varies with temperature (Figure IV.6). This is why many scientists invoke the non-Arrhenius and dispersive nature of NBTI degradation.

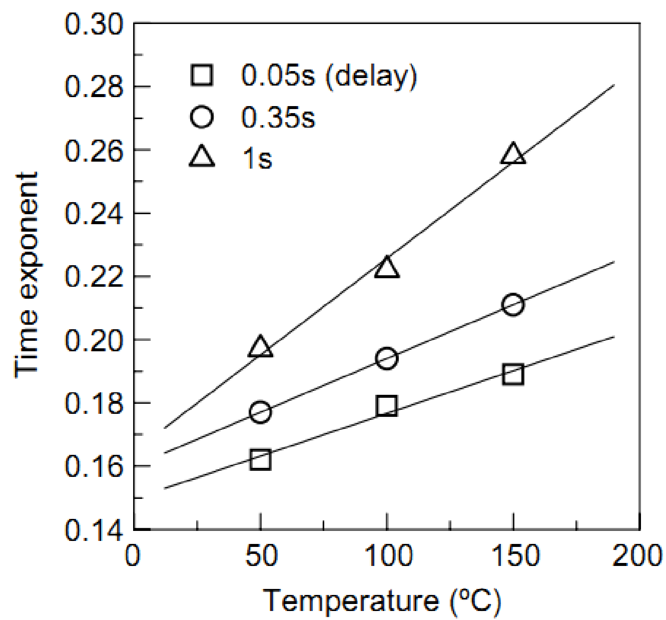

Figure IV.6 Temperature dependence of measured NBTI time exponent. [42]

Figure IV.7 is a schematic illustration of dispersive transport where the dielectric contains hydrogen traps of different energy. The trapping probability at each trap is the same. But for de-trapping it is different; deeper traps present a higher barrier than the shallow ones. Transport hydrogen species spend most of their lifetime in the deeper traps, which thus control their transport properties.

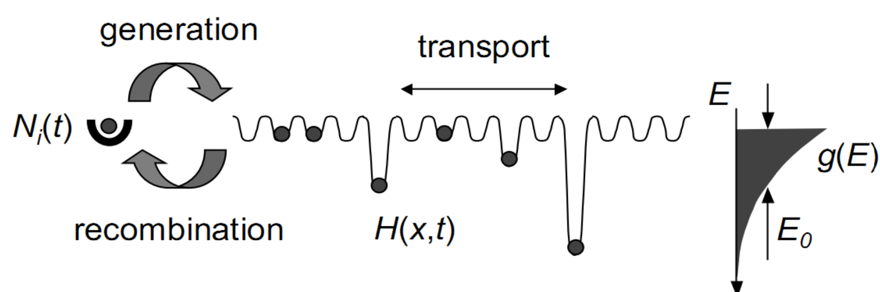

Figure IV.7 Schematic representation of the dispersive transport of hydrogen species.

N_{it} is then given by [33]

$$N_{it}(t) \infty \left(\frac{k_{f0} N_0}{K_{r0}} \right)^m \left(\frac{D_{H_0}}{\upsilon} \right)^n e^{-\frac{m(E_F - E_R)}{KT}} (\upsilon t)^{n(1-\alpha)} \tag{IV.21}$$

Where

- υ is the hopping frequency of hydrogen
- α is the dispersive parameter. It can vary between 0 (conventional transport) and 1 (strongly dispersive transport).

The conventional RD model (involving dimerization of H to H2) is found to be incompatible in the stochastic domain [56],. Instead, the “double-interface” RD model, first proposed in [47] and later refined in [57] is used. In this model , illustrated using **Figure IV.8**, released H atoms from depassivated defects at the Si/SiO2 interface during stress diffuse and subsequently react with H passivated bulk insulator defects to create additional defects at the gate insulator bulk (in tune with [2,13,34]) and H2 molecules, the latter diffuse away and control the long time kinetics of ΔN_{IT} (power law time slope of n ~ 0.16) during stress. The reverse processes of H/H2 back diffusion and defect re-passivation in the gate insulator bulk and subsequently at the Si/SiO2 interface control the kinetics of ΔNIT recovery after stress. In this “double-interface” RD model, all H passivated bulk gate insulator defects are placed at a suitable “second interface” inside the gate insulator for simplicity, the “first interface” being that at the Si/SiO2 interface.

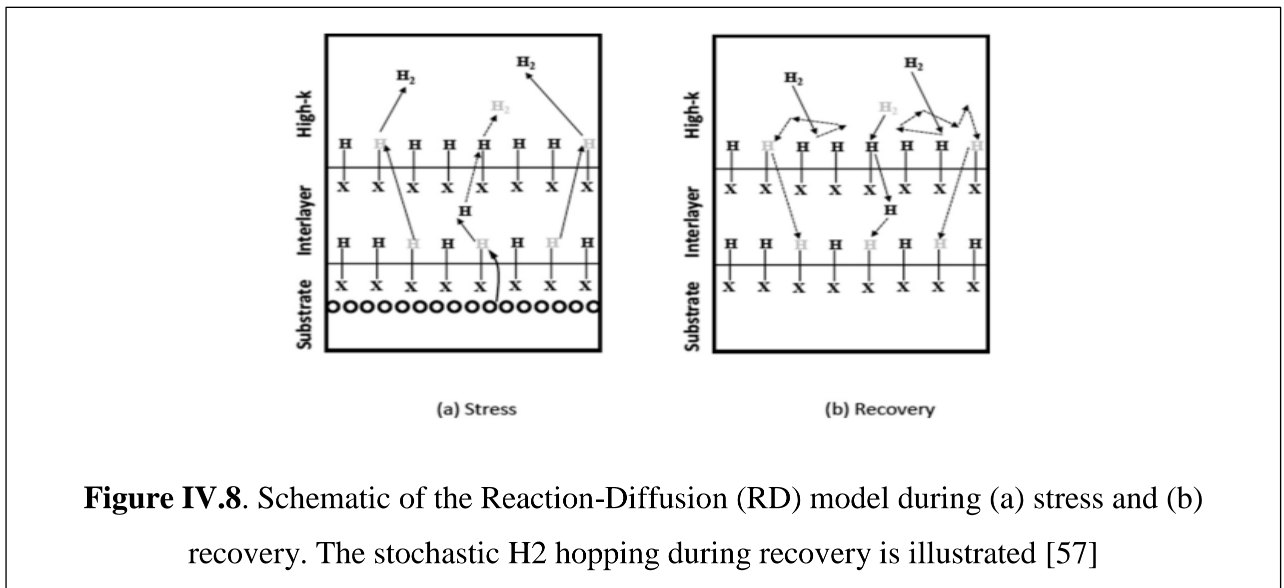

Figure IV.8. Schematic of the Reaction-Diffusion (RD) model during (a) stress and (b) recovery. The stochastic H2 hopping during recovery is illustrated [57]

IV.2 Hole-trapping detrapping based model

In spite of its success in describing many experimental results of NBTI degradation, R-D model faces growing criticism from many research labs. It is especially pointed out that [58][59][30][60]:

- Generated interface traps do not show any recovery,
- The logarithmic dependence on time of the recovery,
- The cyclic behavior of the NBTI stated by Ang et al.

IV.3.1 Two Stage Model

A more elaborated multi-mechanism explanation is the two stage model proposed by T. Grasser, et al. [50]. In this theory the precursor for the phenomenon is a neutral interfacial oxygen vacancy, which upon the capture of a hole, creates a positive defect called an E'_{γ} center. Next, the emission of the captured hole (electron capture) neutralizes the defect at which point the structure can either relax back to the original oxygen vacancy precursor, or re-capture a hole and return to the E'_{γ} state. This is the mechanism believed to account for the rapid charging and recovery dynamics observed in NBTI. As for the second mechanism, the E'_{γ} center can interact with the hydrogen passivating a neighboring silicon dangling bond at the interface. Lenahen and Campell [61] demonstrate that it is energetically favorable for the hydrogen to migrate to the E'_{γ} center leaving behind an interface state whose charge will depend on the position of the Fermi-level.

Figure III.8 illustrates the principal of the two stage model proposed by T. Grassor.

By considering a trap level E_T located at a distance x away from the interface as shown in Figure IV.10, the hole capture and emission rates are then approximately given by [50]:

$$K_p^c = p\upsilon_p^{th}\sigma_p e^{-\frac{x}{x_{p,0}}} e^{-\beta\Delta E}\theta(E_{VT}e^{-\beta E_{VT}},1)e^{\frac{F^2}{F^2}} \qquad \text{(IV.22)}$$

$$K_p^e = p\upsilon_p^{th}\sigma_p e^{-\frac{x}{x_{p,0}}} e^{-\beta\Delta E}\theta(E_{VT}e^{-\beta E_{VF}},e^{-\beta E_{TF}}) \qquad \text{(IV.23)}$$

Figure IV.9 Two stage model principle. Stage one is based on the hole-trapping detrapping model for switching traps. Stage two illustrates a hydrogen transitions that results in the creation of an interface state. [50]

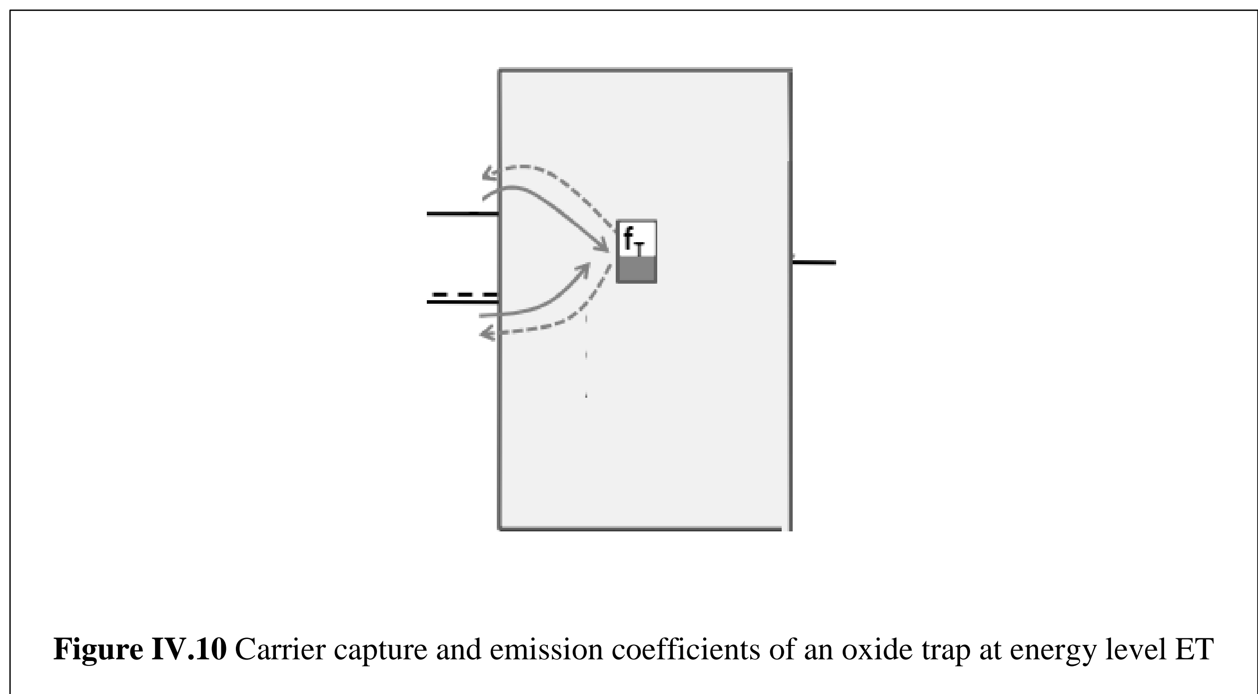

Figure IV.10 Carrier capture and emission coefficients of an oxide trap at energy level ET

while the corresponding rates for electrons is:

$$K_n^c = n\upsilon_n^{th}\sigma_n e^{-\frac{x}{x_{n,0}}} e^{-\beta\Delta E}\theta(E_{TC}e^{-\beta E_{TC}},1) \quad \text{(IV.24)}$$

$$K_n^e = n\upsilon_n^{th}\sigma_n e^{-\frac{x}{x_{n,0}}} e^{-\beta\Delta E}\theta(E_{TC}e^{-\beta E_{FC}},e^{-\beta E_{TF}}) \quad \text{(IV.25)}$$

Where

- p and n are the hole and electron concentrations in the channel,
- $v^{th}{}_p$ and v^{th} are their thermal velocities,
- σ_p and σ_n are their capture cross sections,
- E_F is the Fermi-level in the channel, E_V and E_C are the valence and conduction bands directly at the interface (classical approximation),
- ΔE is the multiphonon emission barrier,
- Fc is the reference field for the multiphonon-field- assisted tunneling mechanism, $x_{n,0}$ = 0.8 A for electrons; and $x_{p,0}$ =0.5 A for holes.
- θ is the auxiliary function. It is used to account for the fact that thermal activation is required for hole capture into a trap below E_V while capture in a trap above E_V proceeds without activation, and vice-versa for electrons.

$$\theta(E_{swich},a,b = \begin{cases} a & E_{switch} \geq 0 \\ b & E_{switch} < 0 \end{cases} \quad \text{(IV.26)}$$

a) First stage

Initially the defects before stress are in state 1 (Figure IV.8). The trap energy lies at E_T has a multiphonon emission (MPE) barrier of ΔE_B, and a multiphonon-field-assisted tunneling (MPFAT) reference field F_c.

After the application of the stress, defects starts to transform from state “1” to state “2” by capturing a hole from the inversion layer with a rate of , where f_1 is the probability of the defects to be in state “1” and k_{12} is the rate of transformation from state “1” to “2”.

Being in state “2” (charged E’γ center) the defects can transform to state “3” with a rate of or

pass to state “4” by capturing a hydrogen from the Si-H bonds.

Defects in state “3” (neutral E’γ) can transform back to state “2” by emitting the captured hole with a rate of or totally anneal and returns back to state “1”
In general, the rate equations describing the transitions between the three states are given by:

$$\frac{\partial f_1}{\partial t} = -f_1 k_{12} + f_3 k_{31} \quad \text{(IV.27)}$$

$$\frac{\partial f_2}{\partial t} = +f_1 k_{12} - f_2 k_{23} + f_3 k_{32} \quad \text{(IV.28)}$$

$$\frac{\partial f_3}{\partial t} = +f_2 k_{23} - f_3 k_{32} + f_3 k_{31} \quad \text{(IV.29)}$$

f_1, f_2 and f_3 are the probability of the trap to be in state 1, 2, and 3 respectively.

The rate of transition between states 1 to 2 is given by:

$$k_{12} = K_p^c(E_T, \Delta E_B, F_C) + k_n^e(E_T, \Delta E_B, F_C) \quad \text{(IV.30)}$$

In a similar way, the transition from state 2 to state 3 are described by:

$$k_{23} = K_p^e(E_T^{'}, \Delta E_C, 0) + k_n^c(E_T^{'}, \Delta E_C, 0) \quad \text{(IV.31)}$$

$$k_{32} = K_p^c(E_T^{'}, \Delta E_C, 0) + k_n^e(E_T^{'}, \Delta E_C, 0) \quad \text{(IV.32)}$$

$$k_{32} = \upsilon e^{-\beta \Delta E_A} \quad \text{(IV.33)}$$

b) Second stage

Stage two of the model deals with the interface traps generation. By the end of stage one created interfacial E’γ triggers the hydrogen dissociation from the Si-H bonds. The transition rates between state 2 and 4 are modeled as follows:

$$k_{24} = \upsilon e^{-\beta(\Delta E_D - E_2 - \gamma F)} \tag{IV.34}$$

$$k_{42} = \upsilon e^{-\beta(\Delta E_D - E_4 - \gamma F)} \tag{IV.35}$$

IV.3.2 Threshold Voltage Shift Expression

By determination of the oxide charge Q_{ox} and the interface charge Q_{it} , the threshold shift is given by:

$$\Delta V_{th}(t) = -\frac{\Delta Q_{ox}(t) + \Delta Q_{it}}{C_{ox}} \tag{IV.36}$$

In the context of the Two stage model Q_{ox} is the density in the bulk of E’ centers that are in state “2”

$$Q_{ox}(t) = q\frac{1-x}{t_{ox}}\langle f_2(t)\rangle \tag{IV.37}$$

And

$$\Delta Q_{ox}(t) = Q_{ox}(t) - Q_{ox}(0) \tag{IV.38}$$

The interface trap charge Q_{it} is given by the average of the probability of having depassivated dangling bonds (state 4) times the probability that the created electrical level of the donor-like defect is unoccupied:

$$Q_{it} = q\left\langle f_4(1-f_{it})\right\rangle \qquad \text{(IV.39)}$$

The **NBTI** literature is full of modeling attempts to refine both conventional R&D models and two-stage models. The following table summarizes the most important of them:

NBTI base model	permanent	Recoverable	Precursor	Correlation	Reference
R-D	Nit	Nit	Interface Si-H	-	[62][40][63]
R-D	Nit	Nit +Not	Interface Si-H + Pre-existing defect	uncorrelated	[30] [64][57]
Hole trapping detrapping	Nit	E' center	Oxygen vacancy	correlated	[50][59][11][11], [65]
Deep level positive trap	Nit	Deep level positive trap	Trap precursor	uncorrelated	[38]
Hole trappind detrapping	ANHT	CPC	AHT	correlated	[66]

Table IV.2 List of the most relevante NBTI models in the literature

IV.3 Conclusion

This chapter discussed the NBTI models based on hydrogen diffusion and hole trapping-detrapping formalism. Early works have adopted the hydrogen diffusion formalism based on the R-D model which is based on the generation of the interface trap also known as a permanent component upon the application of stress. With the development of measurement techniques and focusing on the recovery regime, the R-D base model has been proved to be limited and other modeling approaches based on hole trapping detraining have surged.

I have investigated two models for the negative bias temperature: the classical reaction-diffusion model and the two stage model proposed by T.Grassor. The first model is a

hydrogen-diffusion based model whereas the latter is a hole-trapping detrapping based model.

None of them is able to reproduce all the experimental signatures of the NBTI. This is explained by the fact that NBTI is heavily dependent on the oxide process and that the experimental results themselves do not reflect the intrinsic behavior of the NBTI degradation because of the recovery effect which cannot be eliminated during measurements.

Chapter V

NBTI Proposed model

Negative bias temperature instability (NBTI) is one of the most longstanding reliability issues in CMOS technologies. Despite of many models that have been developed, none of them gets the consensus especially on the microscopic origin of fast and permanent components. NBTI is the consequence of gradual and time dependent buildup of positive charges in the substrate-oxide interface and/or in the gate insulator of a MOS based transistor under the application of a negative stress bias and relatively high temperature. The generated positive charges cause a shift in transistor parameters such as threshold voltage, transconductance, subthreshold slope...etc. [23]Some of NBTI distinguishing signatures are the power law behavior during stress period and fast recovery alongside with long term degradation that lasts for many decades [25].

It is important to understand the physical mechanism of NBTI and develop a robust models to predict the time as well as the temperature dependence of the degradation to determine NBTI limited device lifetime. The byproduct of any NBTI model is to determine the microscopic species behind NBTI and precise which of them is responsible for the fast and the long recovery. The proposed models in the literature can be split into two big categories: Hydrogen based models or Reaction-Diffusion (RD) models and hole trapping detrapping models also called Energy Well (EW) models [25], [67]. Some authors agreed to propose models that combine both hydrogen and hole contribution, but they diverge on which of them is behind the permanent part or the fast recovery one. Although NBTI is extensively studied and several models have been proposed in the past, its physical mechanism has remained a field of great debate.

In this chapter, a new physical based model, which extends the two-stage model [50] to account the hydrogen diffusion in the oxide, has been proposed. In our model holes in correlation with hydrogens in the oxide are responsible of NBTI and in contrast to any other proposed model both hole and hydrogen related defects contribute to fast and long term recovery. The validity of the model equations is checked using COMSOL Multiphysics simulator.

V.1 Positive charge classification

Positive charge in the oxide and the substrate-oxide interface are the major cause of bias instabilities. Their comprehensive classification is the best start towards à robust model.

In this work we adopt the classification proposed by J.F Zhang because it seems to us to fit naturally to NBTI degradation [68] [21][21].

Positive charge are classified as follows (figure V.1):

- AHT : as grown hole traps – oxygen vacancy precursors
- CPC : Cyclic positive charges – Fast states
- ANHT : antineutralization hole traps – Slow states

We add to this classification the obvious interface states Nit.

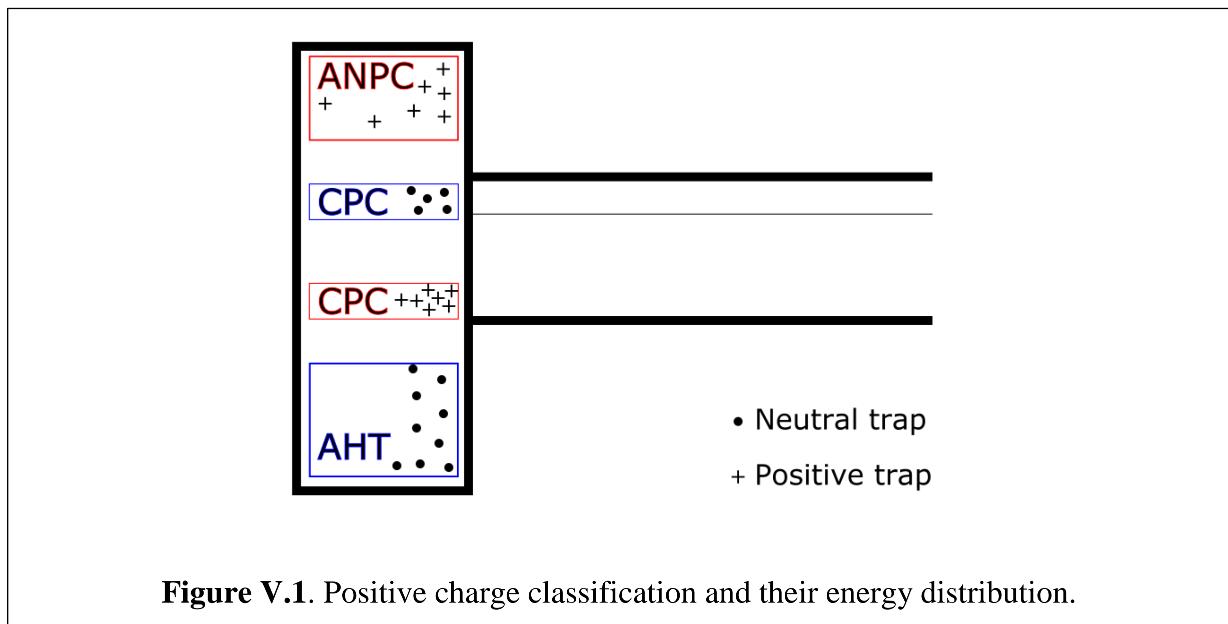

Figure V.1. Positive charge classification and their energy distribution.

Based on this framework of oxide charge classification and the Two-Stage model proposed by Tabor Grasser [50]our model is built. The Two-Stage model extends the Harry Diamond Laboratory model [69], [69] by extending it with a second stage to account for the NBTI permanent part.

V.2. Model derivation:

Figure V.2 shows all dynamics of the proposed model and Figure V.3 illustrates the defects supposed to cause NBTI degradation highlighting their energy distribution with respect to the silicon substrate band gap. These tow figures will be heavily referenced during our steps of model derivation.

These two figures will be heavily referenced during our steps of model derivation.

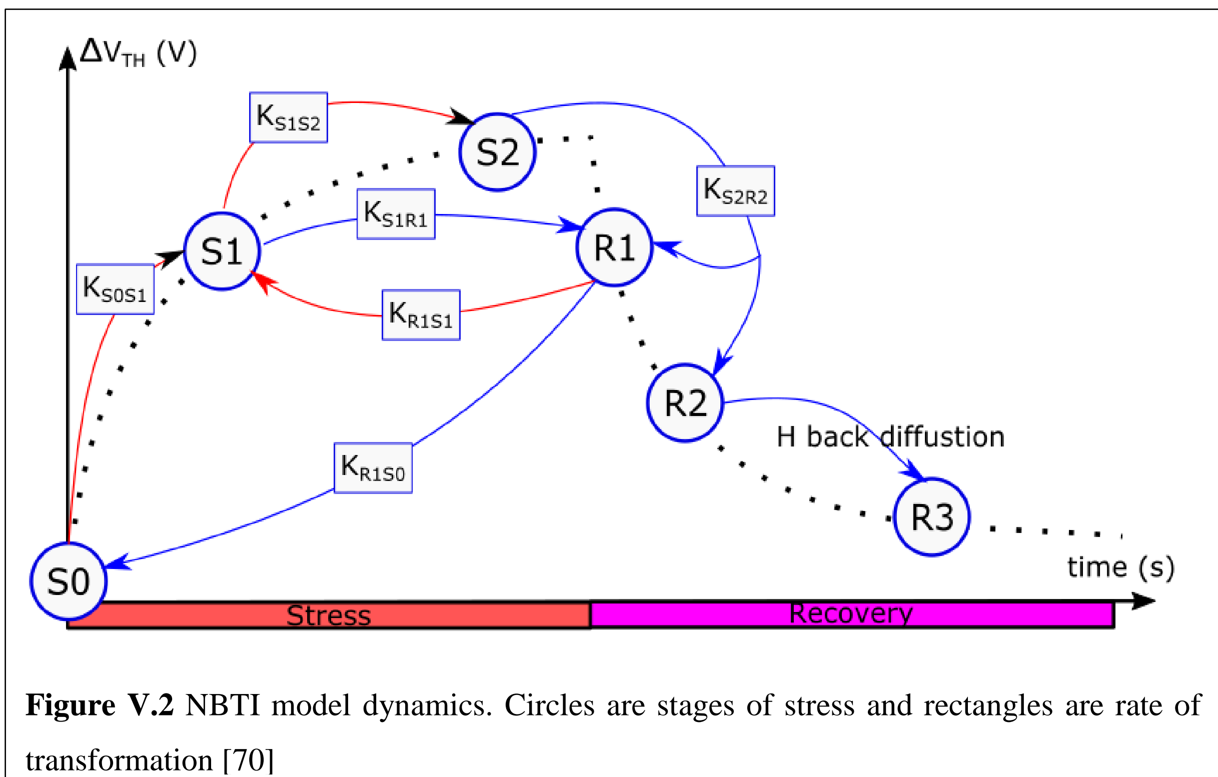

Figure V.2 NBTI model dynamics. Circles are stages of stress and rectangles are rate of transformation [70]

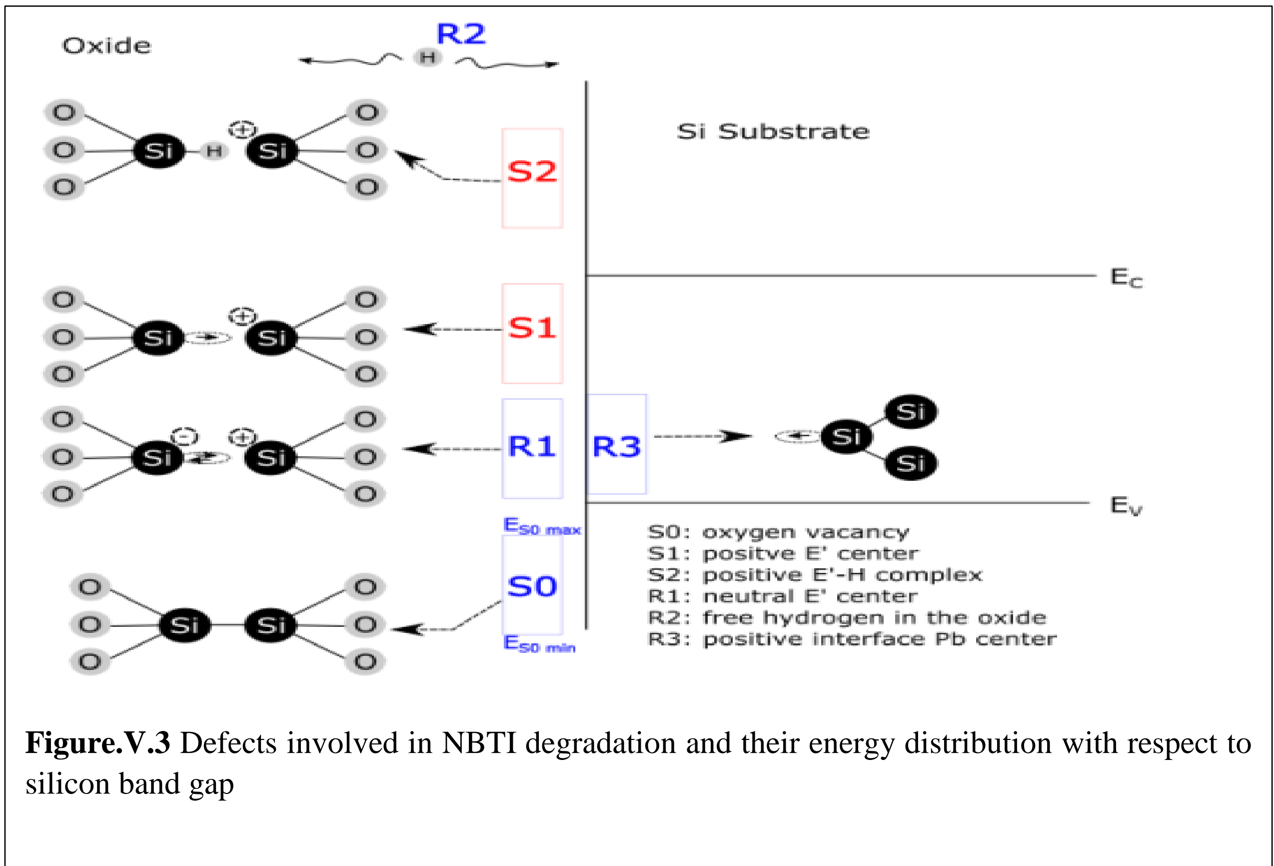

Figure.V.3 Defects involved in NBTI degradation and their energy distribution with respect to silicon band gap

our model can be explained as follows [70]:

V.2.1 Stress Period

During the stress period, the device is subjected to a negative bias under relatively high temperature. This period is characterized by the increase of channel hole concentration which plays a major role in oxide trap charging. In this developed model, the stress period passes through three stages as depicted in Figure.V.2.

Stage zero of stress (S0): this stage represents the device before stress. The NBTI related defect precursors are taken to be oxygen vacancies. Oxygen vacancies energy is distributed below the silicon upper valence band energy (S0 in Figure.V.3). It is randomly distributed from 1.4 eV to 0.32 eV below the upper valence band [71].

Stage one of stress (S1): Upon application of the stress, substrate holes pile up near the Si-SiO_2 interface. Some of these holes acquire energy so that they have a non-negligible probability to tunnel to the nearby interfacial oxygen vacancies. Once an oxygen vacancy captures a hole, the bond between Si atoms is broken and hence one Si atom becomes a positive

charge and the other stays neutral with one dangling bond. This new configuration of the oxygen vacancy is called E’ center with a positive charge (S1 in Figure.V.3).

The creation of E’ center is accompanied by structural relaxation, which leads the energy level of the defect to shift. The energy of the newly created E’ centers lays in the upper half of the Si band gap (S1 in Figure.V.3). Within these energy levels, E’ center has been positively charged and it will play a crucial role in the trapping/detrapping process of the proposed NBTI model.

By taking the oxygen vacancy concentration in the oxide to be N_{S0} [cm^{-3}] and the newly created E’ center to be N_{S1} [cm^{-3}] (Subscript S represents stress; and 1, 2 for stage one and two respectively), the rate equations of transformation are given by:

$$\frac{dN_{S0}}{dt} = -K_{S0S1}N_{S0} \qquad \text{(V.1)}$$

$$\frac{dN_{S1}}{dt} = K_{S0S1}N_{S0} \qquad \text{(V.2)}$$

$$K_{S0S1} = p\upsilon_p^{th}\sigma_p e^{-\frac{x}{x_{p0}}} e^{-\beta\Delta E_{S0S1}}\theta(E_V - E_{S0}, e^{-\beta(E_V - E_{S0})}, 1)e^{\frac{F^2}{F_c^2}} \qquad \text{(V.3)}$$

where

- K_{S0S1} is the rate of transformation from stage S0 to stage S1,
- p is the channel hole concentration, υ_p^{th} is the hole thermal velocity,
- σ_p hole capture cross-section,
- $\beta = 1/K_BT$, ΔE_{S0S1} is the energy barrier that should be exceeded then a hole will be captured by oxygen vacancy,
- E_{S0} refers to the energy level of defects in state S0,
- F is the electric field,
- F_c is the reference field for the multiphonon-field-assisted tunneling mechanism [50], and

$$\theta(E_{S0}, e^{-\beta E_{S0}}, 1) = \begin{cases} e^{-\beta E_{S0}} & E_V - E_{S0} \geq 0 \\ 1 & E_V - E_{S0} < 0 \end{cases} \qquad \text{(V.4)}$$

It is important to note that these equations are preliminary and are subject to modification as long as the proposed model is derived.

Stage two of stress (S2): Being in state S1, hydrogen atoms bonded to the interfaces can move to the next E' center and form E'-H complex and leave behind it an interface dangling bond Pb center, which means that the formation of E'-H and Pb centers are tightly coupled [50]. The new created E'-H complex forms the permanent component of the NBTI.
Naming the E'-H concentration by N_{S2}, the rate of generation of the latter is:

$$\frac{dN_{S2}}{dt} = K_{S1S2}N_{S1} \quad \text{(V.5)}$$

$$K_{S1S2} = \upsilon e^{(-\beta\Delta E_{S1S2} - E_{S2} - \gamma F)} \quad \text{(V.6)}$$

where K_{S1S2} is the rate of transformation from stage S1 to stage S2, ν is the attempt frequency, ΔE_{S1S2} is the energy barrier that a hydrogen bond should overpass to form the E'-H complex, E_{S2} is energy level of defects in the S2 state and γ is the field acceleration parameter.

Now, the rate of change of N_{S1} in equation (V.2) becomes:

$$\frac{dN_{S1}}{dt} = K_{S0S1}N_{S0} - K_{S1S2}N_{S1} \quad \text{(V.7)}$$

At the end of the stress period, three types of positive charges are created:

– E' centers: created during stage S1;
– E'-H centers: created during stage S2;
– Nit interface states or Pb centers: created during stage S2.

The created E'-H centers and Pb centers are tightly coupled. FigureV.3 shows the energy distribution inside the oxide band gap.

V.2.2 Relaxation (Recovery) Period

During recovery, the stress is removed and eventually a positive voltage can be applied. The relaxation period is featured by the increase of substrate electron concentration in the channel which will play a major role in trap discharging.

Stage one of relaxation (R1): After removing the stress, electrons pile up at the substrate channel. Some of these electrons can rapidly tunnel back to the positive E' (stage S1) center and neutralize it. The capture of an electron by E' center shifts the energy level of the trap down near to the upper band of the silicon valence.

Being in this stage, a neutral E' center can rapidly capture a hole from the valence band and becomes again positively charged and its energy level shifts up. E' center switches between two states: positively charged if it captures a hole or neutral if it captures an electron.

Taking N_{R1} to be the concentration of neutral E' center in stage R1 (R stands for relaxation and 1 for stage one), the rate of change of N_{R1} is:

$$\frac{dN_{R1}}{dt} = K_{S1R1}N_{S1} - K_{R1S1}N_{R1} \qquad \text{(V.8)}$$

where K_{S1R1} and K_{R1S1} are the rates of transformation from stage S1 to stage R1 and back from R1 to S1 respectively which can be written as follows:

$$K_{S1R1} = n\upsilon_p^{th}\sigma_n e^{-\frac{x}{x_{n0}}} e^{-\beta\Delta E_{S1R1}}\theta(E_{S1} - E_C, e^{-\beta(E_{S1}-E_C)}, 1) \qquad \text{(V.9)}$$

and,

$$K_{R1S1} = p\upsilon_p^{th}\sigma_p e^{-\frac{x}{x_{p0}}} e^{-\beta\Delta E_{R1S1}}\theta(E_V - E_{R1}, e^{-\beta(E_V-E_{R1})}, 1) \qquad \text{(V.10)}$$

For this stage, equation (V.7) becomes:

$$\frac{dN_{S1}}{dt} = K_{S0S1}N_{S0} - K_{S1S2}N_{S1} - K_{S1R1}N_{S1} + K_{R1S1}N_{R1} \qquad \text{(V.11)}$$

In this stage, an E' center that does not capture a hole for a long time can recover back to an oxygen vacancy.
Taking this into consideration equations (V.1) and (V.8) we obtain:

$$\frac{dN_{S0}}{dt} = -K_{S0S1}N_{S0} + K_{R1S0}N_{R1} \qquad \text{(V.12)}$$

and,

$$\frac{dN_{R1}}{dt} = K_{S1R1}N_{S1} - K_{R1S1}N_{R1} - K_{R1S0}N_{R1} \quad \text{(V.13)}$$

where K_{R1S0} is the rate of transformation from stage R1 to stage S0, which is given by:

$$K_{R1S0} = \upsilon e^{-\beta \Delta E_{R1S0}} \quad \text{(V.14)}$$

Stage two of relaxation (R2): Electrons in the channel, depending on the temperature and the positive bias voltage, can acquire the necessary energy to overcome the energy barrier and capture the positive E'-H centers.

Being in the neutral state, E'-H complex has a non-zero probability to be dissociated and release its hydrogen in the oxide.

We argue that a positive E'-H complex has a neglected probability to release hydrogen in the oxide. Effectively, when the E'-H complex captures an electron from the silicon channel, the probability of releasing its hydrogen increases. This fact can be understood based on quantum mechanics principles.

The captured electron is located near the positively charged Si atom of the Si-H complex. According to quantum mechanics, the captured electron has a non-zero probability to be near the Si atom that is passivated by the hydrogen. Where the electron weakens the Si-H bond and hydrogen can be released into the oxide due to thermal agitation. After releasing the hydrogen, the E'-H complex returns back to a neutral E' center (see stage R1 in Figure.V.2 and Figure.V.3).

Naming the species at this stage by N_{R2} (hydrogen atoms in the oxide), the rate of change of N_{R2} is given by:

$$\frac{dN_{R2}}{dt} = K_{S2R2}N_{S2} \quad \text{(V.15)}$$

$$K_{S2R2} = n\upsilon_p^{th}\sigma_n e^{-\frac{x}{x_{n0}}} e^{-\beta \Delta E_{S2R2}} \theta(E_{S2} - E_C, e^{-\beta(E_{S2}-E_C)}, 1) \quad \text{(V.16)}$$

And equations (V.5) and (V.13) will be rewritten as:

$$\frac{dN_{S2}}{dt} = K_{S1S2}N_{S1} - K_{S2R2}N_{S2} \quad \text{(V.17)}$$

$$\frac{dN_{R1}}{dt} = K_{S1R1}N_{S1} - K_{R1S1}N_{R1} - K_{R1S0}N_{R1} + K_{S2R2}N_{S2} \quad \text{(V.18)}$$

Stage three of the relaxation (R3): The released hydrogen can diffuse into the oxide or came back and passivate a silicon–oxide interfacial dangling bond. The behavior is similar to what the RD model is in the recovery phase [10].

Equation (V.15) becomes:

$$\frac{dN_{R2}}{dt} = K_{S2R2}N_{S2} + D_H \frac{d^2N_{R2}}{dx^2} - K_r N_{it} D_{R2} (at \quad x = 0) \quad \text{(V.19)}$$

Where:

- D_H is the hydrogen diffusion coefficient in the oxide,
- K_r is the back interface reaction as defined in the context of RD model,
- N_{it} is the interface state concentration.

At the end of this relaxation period, the recovery of NBTI is the sum of three independent processes:

1- The capture of substrate electrons by positive E’ centers (stage R1);
2- The capture of high energy electrons by the positive E’-H centers (stage R2); and
3- The back diffusion of hydrogen in the oxide to passivate a Pb center (stage R3).

The final equations of the developed model are:

$$\frac{dN_{S0}}{dt} = -K_{S0S1}N_{S0} + K_{R1S0}N_{R1} \quad \text{(V.20)}$$

$$\frac{dN_{S1}}{dt} = K_{S0S1}N_{S0} - K_{S1S2}N_{S1} - K_{S1R1}N_{S1} + K_{R1S1}N_{R1} \quad \text{(V.21)}$$

$$\frac{dN_{S2}}{dt} = K_{S1S2}N_{S1} - K_{S2R2}N_{S2} \quad \text{(V.22)}$$

$$\frac{dN_{R1}}{dt} = K_{S1R1}N_{S1} - K_{R1S1}N_{R1} - K_{R1S0}N_{R1} + K_{S2R2}N_{S2} \tag{V.23}$$

$$\frac{dN_{R2}}{dt} = K_{S2R2}N_{S2} + D_H \frac{d^2N_{R2}}{dx^2} - K_r N_{it} D_{R2} \,(at \quad x = 0) \tag{V.24}$$

The quantity of N_{it} can be obtained from:

$$\frac{dN_{it}}{dt} = -K_{S1S2}N_{S1} + K_r N_{it} N_{R2} \tag{V.25}$$

The total shift of the threshold can be evaluated by:

$$\Delta V_{TH} = -\frac{q}{C_{ox}}\left(\int_0^{t_{ox}}\left(1 - \frac{x}{t_{ox}}\right)(N_{S1} + N_{S2})\,dx + N_{it}\right) \tag{V.26}$$

V.3 Model simulation

To validate the developed model, numerical simulations on a pMOSFET structure with an oxide thickness of 4 nm have been performed using COMSOL Multi-physics simulator [72]. Defect energy distribution and barriers between states are predefined to follow a random uniform distribution (except for the S1-S2 transition barrier for which it uses Gaussian-like Fermi-derivative distribution) [71] . Table 1 gives the values of energy distribution and barriers between stages as used in these simulations.

Stage	Energy spread [eV]		Barrier	Energy spread [eV]	
S0 (Oxygen vacancy)	E_{S0} min	– 1.14	S0S1	E_{S0S1} min	0.01

	E_{S0} max	– 0.31		E_{S0S1} max	1.14
S1 (positive E' center)	E_{S1} min	0.57	S1S2	E_{S1S2} mean	1.46
	E_{S1} max	1.11		E_{S1S2} std. dev	0.44
S2 (E'-H complex)	E_{S2} min	1.13	S1R1	E_{S1R1} min	0.4
	E_{S2} max	2.13		E_{S1R1} max	0.4
R1 (neutral E' center)	E_{R1} min	0.1	R1S1	E_{R1S1} min	0.4
	E_{R1} max	0.55		E_{R1S1} max	0.4
R2 (free hydrogen)	–	–	R1S0	E_{R1S0} min	0.7
	–	–		E_{R1S0} max	1.2
R3 (Pb centers)	–	–	S2R1	E_{S2R1} min	0.3
				E_{S2R1} max	0.9

Table 1 – Energy distribution and barrier used in simulation

For details steps of model implementation using COMSOL Multi-physics simulator see appendix 1.

The predictability of our model is investigated against some of the most accepted features of NBTI in the literature.

V.3.1 Fast Recovery and Long Term Recovery

Figure. V.4 shows the threshold voltage shift (ΔV_{th}) evolution during the stress at – 1.5 V and relaxation at 0 V. The total NBTI threshold voltage shift is the result of the superposition of interface trap generation contribution and oxide hole trapping contribution for stress period, and interface passivation and hole detrapping for the recovery period.

The generation of interface state is strongly coupled to the E'-H complex generation rate which results from the transfer from stage S1 to stage S2. This correlation between N_{it} and E'-H is lost during recovery period because the released hydrogen (the byproduct of S2 to R2 transformation) can diffuse freely into the oxide and only hydrogen atoms at the interface are responsible for interface passivation.

Our model predicts that the long-term NBTI recovery is limited by the diffusion of the hydrogen atoms towards the interface in concordance with many experimental results that highlight the role of hydrogen diffusion in NBTI degradation. In contrast to our model, the Two-Stage model fails to predict this long-term recovery of NBTI [50].

Alongside with the long-term recovery prediction capability of our model, it also succeeded in reproducing the fast early recovery of the degradation. It is the fast switch between Stage S1 and Stage R1 and back forth that is the behind the fast recovery of the NBTI.

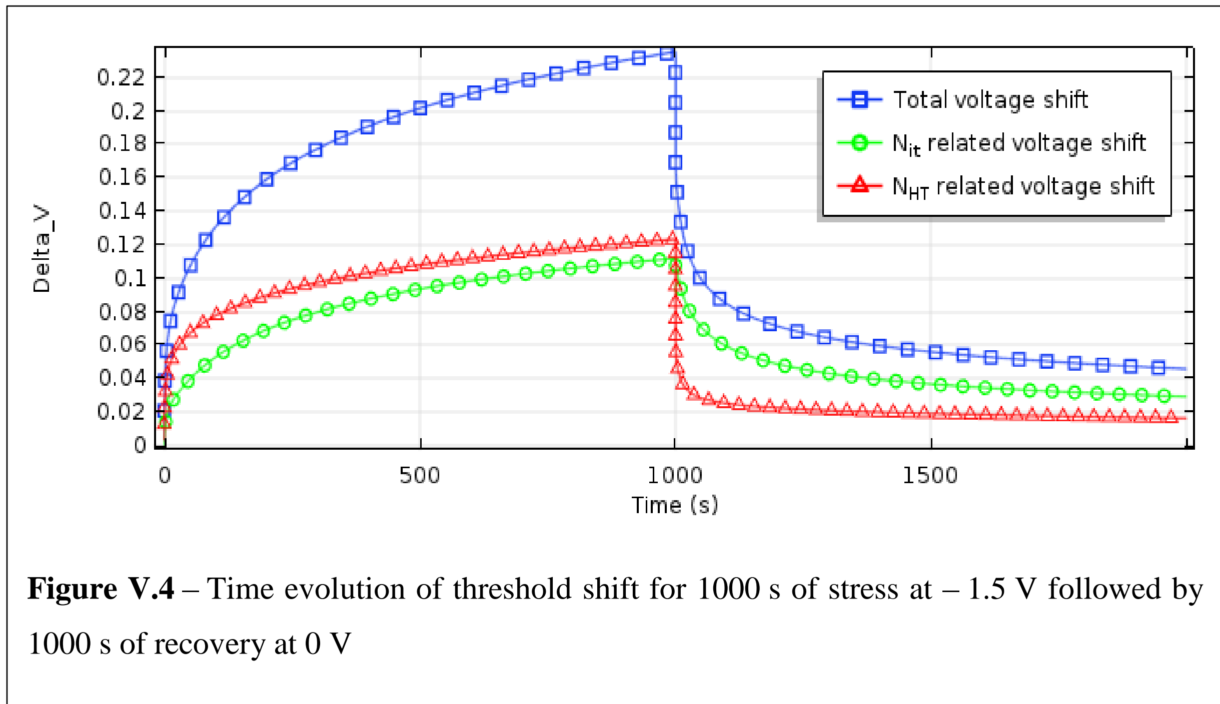

Figure V.4 – Time evolution of threshold shift for 1000 s of stress at – 1.5 V followed by 1000 s of recovery at 0 V

V.3.2 Power Law and Time Exponent

Our model predicts that the NBTI degradation follows a power low characteristic with time exponent of 0.26 as illustrated in Fig. 4. Although a 0.25 time exponent is reported in the literature, the 0.16 time exponent is the most accepted by researchers in the field especially after the introduction of ultra-fast measurement technique and on-the-fly ones.

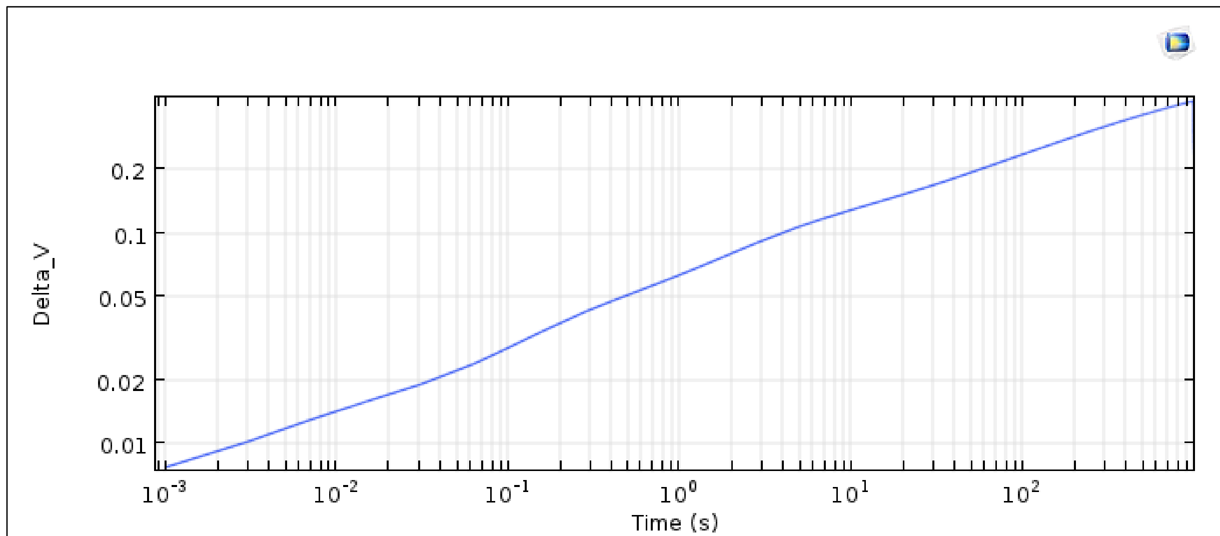

Figure V.5 – Threshold shift in a log-log scale. The extract power law time exponent is 0.26

V.3.3 Stress Voltage and Temperature Dependence

Fig. 5 and Fig. 6 show that our model is able to predict the stress voltage sensibility of the NBTI degradation as well as its temperature dependence. The stress voltage dependence is attributed to the $\exp(F^2/Fc^2)$ in the rate of transformation from S0 to S1, whereas the temperature dependence of the NBTI is included in the energy barriers that should be exceeded to transit between stages.

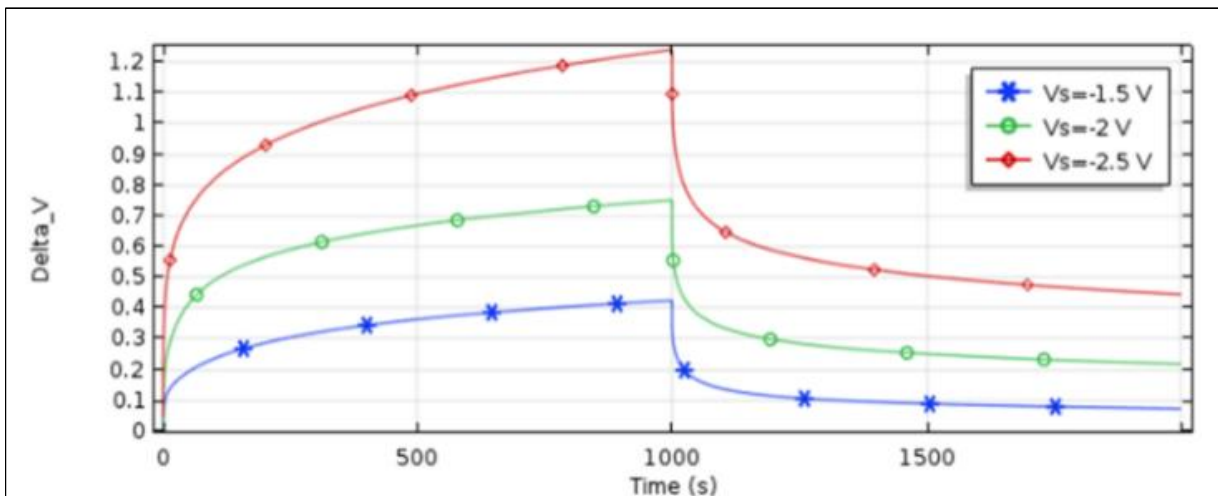

Figure V.6 – NBTI degradation for different voltage stress at T = 200 °C

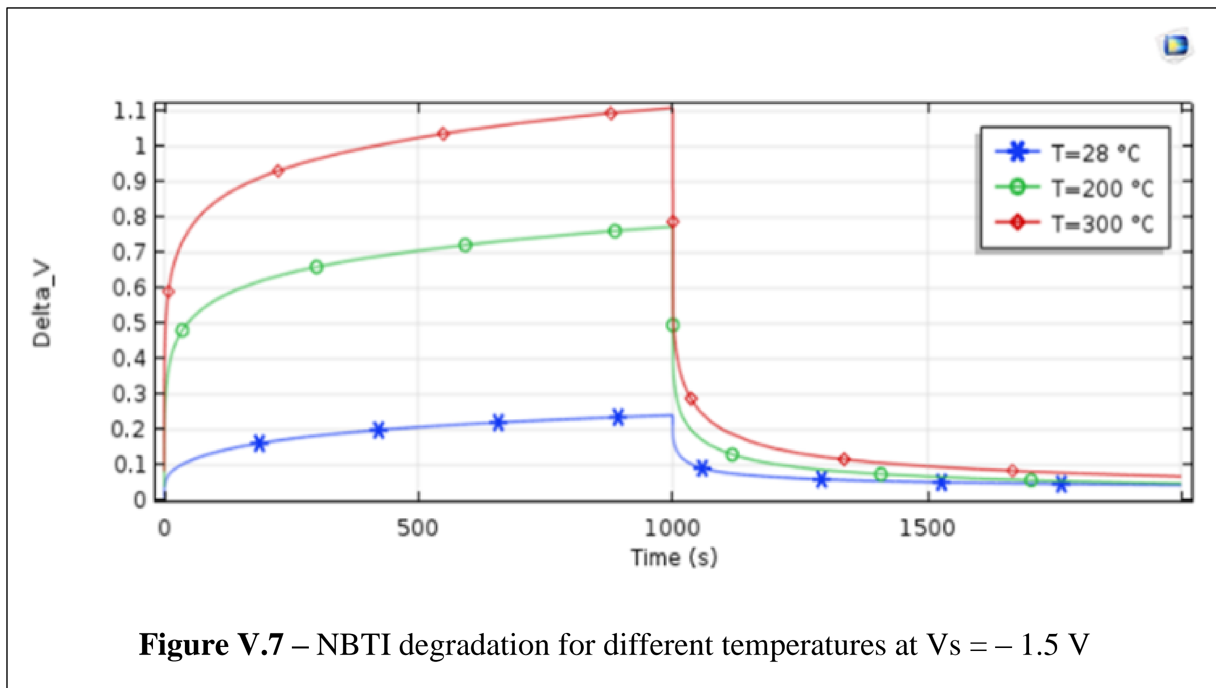

Figure V.7 – NBTI degradation for different temperatures at Vs = – 1.5 V

V.3.4 Magnetic Field Effect:

The magnetic field effect on the NBTI degradation dynamics can be understood in the context of the following facts:

- The applied magnetic field tends to favor one spin orientation (either up or down spin).
- Pauli Exclusion Principle, which states that two electrons, cannot have the same quantum state. This means that two electrons in the same orbital must have opposite spins [76].
- Our proposed model is based on the creation and passivation of oxygen vacancy, Pb and E' centers. Those defects are paramagnetic; that is, they have an unpaired electron in their external orbitals.

With application of magnetic field, the probability that electrons (holes) in the defects and in the substrate channel to have the same spin orientation increases. Consequently, the probability of capturing a hole by a paramagnetic defects decreases which influences the K_{S0S1} and K_{S1R1} rate equations of our model because they depend on the hole capture cross section.

The probability of an electron to change its spin is proportional to the strength of the magnetic

field and inversely proportional to the temperature (thermal agitation) [77].

To account of the magnetic field in our model we change the hole capture cross section in equations (V.3) and (V.10) with:

$$\sigma_p = \sigma_{p0}(1 - \alpha \frac{B}{T}) \qquad (V.27)$$

where:

- σ_{p0} is the hole capture cross section without magnetic field;
- B is the magnetic field;
- T is the temperature and
- α is a coefficient of the proportionality.

Fig. 8 plots the threshold voltage shift of a 1000s period of stress follow with the same period of recovery under different magnetic field values.

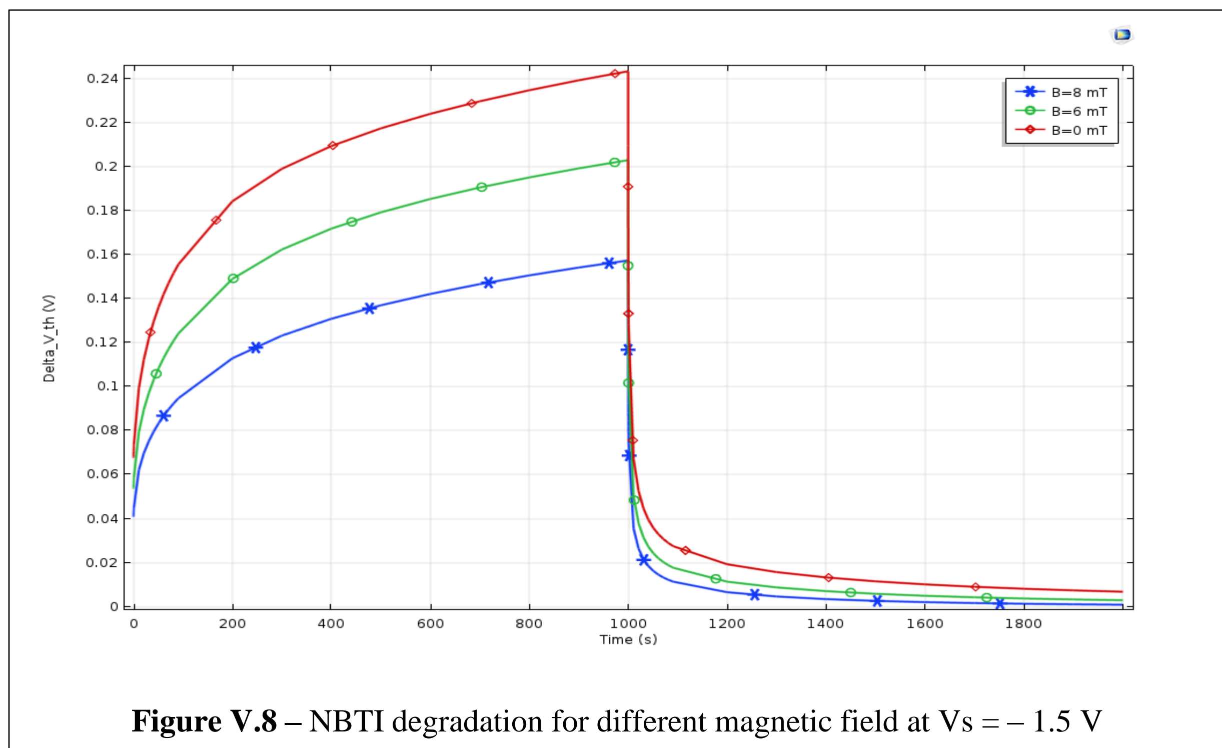

Figure V.8 – NBTI degradation for different magnetic field at Vs = – 1.5 V

V.4. Conclusion

In this chapter, I presented the proposed model of NBTI degradation. The model is based on the Two-stage model and extend it by taking into consideration the hydrogen diffusion in the oxide. The dynamics and mathematical derivation of our model have been presented. The model predicts that both hydrogen and hole trapping-detrapping play a major role in NBTI degradation. The generation of the E'-H complex is a consequence of the transformation from state S1 to S2, which is tightly coupled to sub-strate hole trapping in E' center. The fast component of NBTI degradation is caused by the switching character of E' centers. Whereas the permanent part of the degradation is ascribed to the E'-H complex and hydrogen back diffusion in the oxide.

Chapter VI

Conclusion and perspectives

The main purpose of this thesis was the evaluation of a new model for the Negative Bias Temperature in pure-oxide. The work performed during this thesis allowed us to study in-depth the NBTI from the microscopic defects related to NBTI to the simulation of the proposed model.

As NBTI is heavily related to the structure of the oxide, our starting point was the amorphous structure of SiO_2 and its electrically active defects. The hydrogen's role in the annealing process is discussed and the classification of positive charge in the oxide is shown. Understanding the microscopic structure of the oxide is a crucial step towards elaborating a reliable NBTI model.

NBTI is distinguished from other reliability problem by the fact that under moderate negative bias and a relatively high temperature it shows the following characteristics:

- Power law behavior of the time evolution when plotted on a log-log scale. Different values of the time exponent have been quoted. They range from 0.25 to 0.16
- Initial high time exponent (with in 10s).
- Logarithmic time dependence of the recovery
- Temperature activated process.

The modeling of the NBTI is a problematic task because:

- NBTI recovery makes the experimental data less accurate even when ultrafast switching or On-The-Fly methods are used.
- NBTI hardly dependent on the oxidation process. Pb, E' and nitrogen concentration and their distribution in the oxide is proved to influence NBTI degradation

NBTI modeling attempts that dates from the mid-70s, can be classified in to big tendencies:

- The first one focuses on hydrogen species and give it a big part of the responsibility of NBTI degradation. The reaction-diffusion model is widely accepted to better reproduce the NBTI behavior. It is based on the dissociation of Si-H bonds to Pb centers and free hydrogen atoms and the subsequent diffusion of the H into the oxide. Many attempts have been conducted to refine the Reaction-Diffusion model to overcome its weaknesses revealed from most advanced measurement techniques.
- The second tendency has been revolving around E' centers and hole trapping/detrapping in the oxide (commonly named switching traps).

Despite the apparent discrepancy between the two tendencies, both agree that behind NBTI degradation there are two components; one permanent and the other recoverable. The relationship between the two components and their microscopic origin is under heavy debate. In general, NBTI models proposed in the literature are trying to answer the following questions:

- Q1: What are the microscopic origins of the two components? And which of them is permanent (slow) or recoverable (fast)?
- Q2: What is the relation (correlation) between the two components: coupled (dependent) or decoupled (independent)?

The model proposed in this thesis is built upon the Two-Stage model and extend it by considering the hydrogen diffusion in the oxide. The proposed model answers to the above-mentioned two questions.

- The degradation is originated from Pb centers at the interface, E' centers in the oxide and E'-H complexes in the border of the Si-SiO2 interface. The fast component is related to E' center trapping/detrapping, where-as the slow component is shared between E'-H complex and Pb centers.
- The two components are coupled and decoupled at the same time. They are tightly coupled during stress and fairly decoupled during recovery.

As we stated before none of the proposed models in the literature has succeeded in explaining all the experimental features of NBTI and our proposed model is not an exception. Our

simulation result suggests the power law exponent to be 0.25 which is an old value that has abounded in favor of 0.16 values.

It should be noted that the proposed model is only useful for pure SiO_2. However, the oxides, used in modern devices, are generally doped with impurities, especially with nitrogen. Therefore, the study of the effects of these impurities on NBTI should be included in the proposed model. This can be done by comparing the NBTI behavior of pure and doped oxides of the same thickness, under the same stress conditions and using the same characterization technique.

Based on our proposed model, we can say that the effect of nitrogen on NBTI can be explained by the fact that the introduction of nitrogen into the oxide can modify the energy distribution of the defect centers (E' center, oxygen vacancy and E'-H complex). In our simulation study, we take the most accepted defect energy distribution for SiO_2, (some of them are supposed to be uniform). The rate equations (K_{s0s1}, K_{r1s1}, ….) strongly depend on the energy distribution of the defects and any change in the latter can totally modify the final result of the model. It is in this context that we can understand the influence of the introduction of nitrogen.

Appendix 1

NBTI Model

Report date	Apr 11, 2020 9:08:02 PM

1 Global Definitions

Date	Apr 28, 2018 10:42:20 AM

GLOBAL SETTINGS

Name	2018-05-18 # 2d NBTI 2Stage.mph
Path	E:\MELLATI_Search Gate\Two Stage\My paper\simulation\2018-05-18 # 2d NBTI 2Stage.mph
COMSOL version	COMSOL 4.0.0.982
Unit system	SI

USED PRODUCTS

COMSOL Multiphysics

1.1 PARAMETERS 1

PARAMETERS

Name	Expression	Value	Description
Vs	-1.5[V]	−1.5 V	
Vr	0[V]	0 V	Recovery voltage
T	26.8[degC]	299.95 K	
KB	8.61733e-5[eV/K]	1.3806E−23 J/K	Boltzmann constant
d_ox	4e-07[cm]	4E−9 m	
ni	1.5e10[1/cm^3]	1.5E16 1/m³	
Nd	1.5e16[1/cm^3]	1.5E22 1/m³	
v_th_h	1.65e7[cm/s]	1.65E5 m/s	
v_th_n	2.3e7[cm/s]	2.3E5 m/s	
segma_h	3e-14[cm^2]	3E−18 m²	
segma_n	3e-14[cm^2]	3E−18 m²	
x_p0	0.05[nm]	5E−11 m	
x_n0	0.08[nm]	8E−11 m	
Ev	0	0	
Ec	1.12[eV]	1.7944E−19 J	
q	1.6e-19[C]	1.6E−19 C	
Fc	2.8e6[V/cm]	2.8E8 V/m	Critical oxide electrique field
nu	1e13[1/s]	1E13 1/s	
E1_mean	-0.725[eV]	−1.1616E−19 J	
E1_range	0.83[eV]	1.3298E−19 J	
E12_mean	0.58[eV]	9.2926E−20 J	

Name	Expression	Value	Description
E12_range	1.14[eV]	1.8265E−19 J	
E2_mean	0.2[eV]	3.2044E−20 J	
E2_range	0.2[eV]	3.2044E−20 J	
E23_mean	0.4[eV]	6.4087E−20 J	
E23_range	0[eV]	0 J	
E3_mean	0.92[eV]	1.474E−19 J	
E3_range	0.2[eV]	3.2044E−20 J	
E32_mean	0[eV]	0 J	
E32_range	0[eV]	0 J	
E31_mean	0.98[eV]	1.5701E−19 J	
E31_range	0.54[eV]	8.6518E−20 J	
E24_mean	0.96[eV]	1.5381E−19 J	
E24_spread	0.2[eV]	3.2044E−20 J	
phi_s	-2*KB*T/1.6e-19[C]*log(Nd/ni)	−0.71517 V	
Kr	8e-3[cm^3/s]	8E−9 m^3/s	
DH	2.8e-16[cm^2/s]	2.8E−20 m^2/s	
N0	1e14[1/cm^2]	1E18 1/m^2	
E4_mean	1.16[eV]	1.8585E−19 J	
E4_range	0.4[eV]	6.4087E−20 J	
E45_mean	0.58[eV]	9.2926E−20 J	
E45_range	0.58[eV]	9.2926E−20 J	

1.2 VARIABLES

1.2.1 Variables 2

SELECTION

Geometric entity level	Entire model

Name	Expression	Unit	Description
p	(F<0)*Nd + (t>20)*(F>=0)*ni^2/Nd	1/m^3	
n	(F<0)*ni^2/Nd + (F>=0)*Nd	1/m^3	
F	((t<=1000) + (t>2000 && t<=3000))*((Vs - phi_s)/d_ox)	V/m	

2 Model 1

Date	Apr 28, 2018 10:43:19 AM

COMPONENT SETTINGS

Unit system	SI
Geometry shape order	automatic

2.1 DEFINITIONS

2.1.1 Variables

Variables 1

SELECTION

Geometric entity level	Entire model

Name	Expression	Unit	Description
K12	p*v_th_h*segma_h*exp((F/Fc)^2)*exp(-x/x_p0)*exp(-rn_E12(x, y)/(KB*T))*((Ev - (rn_E1(x, y) - q*x*F)>=0)*exp(-(Ev - (rn_E1(x, y) - q*x*F))/(KB*T)) + (Ev - (rn_E1(x, y) - q*x*F)<0)*1)		
K23	n*v_th_n*segma_n*exp(-x/x_n0)*exp(-rn_E23(x, y)/(KB*T))*((rn_E2(x, y) - q*x*F - Ec>=0)*exp(-(rn_E2(x, y) - q*x*F - Ec)/(KB*T)) + (rn_E2(x, y) - q*x*F - Ec<0)*1)		
K32	p*v_th_h*segma_h*exp(-x/x_p0)*exp(-rn_E32(x, y)/(KB*T))*((Ev - (rn_E3(x, y) - q*x*F)>=0)*exp(-(Ev - (rn_E3(x, y) - q*x*F))/(KB*T)) + (Ev - (rn_E3(x, y) - q*x*F)<0)*1)		
K31	nu*exp(-rn_E31(x, y)/(KB*T))		
K24	nu*exp(-rn_E24(x, y)/(KB*T))		
K45	n*v_th_n*segma_n*exp(-x/x_n0)*exp(-rn_E45(x, y)/(KB*T))*((rn_E4(x, y) - q*x*F - Ec>=0)*exp(-(rn_E4(x, y) - q*x*F - Ec)/(KB*T)) + (rn_E4(x, y) - q*x*F - Ec<0)*1)		
Nit	intop1(N4) + intop1(N5)	m^2	

2.1.2 Functions

Random 1

Function name	rn_E1
Function type	Random

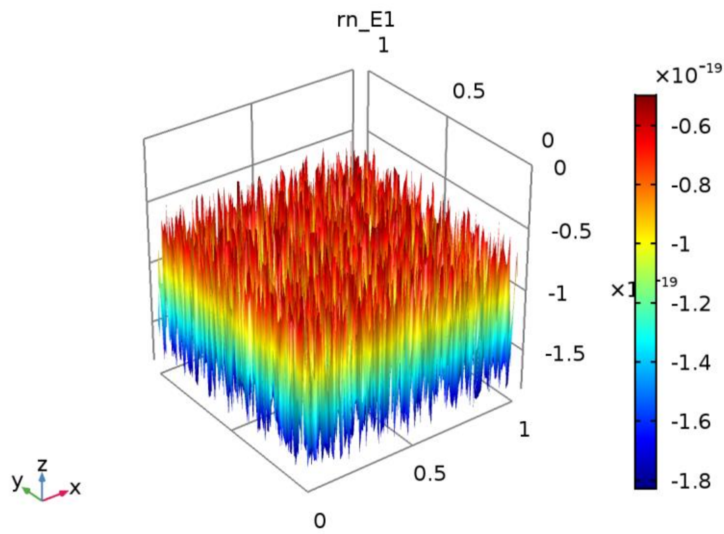

Random 1

PARAMETERS

Description	Value
Number of arguments	2
Distribution	Uniform

SETTINGS

Description	Value
Mean	E1_mean
Range	E1_range

Random 2

Function name	rn_E12
Function type	Random

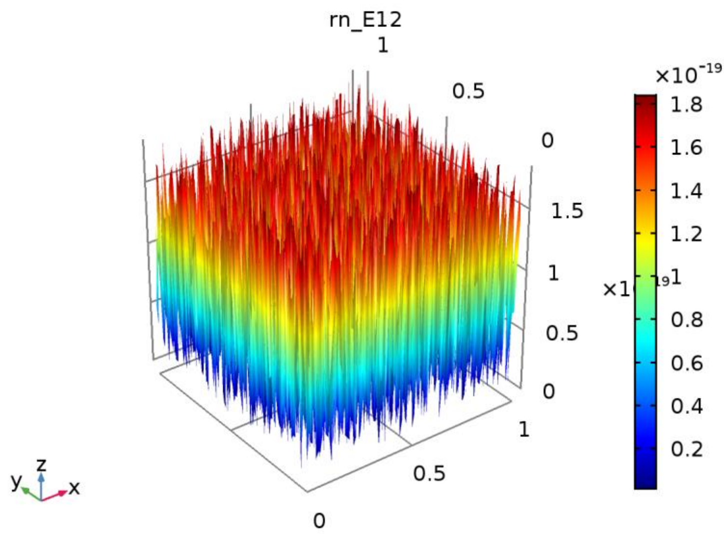

Random 2

PARAMETERS

Description	Value
Number of arguments	2
Distribution	Uniform

SETTINGS

Description	Value
Mean	E12_mean
Range	E12_range

Random 3

Function name	rn_E2
Function type	Random

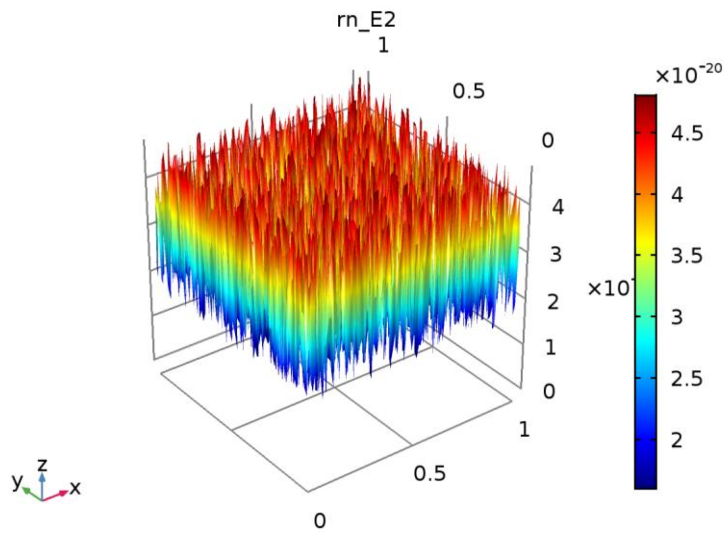

Random 3

PARAMETERS

Description	Value
Number of arguments	2
Distribution	Uniform

SETTINGS

Description	Value
Mean	E2_mean
Range	E2_range

Random 4

Function name	rn_E23
Function type	Random

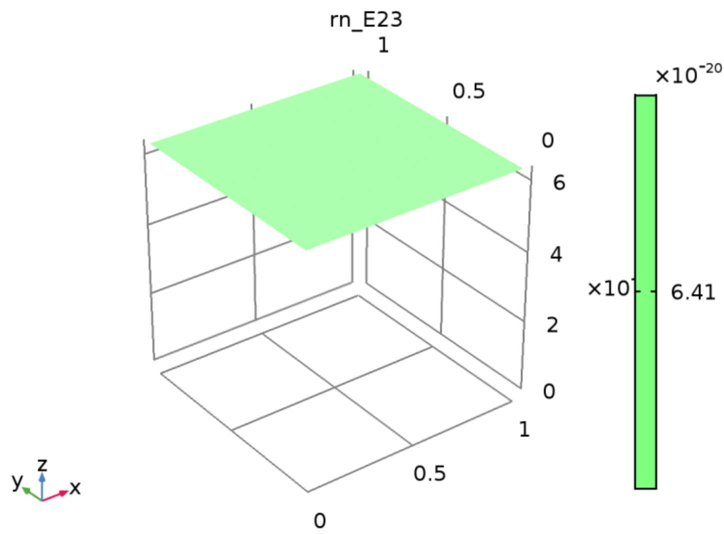

Random 4

PARAMETERS

Description	Value
Number of arguments	2
Distribution	Uniform

SETTINGS

Description	Value
Mean	E23_mean
Range	E23_range

Random 5

Function name	rn_E3
Function type	Random

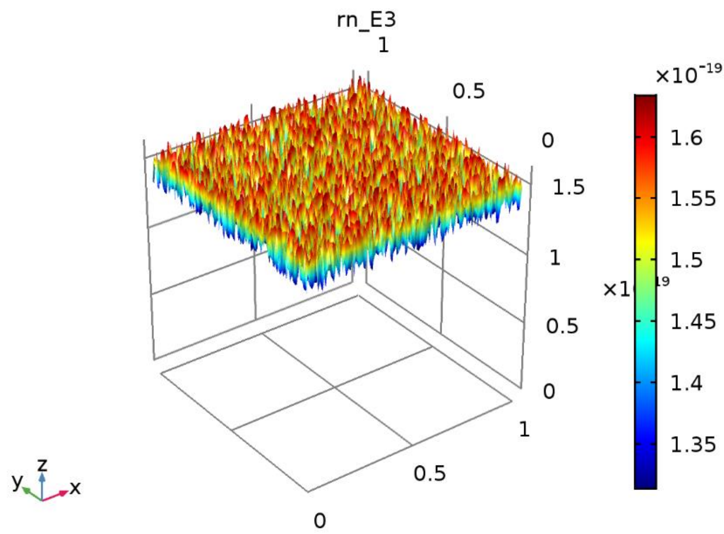

Random 5

PARAMETERS

Description	Value
Number of arguments	2
Distribution	Uniform

SETTINGS

Description	Value
Mean	E3_mean
Range	E3_range

Random 6

Function name	rn_E32
Function type	Random

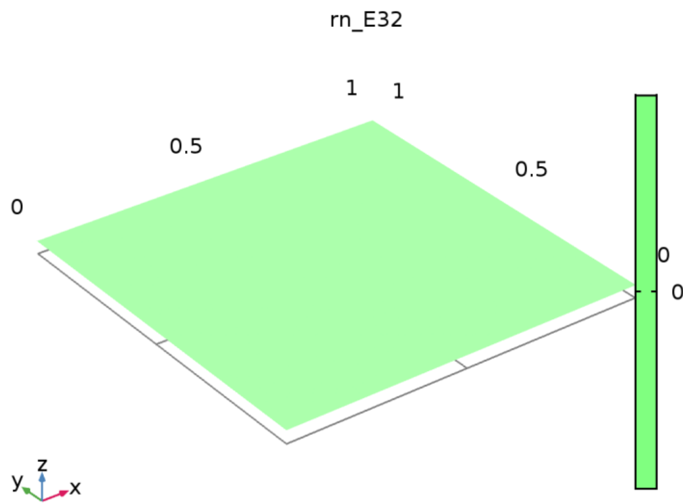

Random 6

PARAMETERS

Description	Value
Number of arguments	2
Distribution	Uniform

SETTINGS

Description	Value
Mean	E32_mean
Range	E32_range

Random 7

Function name	rn_E31
Function type	Random

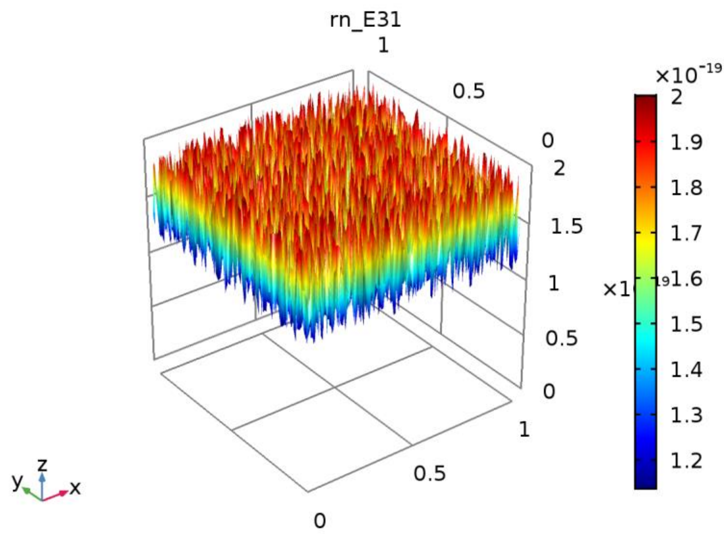

Random 7

PARAMETERS

Description	Value
Number of arguments	2
Distribution	Uniform

SETTINGS

Description	Value
Mean	E31_mean
Range	E31_range

Random 8

Function name	rn_E24
Function type	Random

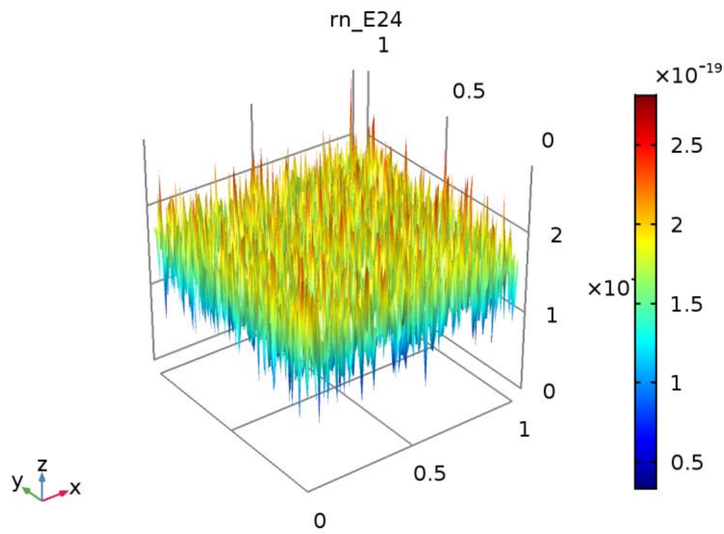

Random 8

PARAMETERS

Description	Value
Number of arguments	2
Distribution	Normal

SETTINGS

Description	Value
Mean	E24_mean
Standard deviation	E24_spread

Random 9

Function name	rn_E4
Function type	Random

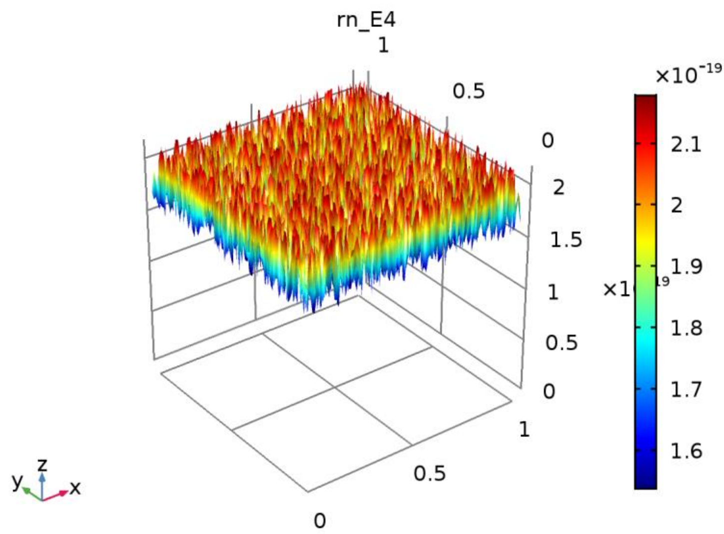

Random 9

PARAMETERS

Description	Value
Number of arguments	2
Distribution	Uniform

SETTINGS

Description	Value
Mean	E4_mean
Range	E4_range

Random 10

Function name	rn_E45
Function type	Random

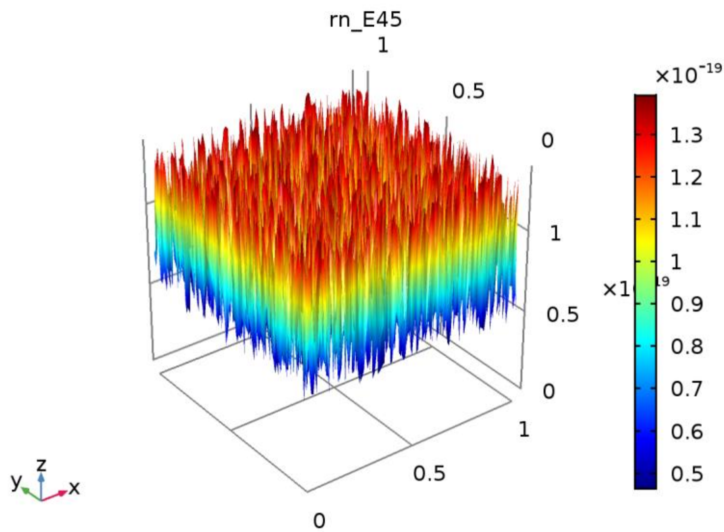

Random 10

PARAMETERS

Description	Value
Number of arguments	2
Distribution	Uniform

SETTINGS

Description	Value
Mean	E45_mean
Range	E45_range

2.1.3 Component Couplings

Integration 1

Coupling type	Integration
Operator name	intop1

SOURCE SELECTION

Geometric entity level	Domain
Selection	Domain 1

Integration 2

Coupling type	Integration
Operator name	intop2

SOURCE SELECTION

Geometric entity level	Boundary
Selection	Boundary 2

2.1.4 Coordinate Systems

Boundary System 1

Coordinate system type	Boundary system
Tag	sys1

COORDINATE NAMES

First	Second	Third
t1	n	to

2.2 GEOMETRY 1

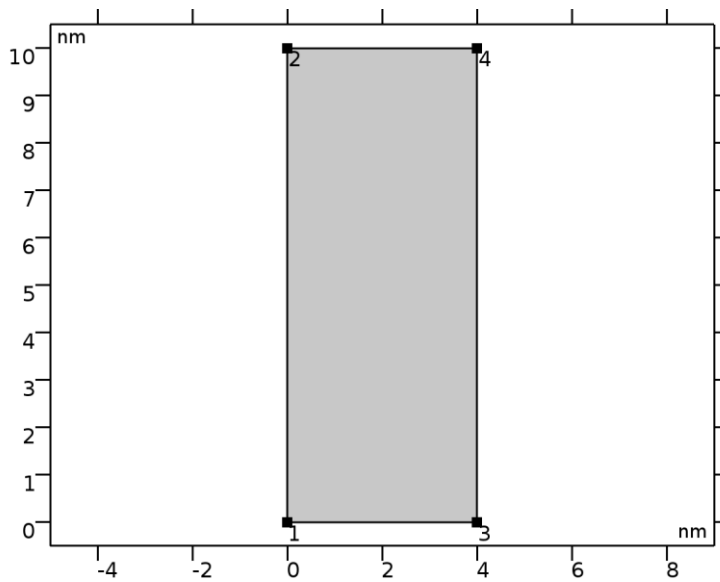

Geometry 1

UNITS

Length unit	nm
Angular unit	deg

GEOMETRY STATISTICS

Description	Value
Space dimension	2
Number of domains	1
Number of boundaries	4
Number of vertices	4

2.2.1 Rectangle 1 (r1)

POSITION

Description	Value
Position	{0, 0}

SIZE

Description	Value
Width	d_ox
Height	10

2.3 N

USED PRODUCTS

COMSOL Multiphysics

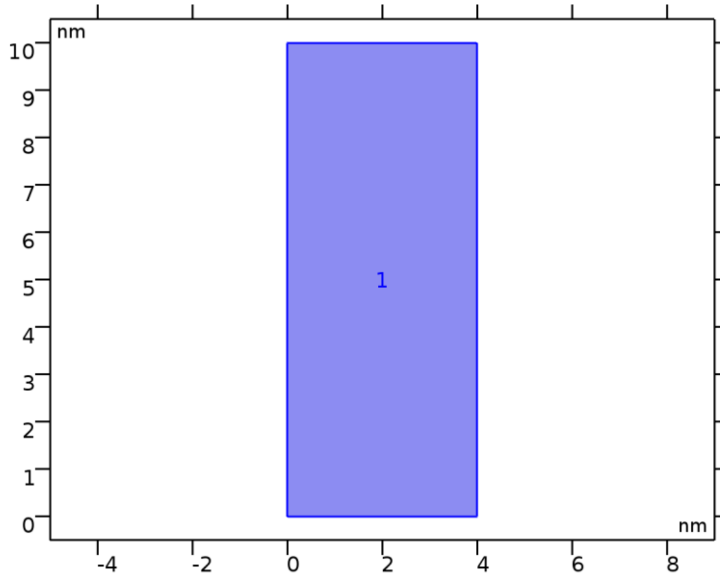

N

SELECTION

Geometric entity level	Domain
Selection	Domain 1

SETTINGS

Description	Value
Element order	Quadratic
Compute boundary fluxes	Off
Shape function type	Lagrange
Value type when using splitting of complex variables	Complex
Dependent variable quantity	Dimensionless (1)
Source term quantity	None
Unit	m^ - 2

VARIABLES

Name	Expression	Unit	Description	Selection
c.nx	nx		Normal vector, x component	Boundaries 1–4
c.ny	ny		Normal vector, y component	Boundaries 1–4

Name	Expression	Unit	Description	Selection
c.nz	root.nz		Normal vector, z component	Boundaries 1–4
c.nxmesh	root.nxmesh		Normal vector (mesh), x component	Boundaries 1–4
c.nymesh	root.nymesh		Normal vector (mesh), y component	Boundaries 1–4
c.nzmesh	root.nzmesh		Normal vector (mesh), z component	Boundaries 1–4

2.3.1 Coefficient Form PDE 1

Coefficient Form PDE 1

SELECTION

Geometric entity level	Domain
Selection	Domain 1

EQUATIONS

$$e_a \frac{\partial^2 \mathbf{u}}{\partial t^2} + d_a \frac{\partial \mathbf{u}}{\partial t} + \nabla \cdot (-c \nabla \mathbf{u} - \alpha \mathbf{u} + \gamma) + \beta \cdot \nabla \mathbf{u} + a \mathbf{u} = f$$

$$\mathbf{u} = [N1, N2, N3, N4, N5]^T$$

$$\nabla = [\frac{\partial}{\partial x}, \frac{\partial}{\partial y}]$$

SETTINGS

Description	Value
Diffusion coefficient	{{{{0, 0}, {0, 0}}, {{0, 0}, {0, 0}}, {{0, 0}, {0, 0}}, {{0, 0}, {0, 0}}, {{0, 0}, {0, 0}}}, {{{0, 0}, {0, 0}}, {{0, 0}, {0, 0}}, {{0, 0}, {0, 0}}, {{0, 0}, {0, 0}}, {{0, 0}, {0, 0}}}, {{{0, 0}, {0, 0}}, {{0, 0}, {0, 0}}, {{0, 0}, {0, 0}}, {{0, 0}, {0, 0}}, {{0, 0}, {0, 0}}}, {{{0, 0}, {0, 0}}, {{0, 0}, {0, 0}}, {{0, 0}, {0,

Description	Value
	0}}, {{0, 0}, {0, 0}}, {{0, 0}, {0, 0}}}, {{{0, 0}, {0, 0}}, {{0, 0}, {0, 0}}, {{0, 0}, {0, 0}}, {{0, 0}, {0, 0}}, {{DH, 0}, {0, DH}}}}
Absorption coefficient	{{0, 0, 0, 0, 0}, {0, 0, 0, 0, 0}, {0, 0, 0, 0, 0}, {0, 0, 0, 0, 0}, {0, 0, 0, 0, 0}}
Source term	{-K12*N1 + K31*N3, +K12*N1 - K23*N2 + K32*N3 - K24*N2*(x<=d_ox/10), K23*N2 - K32*N3 - K31*N3 + K45*N4, K24*N2*(x<=d_ox/10) - K45*N4, K45*N4}
Mass coefficient	{{0, 0, 0, 0, 0}, {0, 0, 0, 0, 0}, {0, 0, 0, 0, 0}, {0, 0, 0, 0, 0}, {0, 0, 0, 0, 0}}
Damping or mass coefficient	{{1, 0, 0, 0, 0}, {0, 1, 0, 0, 0}, {0, 0, 1, 0, 0}, {0, 0, 0, 1, 0}, {0, 0, 0, 0, 1}}
Conservative flux convection coefficient	{{{0, 0}, {0, 0}, {0, 0}, {0, 0}, {0, 0}}, {{0, 0}, {0, 0}, {0, 0}, {0, 0}, {0, 0}}, {{0, 0}, {0, 0}, {0, 0}, {0, 0}, {0, 0}}, {{0, 0}, {0, 0}, {0, 0}, {0, 0}, {0, 0}}, {{0, 0}, {0, 0}, {0, 0}, {0, 0}, {0, 0}}}
Convection coefficient	{{{0, 0}, {0, 0}, {0, 0}, {0, 0}, {0, 0}}, {{0, 0}, {0, 0}, {0, 0}, {0, 0}, {0, 0}}, {{0, 0}, {0, 0}, {0, 0}, {0, 0}, {0, 0}}, {{0, 0}, {0, 0}, {0, 0}, {0, 0}, {0, 0}}, {{0, 0}, {0, 0}, {0, 0}, {0, 0}, {0, 0}}}
Conservative flux source	{{0, 0}, {0, 0}, {0, 0}, {0, 0}, {0, 0}}

Variables

Name	Expression	Unit	Description	Selection
domflux.N1x	0		Domain flux, x component	Domain 1
domflux.N1y	0		Domain flux, y component	Domain 1
domflux.N2x	0		Domain flux, x component	Domain 1
domflux.N2y	0		Domain flux, y component	Domain 1
domflux.N3x	0		Domain flux, x component	Domain 1
domflux.N3y	0		Domain flux, y component	Domain 1
domflux.N4x	0		Domain flux, x component	Domain 1
domflux.N4y	0		Domain flux, y component	Domain 1
domflux.N5x	-DH*N5x	m/s	Domain flux, x component	Domain 1
domflux.N5y	-DH*N5y	m/s	Domain flux, y component	Domain 1

Shape functions

Name	Shape function	Unit	Description	Shape frame	Selection
N1	Lagrange (Quadratic)	1	Dependent variable N1	Material	Domain 1

Name	Shape function	Unit	Description	Shape frame	Selection
N2	Lagrange (Quadratic)	1	Dependent variable N2	Material	Domain 1
N3	Lagrange (Quadratic)	1	Dependent variable N3	Material	Domain 1
N4	Lagrange (Quadratic)	1	Dependent variable N4	Material	Domain 1
N5	Lagrange (Quadratic)	1	Dependent variable N5	Material	Domain 1

2.3.2 Zero Flux 1

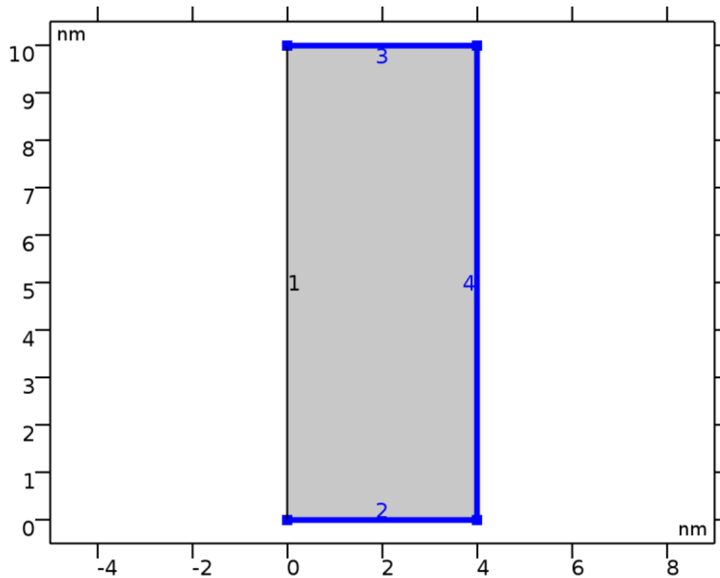

Zero Flux 1

SELECTION

Geometric entity level	Boundary
Selection	Boundaries 2–4

EQUATIONS

$$-\mathbf{n}\cdot(-c\nabla\mathbf{u}-\alpha\mathbf{u}+\gamma)=0$$

$$\mathbf{u}=[N1, N2, N3, N4, N5]^T$$

$$\nabla=[\frac{\partial}{\partial x},\frac{\partial}{\partial y}]$$

2.3.3 Initial Values 1

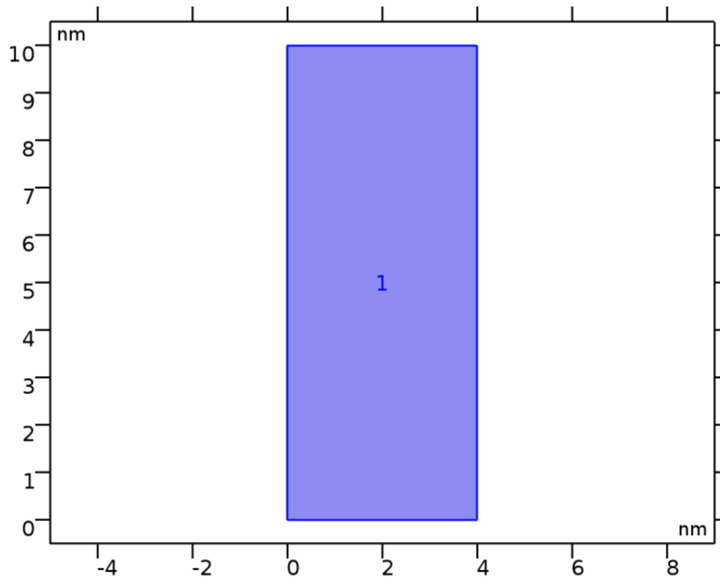

Initial Values 1

SELECTION

Geometric entity level	Domain
Selection	Domain 1

SETTINGS

Description	Value
Initial value for N1	1e15[1/cm^3]
Initial time derivative of N1	0
Initial value for N2	0
Initial time derivative of N2	0
Initial value for N3	0
Initial time derivative of N3	0
Initial value for N4	0
Initial time derivative of N4	0
Initial value for N5	0
Initial time derivative of N5	0

2.3.4 Flux/Source 1

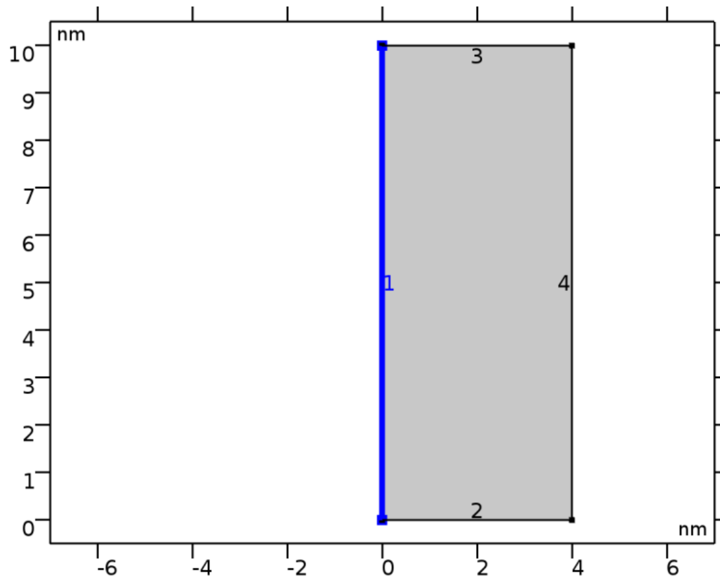

Flux/Source 1

SELECTION

Geometric entity level	Boundary
Selection	Boundary 1

EQUATIONS

$$-\mathbf{n}\cdot(-c\nabla\mathbf{u}-\alpha\mathbf{u}+\gamma)=g-q\mathbf{u}$$

$$\mathbf{u}=[N1, N2, N3, N4, N5]^T$$

$$\nabla=[\frac{\partial}{\partial x},\frac{\partial}{\partial y}]$$

SETTINGS

Description	Value
Boundary flux/source	{0, 0, 0, 0, -Kr*N5*0.01*Nit}
Boundary absorption/impedance term	{{0, 0, 0, 0, 0}, {0, 0, 0, 0, 0}, {0, 0, 0, 0, 0}, {0, 0, 0, 0, 0}, {0, 0, 0, 0, 0}}

Variables

Name	Expression	Unit	Description	Selection
c.g_N1	0	1/m	Boundary flux/source	Boundary 1
c.g_N2	0	1/m	Boundary flux/source	Boundary 1
c.g_N3	0	1/m	Boundary flux/source	Boundary 1
c.g_N4	0	1/m	Boundary flux/source	Boundary 1
c.g_N5	-0.01*Kr*N5*Nit	1/m	Boundary flux/source	Boundary 1

2.4 MESH 1

MESH STATISTICS

Description	Value
Minimum element quality	0.8982
Average element quality	0.987
Triangular elements	1270
Edge elements	98
Vertex elements	4

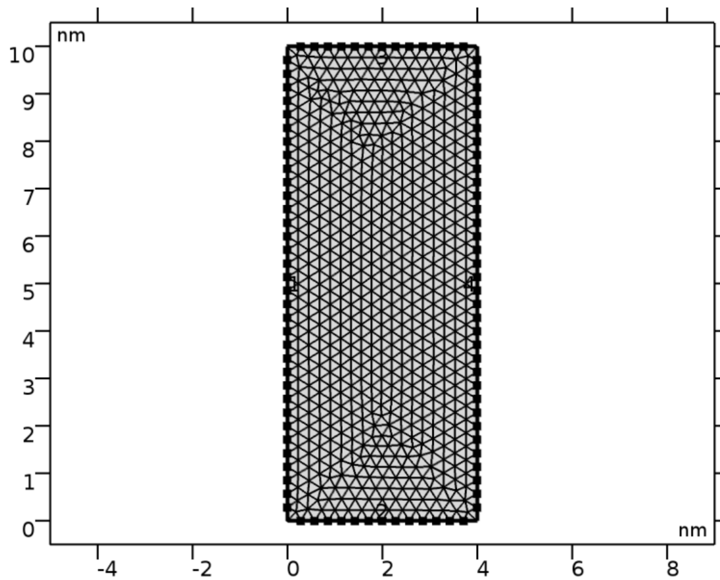

Mesh 1

2.4.1 Size (size)

SETTINGS

Description	Value
Maximum element size	0.3
Minimum element size	0.0030
Curvature factor	0.3
Maximum element growth rate	1
Custom element size	Custom

2.4.2 Free Triangular 1 (auto_f1)

SELECTION

Geometric entity level	Domain
Selection	Geometry geom1

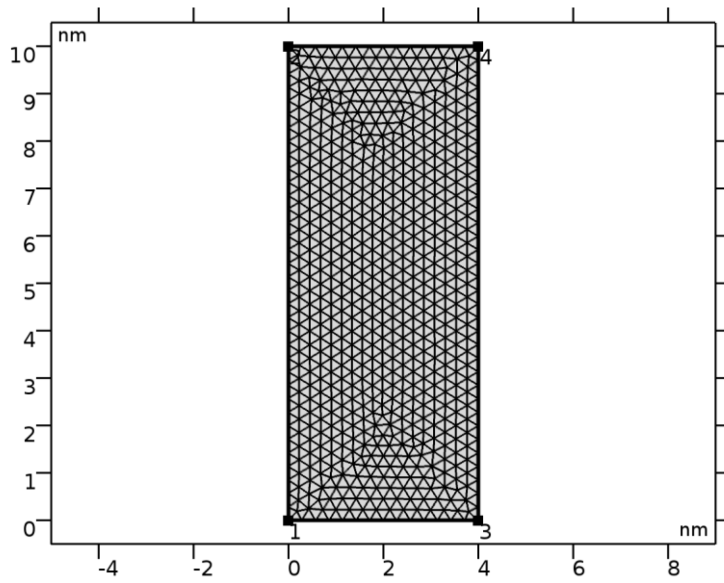

Free Triangular 1

3 Study 1

COMPUTATION INFORMATION

Computation time	
CPU	Intel(R) Core(TM) i5-3470 CPU @ 3.20GHz, 4 cores
Operating system	Windows 10

3.1 SOLVER CONFIGURATIONS

3.1.1 Solver 1

Compile Equations (st1)

STUDY AND STEP

Description	Value
Use study	Study 1

Dependent Variables 1 (v1)

mod1_N2 (mod1_N2)

GENERAL

Description	Value
Field components	mod1.N2

mod1_N1 (mod1_N1)

GENERAL

Description	Value
Field components	mod1.N1

mod1_N3 (mod1_N3)

GENERAL

Description	Value
Field components	mod1.N3

mod1_N4 (mod1_N4)

GENERAL

Description	Value
Field components	mod1.N4

mod1_N5 (mod1_N5)

GENERAL

Description	Value
Field components	mod1.N5

Time-Dependent Solver 1 (t1)

GENERAL

Description	Value
Times	{0, 0.01, 0.02, 0.03, 0.04, 0.05, 0.06, 0.07, 0.08, 0.09, 0.1, 0.2, 0.30000000000000004, 0.4, 0.5, 0.6, 0.7000000000000001, 0.8, 0.9, 1, 11, 21, 31, 41, 51, 61, 71, 81, 91, 200, 300, 400, 500, 600, 700, 800, 900, 1000, 1000.01, 1000.02, 1000.03, 1000.04, 1000.05, 1000.06, 1000.0699999999999, 1000.08, 1000.09, 1000.1, 1000.2, 1000.3000000000001, 1000.4, 1000.5, 1000.6, 1000.7, 1000.8000000000001, 1000.9, 1001, 1011, 1021, 1031, 1041, 1051, 1061, 1071, 1081, 1091, 1200, 1300, 1400, 1500, 1600, 1700, 1800, 1900, 2000, 2000.01, 2000.02, 2000.03, 2000.04, 2000.05, 2000.06, 2000.07, 2000.08, 2000.09, 2000.1, 2000.1999999999998, 2000.3, 2000.3999999999999, 2000.5, 2000.6, 2000.6999999999998, 2000.8, 2000.8999999999999, 2001, 2011, 2021, 2031, 2041, 2051, 2061, 2071, 2081, 2091, 2200, 2300, 2400, 2500, 2600, 2700, 2800, 2900, 3000, 3000.01, 3000.0200000000004, 3000.03, 3000.0400000000004, 3000.05, 3000.0600000000004, 3000.07, 3000.0800000000004, 3000.09, 3000.1, 3000.2, 3000.2999999999997, 3000.4, 3000.5, 3000.6, 3000.7, 3000.7999999999997, 3000.9, 3001, 3011, 3021, 3031, 3041, 3051, 3061, 3071, 3081, 3091, 3200, 3300, 3400, 3500, 3600, 3700, 3800, 3900, 4000}

ABSOLUTE TOLERANCE

Description	Value
Tolerance method	Manual
Absolute tolerance	0.0010
Update scaled absolute tolerance	Off

: MOD1_N2

Description	Value
Tolerance method	Manual

: MOD1_N1

Description	Value
Tolerance method	Manual

: MOD1_N3

Description	Value
Tolerance method	Manual

: MOD1_N4

Description	Value
Tolerance method	Manual

: MOD1_N5

Description	Value
Tolerance method	Manual

TIME STEPPING

Description	Value
Steps taken by solver	Strict
Initial step	0.0010
Fraction of initial step for Backward Euler	1.0

RESULTS WHILE SOLVING

Description	Value
Plot	On
Plot group	1D Plot Group 3
Update at	Time steps taken by solver

LOG

Direct (dDef)

GENERAL

Description	Value
Preordering algorithm	Approximate minimum degree
Out-of-core	Off

Fully Coupled 1 (fc1)

GENERAL

Description	Value
Linear solver	Direct

RESULTS WHILE SOLVING

Description	Value
Probes	Manual

4 Results

4.1 DATA SETS

4.1.1 Solution 1

SOLUTION

Description	Value
Solution	Solver 1
Component	Save Point Geometry 1

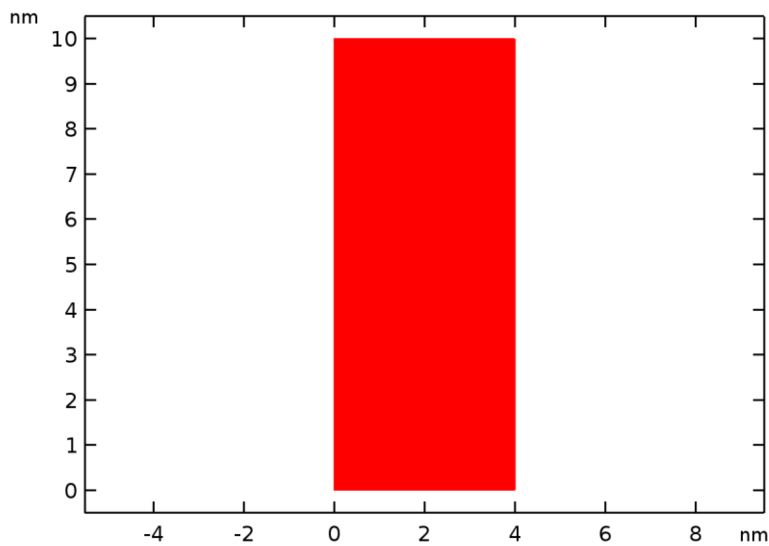

Data set: Solution 1

4.2 DERIVED VALUES

4.2.1 Surface Integration 1

SELECTION

Geometric entity level	Domain
Selection	Domain 1

DATA

Description	Value
Data set	Solution 1

EXPRESSIONS

Expression	Unit	Description
N2		Dependent variable N2

OUTPUT

Evaluated in	Table 2

4.3 TABLES

4.3.1 Table 1

4.3.2 Table 2

Surface Integration 1 (u2)

TABLE 2

4.4 PLOT GROUPS

4.4.1 2D Plot Group 1

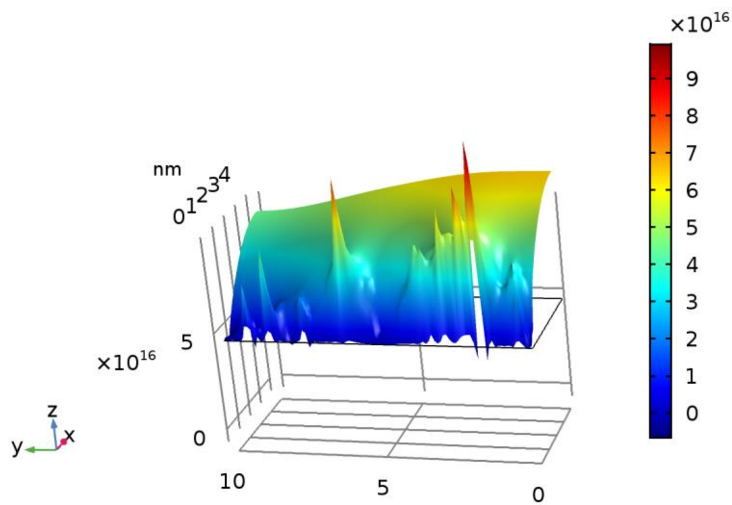

Time=4000 Surface: Dependent variable N5

4.4.2 1D Plot Group 2

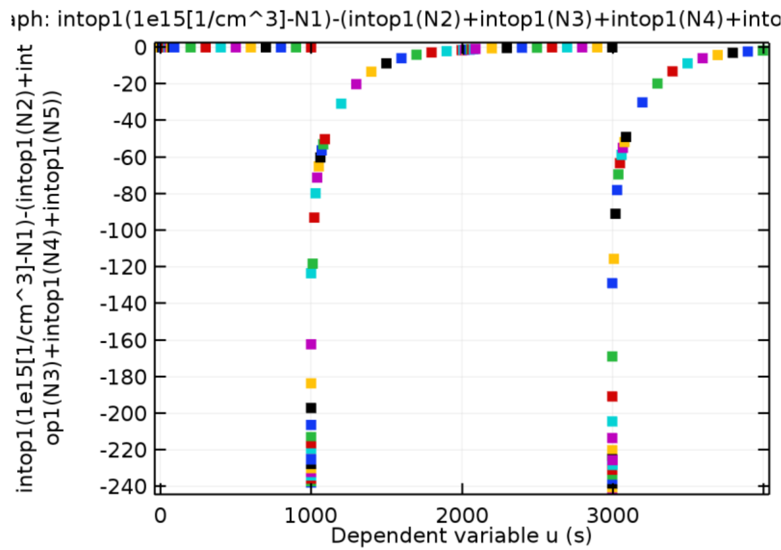

Line Graph: intop1(1e15[1/cm^3]-N1)-(intop1(N2)+intop1(N3)+intop1(N4)+intop1(N5))

4.4.3 1D Plot Group 3

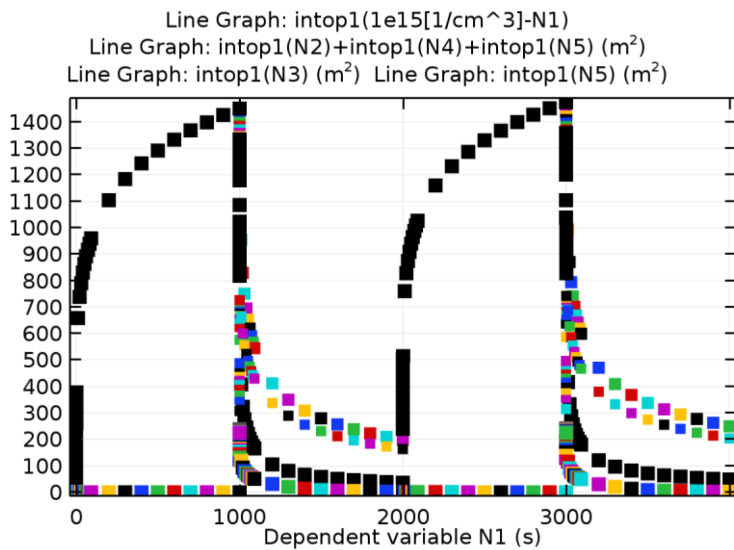

Line Graph: intop1(1e15[1/cm^3]-N1) Line Graph: intop1(N2)+intop1(N4)+intop1(N5) (m^2) Line Graph: intop1(N3) (m^2) Line Graph: intop1(N5) (m^2)

4.4.4 1D Plot Group 4

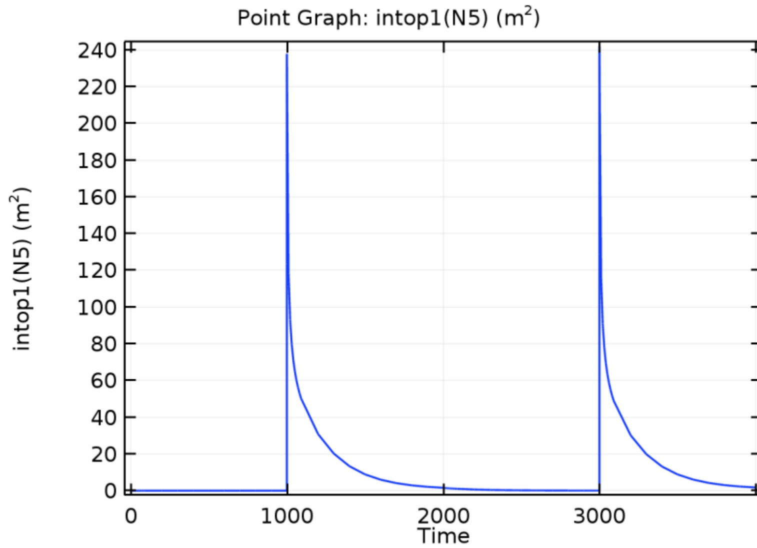

Point Graph: intop1(N5) (m^2)

4.4.5 1D Plot Group 5

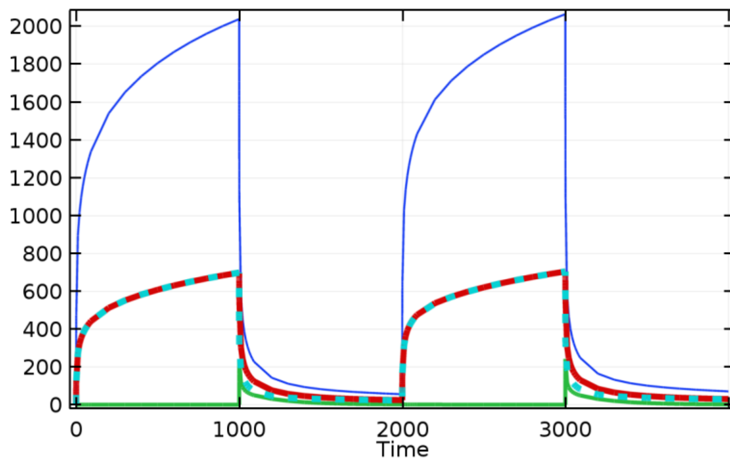

Point Graph: intop1((1-x/d_ox)*N2)+intop1(N4)+intop1(N4)+intop1(N5) (m^2) Point Graph: intop1(N5) (m^2) Point Graph: Nit Point Graph: intop1(N4) (m^2)

References

[1] G. E. Moore and others, “Cramming more components onto integrated circuits,” 1965.

[2] W. H. Zachariasen, “The atomic arrangement in glass,” *Journal of the American Chemical Society*, vol. 54, no. 10, pp. 3841–3851, 1932.

[3] J. Randall, H. Rooksby, and B. Cooper, “13. X-ray Diffraction and the Structure of Vitreous Solids—I,” *Zeitschrift für Kristallographie-Crystalline Materials*, vol. 75, no. 1, pp. 196–214, 1930.

[4] R. Mozzi and B. Warren, “The structure of vitreous silica,” *Journal of Applied Crystallography*, vol. 2, no. 4, pp. 164–172, 1969.

[5] J. Da Silva, D. Pinatti, C. Anderson, and M. Rudee, “A refinement of the structure of vitreous silica,” *Philosophical Magazine*, vol. 31, no. 3, pp. 713–717, 1975.

[6] C. R. Helms and E. H. Poindexter, “The silicon-silicon dioxide system: Its microstructure and imperfections,” *Reports on Progress in Physics*, vol. 57, no. 8, p. 791, 1994.

[7] T. Grasser, *Bias temperature instability for devices and circuits*. Springer Science \& Business Media, 2013.

[8] D. M. Fleetwood and R. D. Schrimpf, *Defects in microelectronic materials and devices*. CRC press, 2008.

[9] M. Walters and A. Reisman, “Radiation-Induced Neutral Electron Trap Generation in Electrically Biased Insulated Gate Field Effect Transistor Gate Insulators,” *Journal of The Electrochemical Society*, vol. 138, no. 9, pp. 2756–2762, 1991.

[10] S. Pantelides, Z.-Y. Lu, C. Nicklaw, T. Bakos, S. Rashkeev, D. Fleetwood, and R. Schrimpf, “The E′ center and oxygen vacancies in SiO2,” *Journal of Non-Crystalline Solids*, vol. 354, no. 2–9, pp. 217–223, 2008.

[11] Z.-Y. Lu, C. Nicklaw, D. Fleetwood, R. Schrimpf, and S. Pantelides, “Structure, Properties, and Dynamics of Oxygen Vacancies in Amorphous S i O 2,” *Physical review letters*, vol. 89, no. 28, p. 285505, 2002.

[12] P. M. Lenahan and J. Conley Jr, “What can electron paramagnetic resonance tell us about the Si/SiO 2 system?,” *Journal of Vacuum Science \& Technology B: Microelectronics and Nanometer Structures Processing, Measurement, and Phenomena*, vol. 16, no. 4, pp. 2134–2153, 1998.

[13] MISSING:goes2008charging, "MISSING:goes2008charging," 2020.

[14] D. L. Griscom, E. Friebele, K. Long, and J. Fleming, "Fundamental defect centers in glass: electron spin resonance and optical absorption studies of irradiated phosphorus-doped silica glass and optical fibers," *Journal of Applied Physics*, vol. 54, no. 7, pp. 3743–3762, 1983.

[15] J. P. Campbell, P. M. Lenahan, A. T. Krishnan, and S. Krishnan, "Observations of NBTI-induced atomic-scale defects," *IEEE Transactions on Device and Materials Reliability*, vol. 6, no. 2, pp. 117–122, 2006.

[16] W. Warren, M. Shaneyfelt, D. Fleetwood, J. Schwank, P. Winokur, and R. Devine, "Microscopic nature of border traps in MOS oxides," *IEEE transactions on nuclear science*, vol. 41, no. 6, pp. 1817–1827, 1994.

[17] D. Fleetwood, "Fast and slow border traps in MOS devices," in *Proceedings of the Third European Conference on Radiation and its Effects on Components and Systems*, 1995, pp. 1–8.

[18] E. H. Poindexter, P. J. Caplan, B. E. Deal, and R. R. Razouk, "Interface states and electron spin resonance centers in thermally oxidized (111) and (100) silicon wafers," *Journal of Applied Physics*, vol. 52, no. 2, pp. 879–884, 1981.

[19] Y. Cheng, "Electronic states at the silicon-silicon dioxide interface," *Progress in Surface Science*, vol. 8, no. 5, pp. 181–218, 1977.

[20] J. Schwank, D. Fleetwood, P. Winokur, P. Dressendorfer, D. Turpin, and D. Sanders, "The role of hydrogen in radiation-induced defect formation in polysilicon gate MOS devices," *IEEE Transactions on Nuclear Science*, vol. 34, no. 6, pp. 1152–1158, 1987.

[21] J. F. Zhang, C. Z. Zhao, A. H. Chen, G. Groeseneken, and R. Degraeve, "Hole traps in silicon dioxides. Part I. Properties," *IEEE Transactions on Electron Devices*, vol. 51, no. 8, pp. 1267–1273, 2004.

[22] C. Z. Zhao, J. F. Zhang, G. Groeseneken, and R. Degraeve, "Hole-traps in silicon dioxides. Part II. Generation mechanism," *IEEE Transactions on Electron Devices*, vol. 51, no. 8, pp. 1274–1280, 2004.

[23] S. Mahapatra and N. Parihar, "A review of NBTI mechanisms and models," *Microelectronics Reliability*, vol. 81, pp. 127–135, 2018.

[24] D. K. Schroder and J. A. Babcock, "Negative bias temperature instability: Road to cross in deep submicron silicon semiconductor manufacturing," *Journal of applied Physics*, vol. 94, no. 1, pp. 1–18, 2003.

[25] J. H. Stathis, S. Mahapatra, and T. Grasser, "Controversial issues in negative bias temperature instability," *Microelectronics Reliability*, vol. 81, pp. 244–251, 2018.

[26] E. Snow, A. Grove, B. Deal, and C. Sah, “Ion transport phenomena in insulating films,” *Journal of Applied Physics*, vol. 36, no. 5, pp. 1664–1673, 1965.

[27] B. E. Deal, M. Sklar, A. S. Grove, and E. H. Snow, “Characteristics of the surface-state charge (Qss) of thermally oxidized silicon,” *Journal of the Electrochemical Society*, vol. 114, no. 3, pp. 266–274, 1967.

[28] K. O. Jeppson and C. M. Svensson, “Negative bias stress of MOS devices at high electric fields and degradation of MNOS devices,” *Journal of Applied Physics*, vol. 48, no. 5, pp. 2004–2014, 1977.

[29] V. Huard, M. Denais, F. Perrier, N. Revil, C. Parthasarathy, A. Bravaix, and E. Vincent, “A thorough investigation of MOSFETs NBTI degradation,” *Microelectronics Reliability*, vol. 45, no. 1, pp. 83–98, 2005.

[30] V. Huard, M. Denais, and C. Parthasarathy, “NBTI degradation: From physical mechanisms to modelling,” *Microelectronics Reliability*, vol. 46, no. 1, pp. 1–23, 2006.

[31] T. Grasser, P.-J. Wagner, P. Hehenberger, W. Goes, and B. Kaczer, “A rigorous study of measurement techniques for negative bias temperature instability,” *IEEE Transactions on Device and Materials Reliability*, vol. 8, no. 3, pp. 526–535, 2008.

[32] G. Groeseneken, H. E. Maes, N. Beltran, and R. F. De Keersmaecker, “A reliable approach to charge-pumping measurements in MOS transistors,” *IEEE Transactions on Electron Devices*, vol. 31, no. 1, pp. 42–53, 1984.

[33] G. Du, D. Ang, Z. Teo, and Y. Hu, “Ultrafast measurement on NBTI,” *IEEE Electron Device Letters*, vol. 30, no. 3, pp. 275–277, 2009.

[34] U. Cilingiroglu, “A general model for interface-trap charge-pumping effects in MOS devices,” *Solid-state electronics*, vol. 28, no. 11, pp. 1127–1141, 1985.

[35] Z. Teo, D. Ang, and K. See, “Can the reaction-diffusion model explain generation and recovery of interface states contributing to NBTI?,” in *2009 IEEE International Electron Devices Meeting (IEDM)*, 2009, pp. 1–4.

[36] Z. Teo, D. Ang, and C. Ng, “Separation of hole trapping and interface-state generation by ultrafast measurement on dynamic negative-bias temperature instability,” *IEEE Electron Device Letters*, vol. 31, no. 7, pp. 656–658, 2010.

[37] Z. Q. Teo, D. S. Ang, and C. M. Ng, “‘Non-hydrogen-transport’ characteristics of dynamic negative-bias temperature instability,” *IEEE Electron Device Letters*, vol. 31, no. 4, pp. 269–271, 2010.

[38] D. Ang, S. Wang, G. Du, and Y. Hu, “A consistent deep-level hole trapping model for negative bias temperature instability,” *IEEE Transactions on Device and Materials Reliability*, vol. 8, no. 1, pp. 22–34, 2008.

[39] D. K. Schroder, "Negative bias temperature instability: What do we understand?," *Microelectronics Reliability*, vol. 47, no. 6, pp. 841–852, 2007.

[40] M. A. Alam and S. Mahapatra, "A comprehensive model of PMOS NBTI degradation," *Microelectronics Reliability*, vol. 45, no. 1, pp. 71–81, 2005.

[41] S. Mahapatra, P. B. Kumar, and M. Alam, "Investigation and modeling of interface and bulk trap generation during negative bias temperature instability of p-MOSFETs," *IEEE Transactions on Electron Devices*, vol. 51, no. 9, pp. 1371–1379, 2004.

[42] M. A. Alam, H. Kufluoglu, D. Varghese, and S. Mahapatra, "A comprehensive model for PMOS NBTI degradation: Recent progress," *Microelectronics Reliability*, vol. 47, no. 6, pp. 853–862, 2007.

[43] S. Mahapatra, P. B. Kumar, T. Dalei, D. Sana, and M. Alam, "Mechanism of negative bias temperature instability in CMOS devices: degradation, recovery and impact of nitrogen," in *IEDM Technical Digest. IEEE International Electron Devices Meeting, 2004.*, 2004, pp. 105–108.

[44] J. H. Stathis and S. Zafar, "The negative bias temperature instability in MOS devices: A review," *Microelectronics Reliability*, vol. 46, no. 2–4, pp. 270–286, 2006.

[45] W. Liu, Z. Liu, D. Huang, C. Liao, L. Zhang, Z. Gan, W. Wong, C. Shen, and M.-F. Li, "On-the-fly interface trap measurement and its impact on the understanding of NBTI mechanism for p-MOSFETs with SiON gate dielectric," in *2007 IEEE International Electron Devices Meeting*, 2007, pp. 813–816.

[46] J. Stathis, G. LaRosa, and A. Chou, "Broad energy distribution of NBTI-induced interface states in p-MOSFETs with ultra-thin nitrided oxide," in *2004 IEEE International Reliability Physics Symposium. Proceedings*, 2004, pp. 1–7.

[47] A. Krishnan, C. Chancellor, S. Chakravarthi, P. Nicollian, V. Reddy, A. Varghese, R. Khamankar, and S. Krishnan, "Material dependence of hydrogen diffusion: Implications for NBTI degradation," in *IEEE InternationalElectron Devices Meeting, 2005. IEDM Technical Digest.*, 2005, p. 4–pp.

[48] S. Tsujikawa, T. Mine, K. Watanabe, Y. Shimamoto, R. Tsuchiya, K. Ohnishi, T. Onai, J. Yugami, and S. Kimura, "Negative bias temperature instability of pMOSFETs with ultra-thin SiON gate dielectrics," in *2003 IEEE International Reliability Physics Symposium Proceedings, 2003. 41st Annual.*, 2003, pp. 183–188.

[49] S. Rangan, N. Mielke, and E. C. Yeh, "Universal recovery behavior of negative bias temperature instability [PMOSFETs]," in *IEEE International Electron Devices Meeting 2003*, 2003, pp. 14–3.

[50] T. Grasser, B. Kaczer, W. Goes, T. Aichinger, P. Hehenberger, and M. Nelhiebel, "A two-stage model for negative bias temperature instability," in *2009 IEEE international reliability physics symposium*, 2009, pp. 33–44.

[51] C. Tahanout, H. Tahi, M. Boubaaya, B. Djezzar, M. Marah, B. Nadji, and N. Saoula, "NBTI stress on power VDMOS transistors under low magnetic field," in *2015 IEEE International Integrated Reliability Workshop (IIRW)*, 2015, pp. 147–150.

[52] S. Merah, B. Nadji, and H. Tahi, "Low magnetic field Impact on NBTI degradation," *Microelectronics Reliability*, vol. 55, no. 9–10, pp. 1460–1463, 2015.

[53] V. Huard, F. Monsieur, G. Ribes, and S. Bruyere, "Evidence for hydrogen-related defects during NBTl stress in p-MOSFETs," in *2003 IEEE International Reliability Physics Symposium Proceedings, 2003. 41st Annual.*, 2003, pp. 178–182.

[54] D. M. Fleetwood, "'Border traps' in MOS devices," *IEEE transactions on nuclear science*, vol. 39, no. 2, pp. 269–271, 1992.

[55] R. Car and M. Parrinello, "Structural, dymanical, and electronic properties of amorphous silicon: an ab initio molecular-dynamics study," *Physical review letters*, vol. 60, no. 3, p. 204, 1988.

[56] F. Schanovsky and T. Grasser, "On the microscopic limit of the modified reaction-diffusion model for the negative bias temperature instability," in *2012 IEEE International Reliability Physics Symposium (IRPS)*, 2012, p. XT–10.

[57] S. Mahapatra, N. Goel, S. Desai, S. Gupta, B. Jose, S. Mukhopadhyay, K. Joshi, A. Jain, A. Islam, and M. Alam, "A comparative study of different physics-based NBTI models," *IEEE transactions on electron devices*, vol. 60, no. 3, pp. 901–916, 2013.

[58] D. Ang, Z. Teo, T. Ho, and C. Ng, "Reassessing the mechanisms of negative-bias temperature instability by repetitive stress/relaxation experiments," *IEEE Transactions on Device and Materials Reliability*, vol. 11, no. 1, pp. 19–34, 2010.

[59] T. Grasser, B. Kaczer, W. Goes, T. Aichinger, P. Hehenberger, and M. Nelhiebel, "Understanding negative bias temperature instability in the context of hole trapping," *Microelectronic Engineering*, vol. 86, no. 7–9, pp. 1876–1882, 2009.

[60] T. Grasser, B. Kaczer, W. Goes, H. Reisinger, T. Aichinger, P. Hehenberger, P.-J. Wagner, F. Schanovsky, J. Franco, M. T. Luque, and others, "The paradigm shift in understanding the bias temperature instability: From reaction-diffusion to switching oxide traps," *IEEE Transactions on Electron Devices*, vol. 58, no. 11, pp. 3652–3666, 2011.

[61] P. M. Lenahan, J. P. Campbell, A. T. Krishnan, and S. Krishnan, "A model for NBTI in nitrided oxide MOSFETs which does not involve hydrogen or diffusion," *IEEE Transactions on Device and Materials Reliability*, vol. 11, no. 2, pp. 219–226, 2010.

[62] Z. Yue, P. Shi, L. Xiao-Yi, C. Qing, M. Xiao-Hua, and H. Yue, "Effects of stress conditions on the generation of negative bias temperature instability-associated interface traps," *Chinese Physics B*, vol. 22, no. 11, p. 117311, 2013.

[63] A. E. Islam, N. Goel, S. Mahapatra, and M. A. Alam, "Reaction-diffusion model," in *Fundamentals of Bias Temperature Instability in MOS Transistors*, Springer, 2016, pp.

181–207.

[64] A. E. Islam, H. Kufluoglu, D. Varghese, S. Mahapatra, and M. A. Alam, “Recent issues in negative-bias temperature instability: Initial degradation, field dependence of interface trap generation, hole trapping effects, and relaxation,” *IEEE Transactions on Electron Devices*, vol. 54, no. 9, pp. 2143–2154, 2007.

[65] T. Aichinger, S. Puchner, M. Nelhiebel, T. Grasser, and H. Hutter, “Impact of hydrogen on recoverable and permanent damage following negative bias temperature stress,” in *2010 IEEE International Reliability Physics Symposium*, 2010, pp. 1063–1068.

[66] M. Chang and J. Zhang, “On positive charge formed under negative bias temperature stress,” *Journal of Applied Physics*, vol. 101, no. 2, p. 024516, 2007.

[67] MISSING:article, “MISSING:article,” 2020.

[68] J. F. Zhang, “Oxide defects,” in *Bias Temperature Instability for Devices and Circuits*, Springer, 2014, pp. 253–285.

[69] A. J. Lelis and T. R. Oldham, “Time dependence of switching oxide traps,” *IEEE transactions on nuclear science*, vol. 41, no. 6, pp. 1835–1843, 1994.

[70] M. Mallati and H. Bentarzi, “New Multi-stages-Hydrogen Diffusion Model for Negative Bias Temperature Instability,” 2019.

[71] S. Gupta, B. Jose, K. Joshi, A. Jain, M. A. Alam, and S. Mahapatra, “A comprehensive and critical re-assessment of 2-stage energy level NBTI model,” in *2012 IEEE International Reliability Physics Symposium (IRPS)*, 2012, p. XT–3.

[72] COMSOL, “12. COMSOL Multiphysics® www.comsol.com. COMSOL AB, Stockholm, Sweden.”

[73] F. Schwierz, H. Wong, and J. J. Liou, *Nanometer CMOS*. Pan Stanford Publishing, 2010.

[74] A. W. Strong, E. Y. Wu, R.-P. Vollertsen, J. Sune, G. La Rosa, T. D. Sullivan, and S. E. Rauch III, *Reliability wearout mechanisms in advanced CMOS technologies*, vol. 12. John Wiley \& Sons, 2009.

[75] B. Kaczer, V. Arkhipov, M. Jurczak, and G. Groeseneken, “Negative bias temperature instability (NBTI) in SiO2 and SiON gate dielectrics understood through disorder-controlled kinetics,” *Microelectronic engineering*, vol. 80, pp. 122–125, 2005.

[76] Ashok K. Singh, “Chapter 3 - Physicochemical, Electronic, and Mechanical Properties of Nanoparticles,” Engineered Nanoparticles, Academic Press, vol. 80, pp. 77 - 123, 2016.

[77] Hammond, Richard T, “Spin flip probability of electron in a uniform magnetic field,” Applied Physics Letters, vol. 100, pp. 112-121, 2012.